



Review article

Selective laser melting of titanium matrix composites: An in-depth analysis of materials, microstructures, defects, and mechanical properties

Jun Fang^{a,b,c}, Yong Chai Tan^{b,*}, Vin Cent Tai^b, Shamini Janasekaran^b, Chia Ching Kee^b, Dongsheng Wang^{a,c,**}, Youwen Yang^d

^a School of Mechanical Engineering, Tongling University, Tongling, AnHui, 244100, China

^b Center for Modelling and Simulation, Faculty of Engineering, Built Environment and Information Technology, SEGi University, Jalan Teknologi, Kota Damansara, 47810, Petaling Jaya, Selangor Darul Ehsan, Malaysia

^c Key Laboratory of Additive Manufacturing of Tongling City, Tongling University, Tongling, AnHui, 244100, China

^d Institute of Additive Manufacturing, Jiangxi University of Science and Technology, Nanchang, 330013, China

ARTICLE INFO

Keywords:

Metal matrix composites
Selective laser melting
Microstructures
Mechanochemical processing
Strengthening mechanism

ABSTRACT

This paper provides an in-depth review of the advancements and challenges associated with Titanium Matrix Composites (TMCs) in Selective Laser Melting (SLM). Material selection, SLM processing parameters, and their influence on the microstructure and properties of TMCs are discussed. The relationship between processing parameters, material characteristics, and the development of defects such as balling, porosity, and cracking is examined. Critical factors influencing the evolution of microstructure and defect formation in TMCs processed by SLM are highlighted. Strengthening mechanisms such as dislocation movements, grain refinement, the Orowan process, and load-bearing capacity are analyzed, and their roles in enhancing hardness, tensile strength, corrosion resistance, and wear resistance are explored. It is indicated by key findings that less than 5 % reinforcement content by volume can significantly enhance mechanical properties, achieving maximum hardness values of approximately 1000 HV and tensile strength close to 1500 MPa. However, this improvement is accompanied by a notable decrease in elongation. The importance of optimizing SLM parameters such as laser power, scan speed, hatch distance, layer thickness, and particle contents to minimize defects and enhance material performance is underscored. Existing research gaps in defect management and material distribution are identified. Future research directions on improving TMCs performance through advanced SLM techniques are suggested.

1. Introduction

Titanium and its alloys have attracted significant interest in various industries, such as aerospace [1], automotive [2], biomedical [3], and defense [4,5]. While these materials exhibit excellent properties like corrosion resistance [6], low density [7], high fatigue resistance [8], reasonable strength [9], and outstanding biocompatibility [10], they fall short in hardness, wear resistance, and heat

* Corresponding author.

** Corresponding author. School of Mechanical Engineering, Tongling University, Tongling, AnHui, 244100, China.

E-mail addresses: tanyongchai@segi.edu.my (Y.C. Tan), wangdongsheng@tlu.edu.cn (D. Wang).

<https://doi.org/10.1016/j.heliyon.2024.e40200>

Received 6 May 2024; Received in revised form 10 October 2024; Accepted 5 November 2024

Available online 8 November 2024

2405-8440/© 2024 Published by Elsevier Ltd.

This is an open access article under the CC BY-NC-ND license

(<http://creativecommons.org/licenses/by-nc-nd/4.0/>).

resistance compared to steel and nickel-based alloys [11,12]. These limitations have restricted their wider applicability in certain demanding applications [13–15].

Titanium matrix composites (TMCs) have emerged as a significant area of research in recent years, offering an effective way to enhance the performance of Ti-based alloys [16]. Their superior physical and mechanical properties position TMCs as promising materials for aircraft engine and airframe applications [17]. If further optimized for performance and cost, TMCs have the potential to replace other metallic materials in a wide range of applications. Numerous manufacturing techniques for TMCs exist today [18,19]. However, traditional methods like powder metallurgy and in-situ casting face challenges such as high interfacial reactivity and poor matrix wettability [20–22]. High interfacial reactivity can result in the formation of cracks or pores, which, in turn, may cause premature failure of the composite material under tensile stress. Current strategies to mitigate this issue primarily involve the implementation of advanced additive manufacturing techniques, optimization of processing parameters, enhancement of reinforced materials, and application of heat treatment to improve interfacial bonding and overall performance, thereby minimizing interface defects [23–25]. Poor wettability can result in the aggregation of reinforcement powders into coarse clumps, which impedes their uniform dispersion throughout the matrix and degrades the surface quality [26]. To address this issue, existing processing methods have devoted substantial efforts to enhancing the wettability between the matrix and reinforcement phase. These strategies include applying metallic coatings to the reinforcement particles, preheating them before their dispersion into the molten matrix, and incorporating reactive components into the melt [27]. The high chemical activity of titanium materials can lead to chemical reactions during processing, potentially affecting material properties and component performance [28,29]. Moreover, the strong van der Waals forces between particles, which are intermolecular forces, become significant when ceramic particles such as TiB, Mo₂C, B₄C, and graphene are incorporated into the titanium matrix and reduced to nanoscale. The increased specific surface area amplifies van der Waals forces, leading to the easy agglomeration of the reinforcement phase [30,31]. This makes it challenging to achieve a uniform distribution of reinforced particles in the matrix, particularly for nanoparticles [27,32].

These challenges underscore the need for alternative manufacturing strategies that can circumvent these issues without adding complexity or cost [29,33,34]. Consequently, the development of additive manufacturing technology has emerged as a promising replacement for producing TMCs [35,36]. This technology provides several benefits, such as the capability to fabricate intricate geometries, minimize material waste, and facilitate customization [37,38]. Furthermore, it enables precise control over the distribution of reinforcing particles within the matrix, resulting in improved material properties and overall performance. For example, a uniformly distributed mixed powder can be achieved by adjusting process parameters, optimizing the mixing time with a planetary ball mill, and employing dynamic imaging techniques [39,40]. In summary, additive manufacturing technology is a promising approach to overcome the limitations of traditional manufacturing methods in producing titanium-based composites [41].

Selective Laser Melting (SLM) is an advanced additive manufacturing process designed for rapid and efficient production of complex-shaped components, minimizing the need for excessive post-processing (Fig. 1) [42]. SLM has become popular in the additive manufacturing of TMCs, offering several advantages: (1) it eliminates the need for special molds or fixtures; (2) it achieves high manufacturing precision; (3) it can produce components with functionally graded materials, allowing for varying material properties within a single component; and (4) it facilitates the integration of complex structural sections into the manufacturing process [43–45]. The principle of forming is that the scraper scrapes the metal powder onto the substrate in the processing room, and then the laser beam selectively melts the metal powder onto the substrate. After the current layer is completed, the horizontal scraper lays a new layer of metal powder, and the laser beam and scraper repeatedly move until the entire component is manufactured. The size and shape of the

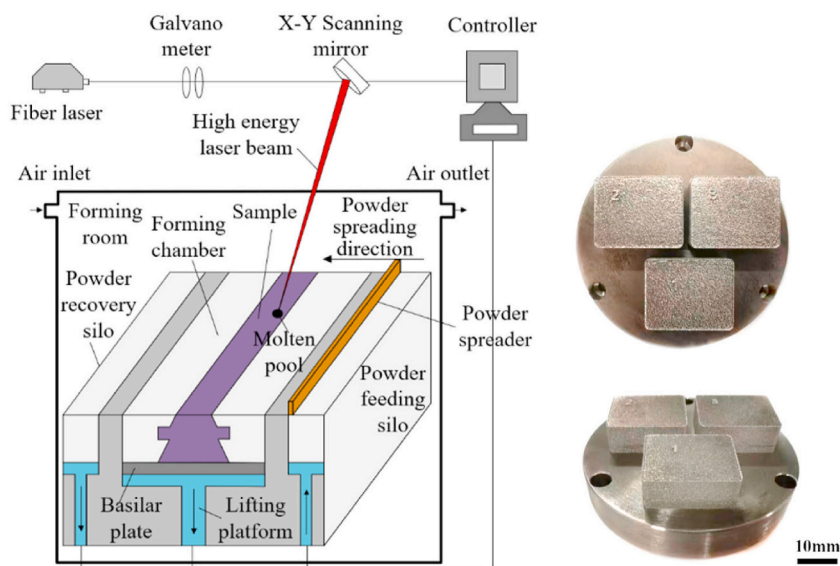


Fig. 1. Process schematics for Selective Laser Melting (SLM) [47,48].

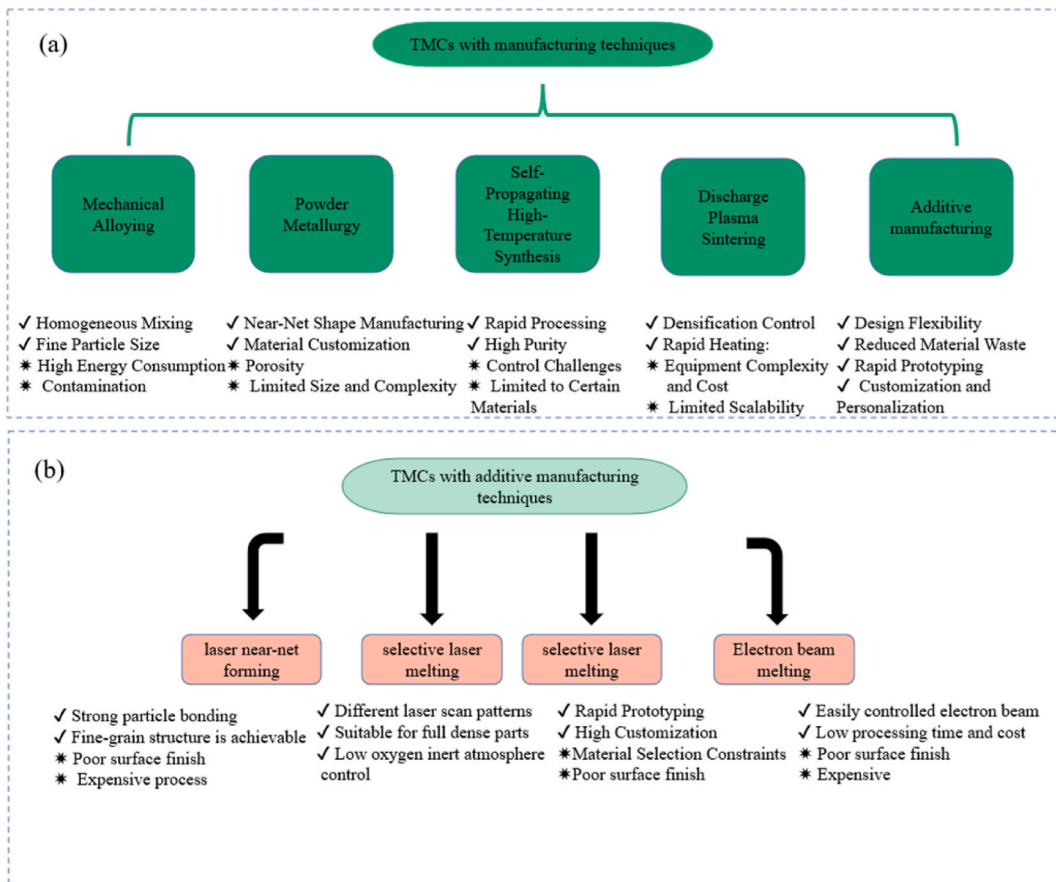


Fig. 2. Summary of the manufacturing techniques for TMCs.

melt pool can be adjusted by controlling laser processing parameters [46].

Existing literature review on SLM of metal matrix composites or pure metals [24,49–51] only provides a brief introduction to particle-reinforced titanium matrix composites (TMCs) produced by SLM and lacks a comprehensive analysis of particle types, defects, properties, and reinforcement mechanisms. This paper addresses these gaps by offering a systematic and detailed analysis of recent advancements and challenges in the field of TMCs, with a particular emphasis on their development through SLM. This paper significantly differs from previous studies by thoroughly collating and discussing critical aspects, ranging from the selection of base and reinforcement materials to the intricate processes involved in SLM. It examines the microstructural characteristics of TMCs and explores the influence of factors such as mechanical milling, reinforcements, SLM parameters, and heat treatment on the microstructures. A significant portion of this review is dedicated to understanding the defects that can arise during the SLM process, such as balling, porosity, cracking, and their impacts on material properties. Furthermore, the paper explores various strengthening mechanisms in TMCs, including dislocation, fine grain, Orowan mechanism, and load-bearing strengthening, and their contributions to the overall mechanical performance of the composites. The review also provides a detailed evaluation of the properties of TMCs, including hardness, tensile properties, corrosion resistance, and wear resistance, offering a comprehensive view of their performance metrics. Finally, the paper concludes with a summary of the current state of the art, outlines prospects, and explores potential research directions in the field of TMCs, aiming to bridge the gap between current challenges and future applications.

The primary novelty of this review lies in its systematic and comprehensive approach to collating and analyzing the multifaceted aspects of TMCs fabricated via SLM. This review provides a cohesive understanding of the state of the art in this field by addressing the selection of materials, SLM process parameters, microstructural characteristics, defect formation, and mechanical performance. This research directly addresses the main question of how various factors influence the properties and performance of TMCs produced through SLM, thereby offering insights that can guide future research and application. The critical analysis and identification of current challenges and potential research directions are intended to inspire further advancements and practical solutions in the development of high-performance TMCs.

2. Materials and processes

TMCs are recognized as cutting-edge materials with substantial potential for a wide range of applications. These composites effectively integrate the superior properties of titanium with those of other reinforcing materials [52]. An overview of the most widely used methods for manufacturing TMCs is provided in Fig. 2. SLM has emerged as a breakthrough method for creating metal matrix composites due to its high material utilization rate and the availability of various material options. Discussing the types and processes of materials and reinforcements is crucial, as they directly impact the performance of laser-fabricated composite materials.

Strict attention to detail is required when selecting reinforcing elements compatible with titanium and its alloys for synthesizing TMCs [20]. Selecting the appropriate reinforcement and matrix materials and optimizing various other factors are crucial steps in the manufacturing process. The procedure for making strategic decisions has an important effect on the composites' overall quality and performance [53,54].

Additionally, Nagarajan et al. (2020) classified the methods affecting SLM products and identified 18 factors that impact performance, including the building chamber atmosphere, powder bed temperature, spot size, support structures, and others. Although these factors affect mechanical properties, there is a lack of studies specifically addressing TMCs produced using the SLM approach. Consequently, this paper examines the current influencing factors [50].

Fig. 3 shows a schematic illustration of the machining principle. Composite materials are composed of a matrix material and a reinforcing material. After ball milling, they are printed layer by layer using SLM equipment and subsequently undergo heat treatment and processed to become ideal products [55].

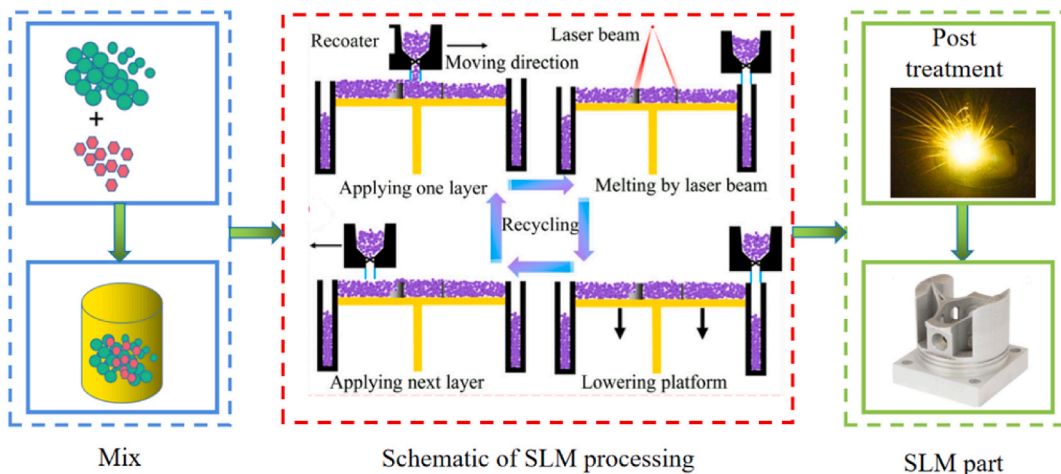


Fig. 3. Processing schematic diagram involved in SLM [55].

Table 1

Comparison of tensile mechanical properties and Vickers hardness of various base materials subjected to SLM.

Based Materials	Condition	Vickers hardness [HV]	Yield strength $\sigma_{0.2}$ [MPa]	Ultimate tensile strength σ_{UCS} [MPa]	Fracture strain ϵ_{max} [%]	Ref.
Ti	SLM	261 ± 13	555	757	19.5	[61]
Ti6Al4V	SLM	409	1110	1267	7.28	[59]
Ti-24Nb-4Zr-8Sn	SLM	220 ± 6	563 ± 38	665 ± 18	13.8 ± 4.1	[62,63]
Ti-6Al-7Nb	SLM	395 ± 10	1029 ± 27	–	–	[64]

2.1. Based materials

In recent research, SLM technology has become widely used in the fabrication of titanium-based composites. Extensive investigations have been conducted on four main categories of substrate materials: pure titanium (Ti) [56], titanium alloy Ti6Al4V [57], Ti-24Nb-4Zr-8Sn, and Ti-6Al-7Nb [58]. The properties of these substrates are meticulously described in Table 1. These materials have received significant attention and scrutiny in the field of SLM, which has profound implications for the advancement and practical application of these advanced materials [59,60].

The Ti6Al4V alloy is widely regarded as the top choice for substrate in SLM research. It possesses exceptional strength and hardness properties, making it highly valued in aerospace, biomedical, and engineering applications [65]. The precision of the SLM technique has played a crucial role in fabricating Ti6Al4V-based composites, leading to extensive research on various aspects such as densification kinetics, microstructural intricacies, and mechanical properties. Apart from the commonly used Ti6Al4V alloy, attention has also been directed towards other titanium-based alloys like Ti-6Al-7Nb and Ti-24Nb-4Zr-8Sn [27,61,66]. These alloys have garnered significant interest in medical applications due to their superior biocompatibility compared to Ti6Al4V and better elongation properties than SLM Ti materials [61]. Furthermore, researchers have conducted extensive studies on the mechanical properties, microstructural evolution, and densification behavior of titanium substrate composites. This comprehensive study has provided valuable insights into the functionality of these substrate materials in composite applications [67].

2.2. Reinforcement materials

SLM must enhance the physical and mechanical properties of titanium-based composites to demonstrate their viability [42]. An appropriate reinforcement phase can improve the composite's overall performance, including its modulus, strength, hardness, lower coefficient of thermal expansion compared to the base material, and thermodynamic stability [68]. However, the large range of possible reinforcing materials may make it difficult to distribute the reinforcing phase evenly throughout the titanium matrix. Unequal temperature gradients could arise from the unequal distribution, and these could ultimately lead to residual stresses and fractures [51]. The most typically used reinforcing phases are TiB [69], TiC [70], B₄C [59], TiB₂ [71], and carbon nanotubes (CNTs) [72]. To mitigate microcracking, trace amounts of impurity elements (Mn and C) and solid solution elements (Co, W, and Mo) have been employed as reinforcements. These additives, which dissolve into the metal matrix, help prevent the formation of undesired pores and cracks [73]. Additionally, dissolved additives can modify ceramic dissolution-enriched regions, thereby reinforcing the matrix and enhancing mechanical properties [62]. Table 2 provides an overview of the characteristics of frequently used and examined reinforcing materials.

Ex-situ methods comprise the independent synthesis or preparation of materials that are then incorporated into the main raw materials in the material synthesis process [89]. This method preserves the powder's original form inside the final composite material without the need for chemical reactions. The performance properties of these composite materials can be finely controlled by meticulously manipulating the amount and mixing method of varied elements [90].

Ceramic materials such as TiB [91], TiC [92], TiN [81], SiC [93], Mo₂C [62], and rare earth elements are commonly used in the ex-situ growth of titanium-based composites using SLM. These materials exhibit thermodynamic stability, with their particles refraining from undergoing chemical reactions and forming new substances during the SLM sintering process [94–96].

Table 2

Characteristics of TMCs reinforcing materials.

Material	Density (g/cm ³)	Melting point (°C)	Coefficient of thermal expansion (*10 ⁻⁶ K ⁻¹)	Young's modulus (GPa)	Ref.
Ti	4.57	1668	8.8	105	[63,74]
TiC	4.99	3433	7.4–8.8	440	[75,76]
B ₄ C	2.51	2720	4.78	445	[31,77]
TiB	4.57	2473	8.6	550	[78,79]
TiB ₂	4.52	3253	4.6–8.1	500	[71,80]
TiN	5.40	3290	9.3	250	[81]
AlN	3.30	2800	5.6	343	[82]
Ti ₅ Si ₃	4.32	2130	9.7	225	[83,84]
Graphene	1.70 - 2.00	~3852	–	1000	[72]
CNTs	2.00	~3379	–	1000	[85]
Rare earth elements	–	–	–	–	[86,87]
Mo ₂ C	9.18	2690	7.0	380–400	[62,88]

Table 3
Maximum densification and ideal machining parameters for a few common SLM-machined TMCs.

Materials	Rotation speed (rpm)	Ball-to-powder weight ratio	Milling time (h)	P (W)	v (mm/s)	h (μm)	d (μm)	Maximum densification obtained	Ref.
Ti-5wt.%TiC	300	8:1	4	100	200	70	50	98.20 %	[23, 76]
Ti-7.5 wt%TiC	200	5:1	4	90	300	50	50	>98.3 %	[23, 83]
Ti-12.5 wt%TiC	200	5:1	4	90	300	50	50	98.30 %	[84]
Ti-15 wt%TiC	200	5:1	4	90	100–400	50	50	>97 %	[84]
Ti-17.5 wt%TiC	200	5:1	4	90	300	50	50	97.20 %	[23, 83]
Ti-22.5 wt%TiC	200	5:1	4	90	300	50	50	94.70 %	[23, 83]
Ti6Al4V-3wt.% TiC	200	1:1	4	200–400	800–1600	120	30	98.7 %	[103]
Ti6Al4V-(0–3) wt.% Mo ₂ C	30	–	24	250	1500	120	40	>0.999 %	[62]
Ti6Al4V-5wt.% TiC	–	–	–	130–250	300–1500	80	30	99.70 %	[104]
Ti-23.8 wt%SiC	300	–	15	80	100–400	50	50	96.90 %	[105]
Ti-5wt.%TiB ₂	200	5:1	2	165–185	118–154	100	100	>99.5 %	[71]
Ti-50 wt%TiB ₂	–	–	2	36–84	80–500	60	25	92	[106]
Ti-(0–5) wt.%B ₄ C	–	–	24	250	1500	85	40	>97.8 %	[31]
Ti6Al4V-0.5 wt% B ₄ C	200	5:1	–	95–260	330–900	60	40	≥99 %	[107]
Ti-24.55 wt% Si ₃ N ₄	250	10:1	8	1000	100–400	150	100	97.70 %	[23, 81]

The in-situ approach is a promising way to create reinforced particles through chemical reactions within the matrix. At the microstructural level, the limitations imposed by the in-situ production process improve the interaction between the reinforced particles and the matrix [76]. Furthermore, there is improved bonding and increased purity at the interface where the reinforced particles and matrix meet. Finer reinforcing effects are produced by the more uniform dispersion of the reinforced particles within the matrix. Several ceramic particles, as well as B₄C [97], TiB₂ [98], SiC [93], and TiN [81], are frequently utilized as in-situ self-generated reinforced particles. Materials incorporating in-situ produced TiB_W and TiC_p particles have exhibited higher overall performance [99]. In addition, carbon materials, such as carbon nanotubes, graphite, and carbon fibers, can react with titanium (Ti) to produce titanium carbide (TiC) reinforced particles, which have found extensive application in the field of titanium-based composites [100].

2.3. Processes

The irregular microstructure of powder particles, including spherical voids, cracks, and surface roughness, can be significantly influenced by the adjustment of process parameters, affecting the overall material properties. A comprehensive understanding and analysis of this phenomenon from an academic perspective are essential [59]. Researchers frequently use laser energy density (E_d) as a fundamental concept to examine the effects of different properties on the material. The impact of process variables, such as laser power (P), scan speed (v), hatch distance (h), layer thickness (d), and scan strategy, on microstructure and process defects is analyzed using this metric [101]. The energy density measurement provides insight into the energy consumption per unit volume of powder material and the influence of process variables on SLM processing [102]. Some examples of popular SLM processing TMCs with optimal processing parameters and maximum densities are provided in Table 3.

$$E_d = \frac{P}{h \times v \times d} \quad (1)$$

Where v represents scanning speed, h represents the hatching distance, d represents the layer thickness, P represents the laser power and E_d is the laser energy density [102].

Additive manufacturing such as SLM, has changed the part-making process [108]. The creation of high-density (>99.5 %) parts, as indicated in Tables 3 and is a crucial objective for process optimization since porosity in SLM parts can result in a decline in mechanical qualities [109]. Energy density is a crucial SLM element because it influences the creation of voids and pores. Low-energy densities lead to hole development, while high-energy densities generate spherical pores and decreased density [110].

To achieve high-density materials, it is essential to control the energy density, maintaining it close to the lower threshold of the powder melting energy. Studies indicate that the optimal energy density range for titanium and its composites in the SLM process is between 50 and 200 J/mm³. Consequently, experimental investigations are necessary to determine the optimal energy density value [23]. Recent studies have demonstrated that SLM may create nearly flawlessly dense components in titanium or pure titanium composites by adjusting the process parameters [111,112]. Several studies have confirmed the existence of small pore effects, indicating that process parameter optimization is required to achieve high-density parts [113,114]. It is important to note that small pore effects can occur if the energy density is higher than required, leading to closed pores.

In conclusion, the matrix materials affect the qualities of TMCs and titanium-based metals are well-liked due to their strength. Various TMCs are produced by incorporating titanium-based metals with different types of reinforcement powders. One important technique is SLM printing, which requires exact conditions for the best mechanical and microstructural results. Heat treatment is one of the post-processing methods that improves the material characteristics. SLM presents a viable path for producing TMCs and provides a variety of applications by refining the technique and selecting the appropriate materials. To advance the performance of SLM-printed TMCs, further research is required to overcome existing challenges.

3. Microstructure of TMCs

The mechanical properties of TMCs are significantly impacted by their microstructural features. The high strength and hardness of the composite are attributed to the small ceramic particles that are present in the matrix, which inhibit dislocation movement and prevent cracking [70]. Moreover, the interface between the matrix and reinforcements is crucial for load transfer; a strong interfacial connection guarantees efficient stress transfer, improving the composite's overall mechanical performance [54,115]. Interfacial strength can be indirectly assessed by using nanoindentation to measure hardness and elastic modulus, along with microstructure analysis to evaluate interface defects between the matrix and reinforcement [116].

3.1. Influence of mechanical milling

High-energy ball milling is a popular and cost-effective method for producing composite powders [117]. In a high-energy ball mill, the powder particles go through many grindings, cold fusion, and regrinding stages. The ball-powder-ball collision causes the ground composite powder to deform significantly on a macroscopic and microscopic level, which presents a great chance for the production of nanostructures between the metal matrix and the ceramic reinforcement [118]. It is anticipated that the final mechanical properties of the nanocomposites made by the additive manufacturing method will be enhanced by the uniform distribution of reinforcing particles and the creation of ultra-fine nanocrystalline structures [119]. High sphericity, homogeneous reinforcement distribution, and excellent flow characteristics are required for composite powders used in SLM processing, as evidenced by previous research [120, 121]. Moreover, studies have demonstrated that ball-milled composite powders show enhanced performance over directly mechanically mixed nanocomposite parts in terms of densification behavior [92]. However, to attain optimal results, variables such as the ball-to-powder ratio and ball-milling time require adjustment. These factors have a direct impact on the mechanical properties and relative density of SLM parts, thus being crucial for ensuring part quality. Table 4 is a list of common materials used in ball milling [23].

Table 4 displays the Ti-TiB₂ TMCs that were milled for varying durations, whereas Fig. 4 illustrates the shape of the milled Ti-TiB₂ powder combination. Images of the microstructure of Ti-TiB₂ composites after SLM treatment of the Ti-TiB₂ powder combination are shown in (Fig. 4c) 2h and (Fig. 4d) 4h, respectively. The Ti-TiB₂ powders from the 2 h of ball milling exhibited a nearly spherical shape because of the homogeneous dispersion of the TiB₂ powders in the titanium matrix and their nearly spherical morphology (Fig. 4c). After 4 h of grinding, the TiB₂ particles were not equally spread around the Ti powder particles and the Ti-TiB₂ powder particles exhibited irregular morphologies (Fig. 4d) [123]. As a result, it was determined that near-spherical powder mixes could be produced and that extending the grinding time would not improve the mechanical properties of Ti-TiB₂ [71]. The primary cause is that milling time alters the uniform distribution of particles, and as milling time increases, the spherical shape of the powder may transform into an irregular shape [119].

Different milling periods resulted in the formation of TiN/Ti₅Si₃, with nanocomposite powders generated in-situ through high-

Table 4
Common ball milling parameters for TMCs powders prepared by SLM.

Materials	Grain Particle Sizes (μm)	Rotation speed (rpm/min)	Blending time (h)	Ref.
Ti-5wt.%TiC	–	200	4	[84]
Ti-7.5 wt%TiC	–	200	4	[83]
Ti-2.5 wt%TiB ₂	–	–	5	[122]
Ti-5wt.%TiB ₂	–	200	1	[71]
Ti-5wt.%TiB ₂	–	200	2	[123]
			4	
Ti-2.5 wt%SiC	10	200	4	[124]
Ti-10 wt%Si ₃ N ₄	12.1	350	5	[125]
	12.1	350	10	
	12.1	350	15	
	12.1	350	20	
Ti6Al4V-0.5 wt%B ₄ C	30.4	200	3	[107]
Ti6Al4V-2wt.%Gr	26.16	300	0	[72]
	29.04	300	5	
	30.10	300	10	
	32.80	300	20	
Ti6Al4V-1wt.%MWCNTs	–	300	2	[126]
	–	300	4	
	–	300	6	

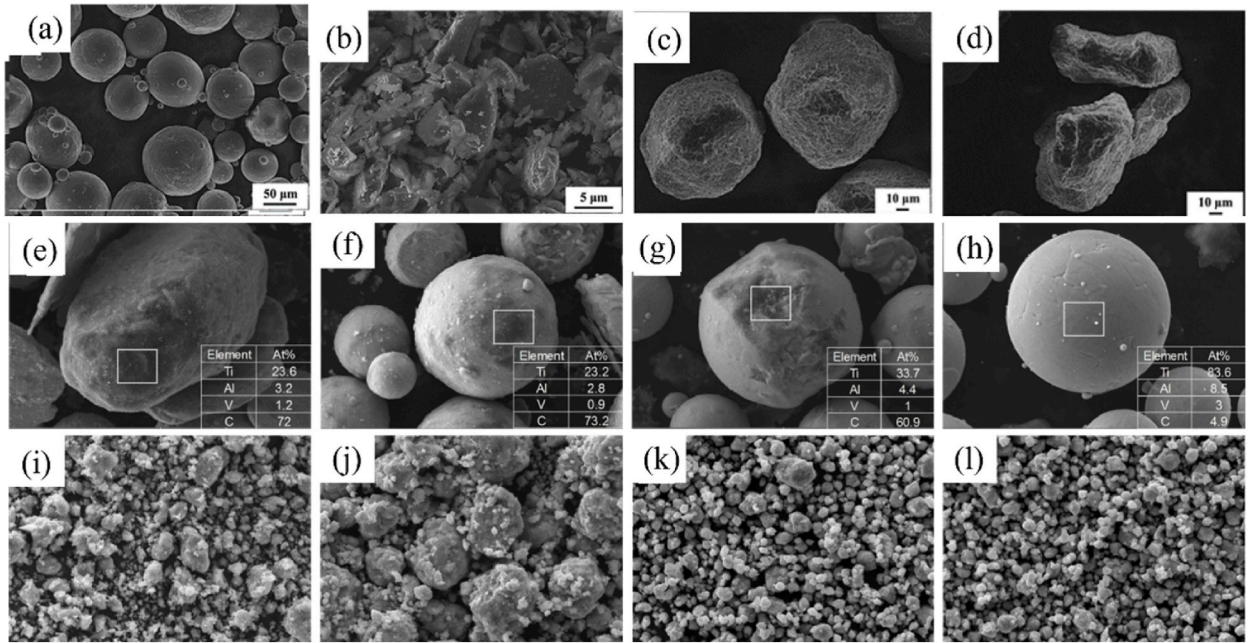


Fig. 4. The particle shape of the starting (a) CP-Ti and (b) TiB₂ powder, and the Ti-TiB₂ powder mixture milled for (c) 2 h and (d) 4 h [123], the graphene powder-TC₄ powder mixture milled for (e) 0 h; (f) 5 h; (g) 10 h; (h) 20 h [123], the Si₃N₄-Ti powder mixture milled for (i) 5 h; (j) 10 h; (k) 15 h; (l) 20 h [125].

energy mechanical alloying of Ti and Si₃N₄ powders. The powders' constituent phases and microstructural properties varied depending on the milling periods (Fig. 4i - l). Fine particles are formed by continuously breaking the powdered powder. Pre-refining, coarsening, and refining were the three stages in which the structure of the TiN/Ti₅Si₃ composite powders changed as the ball milling time increased. The Ti₅Si₃ and TiN phases in-situ usually display a coherent interfacial structure with grain sizes ≤15 nm [125].

The effects of different grinding times on TMCs and graphite are shown in Fig. 4e-h. Due to the strong van der Waals interaction between the nanosheets and the high-density difference between graphite and the metal matrix, graphite tends to agglomerate and not fully attach to the substrate powder [72]. The ball milling procedure can disperse the graphite clusters, but it can also lessen the matrix powder's sphericity, which could have an impact on the composite powder's flowability [127]. To ensure optimal performance during SLM processing, it is crucial to adjust the ball milling parameters to attain a uniform distribution of graphite within the TMCs

Table 5

A summary of the microstructural traits of the several TMCs made using SLM.

Material	Microstructural features and remarks	Ref.
Ti	The Ti parts underwent a successive change as the applied scan speeds increased: relatively coarse lath-shaped α→refined needle-shaped martensitic α'→ further refined zigzag-structured martensitic α'.	[130]
Ti-TiC	The TiC exhibited two typical morphologies: nanoscale lamellar and submicron stripe structures, and showed a uniform network distribution.	[76]
Ti-TiB ₂	Both Ti and TiB ₂ react chemically with each other, resulting in the formation of Ti-TiB composites.	[98]
Ti-B ₄ C	The reinforced B ₄ C particles react with CP-Ti to form prismatic TiB, whisker-like TiB, and granular TiC.	[131]
Ti-Si ₃ N ₄	The in-situ synthesis reaction 9Ti + Si ₃ N ₄ = 4TiN + Ti ₅ Si ₃ . The in-situ TiN reinforcing phase had a refined granular morphology and uniform distribution.	[132]
Ti-SiC	The uniformly dispersed TiC reinforcing phase has a unique network distribution and submicron dendritic morphology.	[105]
Ti-GNPs	TiC particles were formed in the SLM GNPs/Ti.	[133]
Ti6Al4V	The higher the temperature, the more metastable the fine acicular is in the reheating cycle. The fine acicular martensite changes completely to a Widmannstetter structure.	[134]
Ti6Al4V-TiB ₂	The distribution of TiB whisker clusters in primary β-Ti grains is not consistent with a complete dissolution mechanism.	[135]
Ti6Al4V-TiC	Unique nanoscale lamellar and acicular eutectic TiC reinforcement phases.	[103]
Ti6Al4V-LaB ₆	TiB and La ₂ O ₃ with particle-like shapes formed uniformly after the in-situ reaction.	[136]
Ti ₆ Al ₇ Nb-TiB ₂	in situ formation of fine TiB phase.	[64]
Ti6Al4V-Cr	The increase in Cr content increases the amount of β-phase.	[137]
Ti6Al4V-Gr	The composites were mainly composed of α, α' martensite, and α+β structures, TiC was formed.	[138]
Ti6Al4V/ MWCNTs	TiC _x is formed via an in-situ reaction.	[38]
Rare-earth metals	-	[98, 101]

composite powder, while preserving adequate powder flowability.

The primary reason for these variations is that differences in milling time can significantly affect the morphology of powder materials, including their particle shape and size [125]. For instance, after 0 h of ball milling, Ti6Al4V matrix powder maintains its original spherical shape. However, after 5 h of ball milling, some fines are also seen, and the surface becomes rougher. Deformed particles also appear. The average particle size of the composite powder grows somewhat rather than decreases. There is considerably more surface roughening, more distorted particles developed, and the number of fines increases significantly when the ball milling time is extended to 10 h. When the ball milling duration is extended to 20 h, there is a significant increase in the quantity of flattened particles [72]. Additionally, the optimum nanocomposite powder for SLM processing was obtained by ball milling at 300 rpm for up to 4 h after studying the dispersion of multi-walled carbon nanotubes in the matrix powder [126]. In conclusion, various composite materials and mixes react and generate diverse results when subjected to varying ball milling times. The ideal powder mixture is almost spherical and has good mechanical qualities; lengthening the ball milling period has the opposite impact of what is desired. Attar et al. (2017) mixed commercially pure titanium (CP-Ti) with TiB₂ powder and milled them for 2 h and 4 h, respectively. The maximum tensile strength values were 1421 MPa and 883 MPa respectively, and the compressive strain decreased from 17.8 % to 5.5 % [123].

3.2. Influence of the reinforcements

Key microstructural features such as particle distribution, particle-matrix interface, grain size, and phase composition significantly influence mechanical properties [55,128]. Uniform particle distribution enhances strength and ductility, while a strong particle-matrix bond ensures effective load transfer. Grain refinement and preferred grain orientation can affect strength and anisotropy, respectively [24]. Additionally, the secondary phase can impact hardness, toughness, and wear resistance. To optimize mechanical properties and microstructure, careful selection of reinforcement type and volume fraction is essential [25]. Ceramic particles like TiC or SiC are commonly used for their stability and compatibility with the matrix. Typically, a volume fraction of 10–30 % balances strength and ductility. Processing parameters, including laser power and scan speed in SLM, should be optimized to control microstructure evolution [51]. Post-processing treatments can further enhance properties. Experimental validation through techniques like SEM and mechanical testing is necessary to refine and optimize the composite design [129]. Table 5 summarizes the different microstructures formed by various types of reinforcement.

A distinct microstructure will arise from the variations in matrix and reinforcing materials [69]. The selection of these combinations influences the materials' chemical characteristics and performance in addition to their physical characteristics [55]. The microstructure of composites is significantly impacted by the volume proportion of reinforcement, as has been thoroughly investigated and documented in the pertinent literature [124]. Table 6 provides a summary of the impact of varying reinforcement volume percentages on the composite microstructure.

Two primary factors led to this development. First, the effective crystallinity of the TiC nuclei is severely limited by the lack of time for grain formation, which preserves the beneficial nanoscale structure of the TiC reinforcement phase (Fig. 6a and b). Second, Marangoni convection in the pool is the source of the liquid capillary force [141]. Homogenizes the dispersion of the nanoscale TiC reinforcement in the finally formed matrix by acting on the precipitated TiC and speeding its rearrangement in the melt (Fig. 5a and b) [83]. In thermal convection, circular velocity patterns refer to the ring-like flow within a melt caused by temperature gradients and density differences [142]. These include Marangoni convection, which arises from surface tension gradients, creating a ring-shaped flow that enhances mixing and material transfer around the heat source [143]. Temperature gradient convection, driven by thermal differences, results in circular flow from hot regions near the heat source to cooler areas, forming multiple ring-shaped patterns. These circular velocity patterns significantly influence the formation of cellular structures by enhancing uniformity and promoting cellular development, thereby determining the microstructure and properties of the final material [115]. Thus, the creation of the cellular structures was determined by circular thermal convection [31].

In the micrometer range, ceramic particles like SiC [144], TiB [145], and WC [146] are frequently utilized for traditional particle-reinforced TMCs. These particles range in size from a few microns to tens of microns. During typical processing, these very large ceramic reinforcing particles either remain partially fused or unfused [50]. Unfortunately, the restricted wettability of ceramics and metals hinders the interfacial interaction between the ceramic particles and the metal matrix, particularly when bigger ceramic particles are utilized. TMCs may fail early because of fractures in the weak ceramic/metal contacts under mechanical stress [49].

A high relative density (>95 %) from the TMCs is needed [147]. However, due to strong van der Waals interactions, uncontrolled

Table 6
Effect of varied volume fractions of reinforcement on the organizational structure of composites.

Material	Microstructural features and remarks	Ref.
Ti-TiC	nanoscale lamellar shape Ti (TiC 7.5 wt%) → nanoscale lamellar shape (TiC 12.5 wt%) → coarsened, feathery (TiC 17.5 wt%) → different dendritic morphology (22.5 wt%)	[83]
Ti-TiB ₂	phase of α' -Ti (0 wt%) → the mixed phases of α' -Ti, TiB and TiB ₂ (7.5 wt%)	[122]
Ti-B ₄ C	a lath-shaped structure (0 wt%) → a dendritic structure (1 wt%) → a cellular + dendritic structure (2–5 wt%)	[31]
Ti-SiC	acicular α -Ti forms a basketweave structure (0 wt%) → similar columnar structure (2.5 wt%) → columnar grain structure disappears, a network architecture (5 wt%).	[124]
Ti6Al4V-TiB ₂	a quasi-continuous distribution (2 vol % TiB) → full-continuous distribution (5 vol % TiB)	[139]
Ti6Al4V-TiC	α grains and longitudinal-sectional β columnar grains (0.5 wt% SiC) → equiaxed grains (1 wt% SiC)	[140]

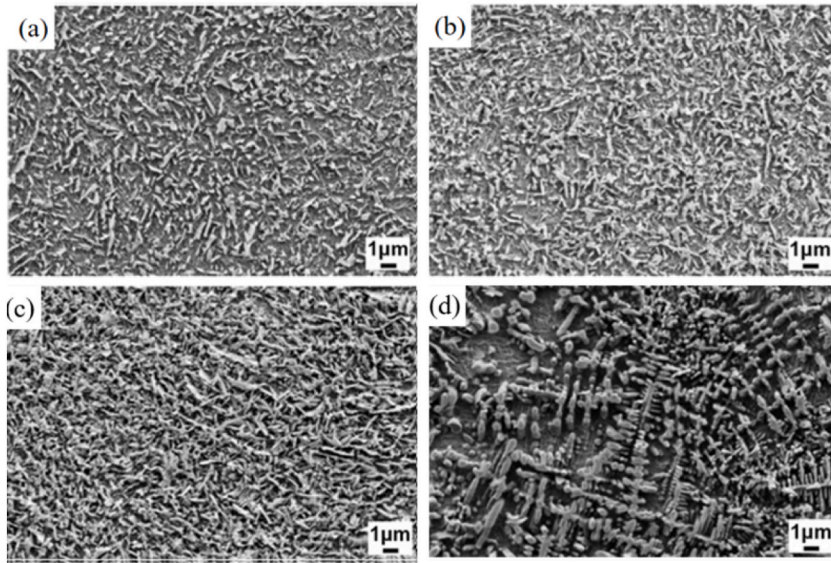


Fig. 5. The state of dispersion of reinforcing components in TiC/Ti nanocomposite parts with different TiC concentrations subjected to SLM processing. (a) 7.5 wt%, (b) 12.5 wt%, (c) 17.5 wt%, (d) 22.5 wt% [83].

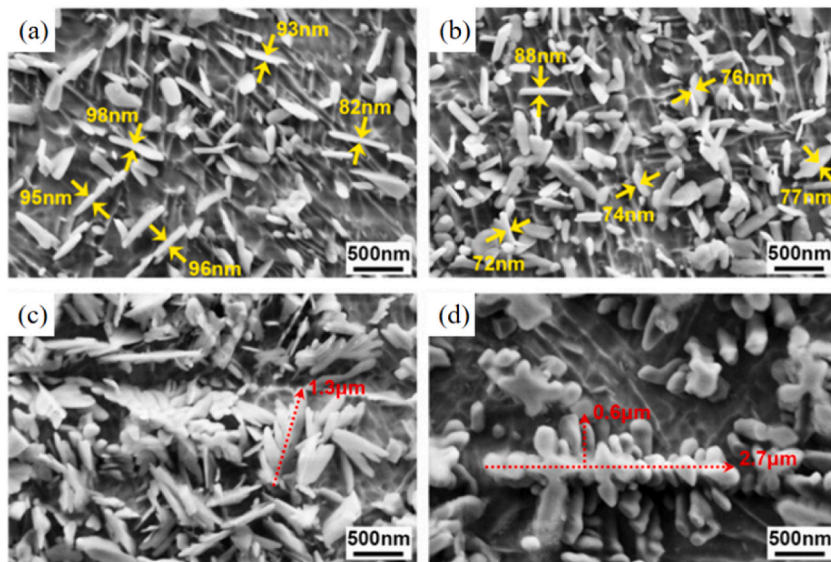


Fig. 6. Typical growth morphology of TiC reinforced material in TiC/Ti parts processed by SLM. (a) 7.5 wt%, (b) 12.5 wt%, (c) 17.5 wt%, (d) 22.5 wt% TiC [83].

aggregation of nanoparticles in bulk portions of ultrafine nanoparticle powders can lead to structural abnormalities or even loss of the original nanoparticle structure [55]. To ensure uniform distribution throughout the matrix and meet higher microstructure standards, nanoceramic reinforcing particles must avoid grain coarsening during processing [84]. Higher microstructure standards refer to the stringent requirements set to optimize the microstructural characteristics and uniformity of these components within composite materials. These standards specifically aim to achieve a uniform grain size distribution, which is essential for maintaining the desired mechanical performance and properties. Inconsistencies in grain size can lead to material performance inhomogeneities [50,55]. Additionally, minimizing grain growth is crucial, as controlling grain growth during processing helps prevent grain coarsening, which can reduce the material’s strength and performance. To adhere to these higher microstructure standards and prevent grain coarsening, specific measures such as selecting appropriate reinforcement particle sizes, optimizing ball milling time, and fine-tuning process parameters can be implemented [140,148].

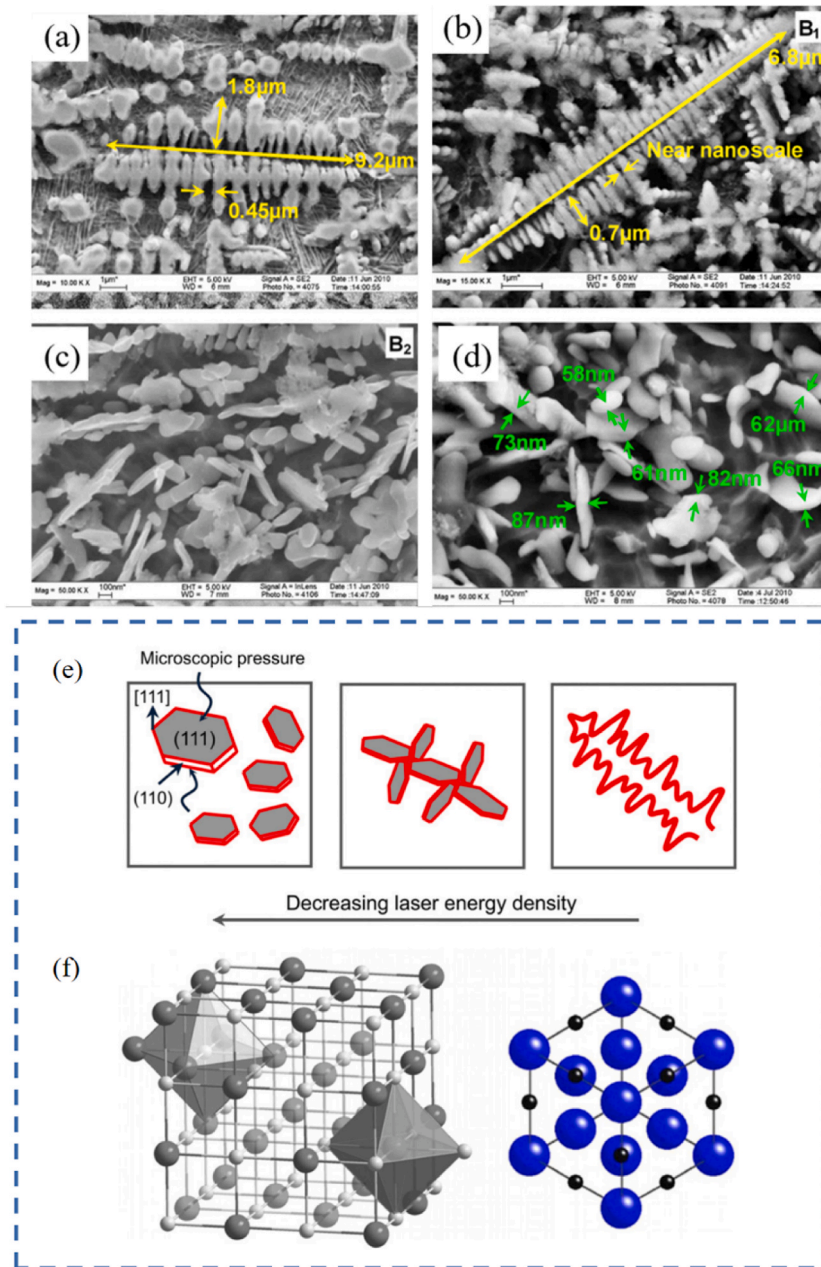


Fig. 7. The characteristic morphologies of TiC reinforcement at different energy densities (a) $E_d = 360 \text{ J/mm}^3$, (b, c) $E_d = 180 \text{ J/mm}^3$, (d) $E_d = 120 \text{ J/mm}^3$, (e) Schematic of microstructural developments of TiC, (f) Crystal structure of TiC and projection of Ti-C atoms along $[109]$ direction [84].

3.3. Influence of the SLM parameters

Numerous studies have demonstrated that the parameters of the particle addition process have a substantial effect on the formation of reinforced phase microstructures. Lower energy densities lead to the formation of nanoscale punctate or sheet-like structures (Fig. 7d) [84,149], whereas higher energy densities induce the reinforced phase to coarsen (Fig. 7a, b, c). For example, during the SLM process used to produce TiC/Ti composites, energy density significantly influences the shape of TiC particles. As the energy density drops, coarse columnar crystals transition to mixed forms with dendritic layers, and then to uniformly distributed TiC layers [76].

Furthermore, other research has indicated that a major aspect of defining the material properties of TiC/Ti nanocomposites is their nanoscale layered structure. Process optimization has produced dense TiC/Ti6Al4V composites with typical coarse columnar grains and ultrafine layered $\alpha+\beta$ microstructures dispersed internally. The needle-shaped nanoscale TiC present in the sub-columnar crystals effectively alters the microstructure and fine-tunes the matrix grain [104]. The issue of coarse columnar grains can be solved by

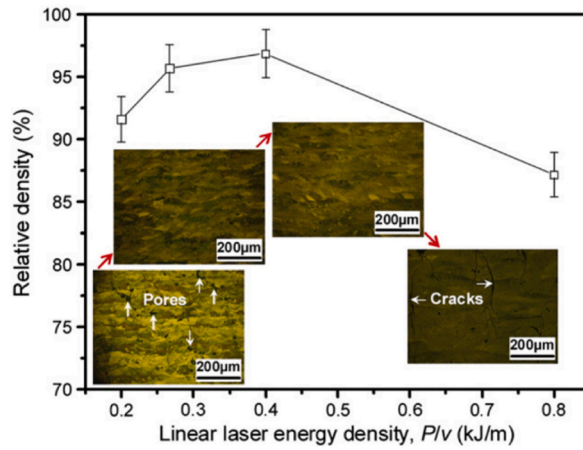


Fig. 8. The relationship between relative density and energy density of in-situ TiC/Ti₅Si₃ composites [105].

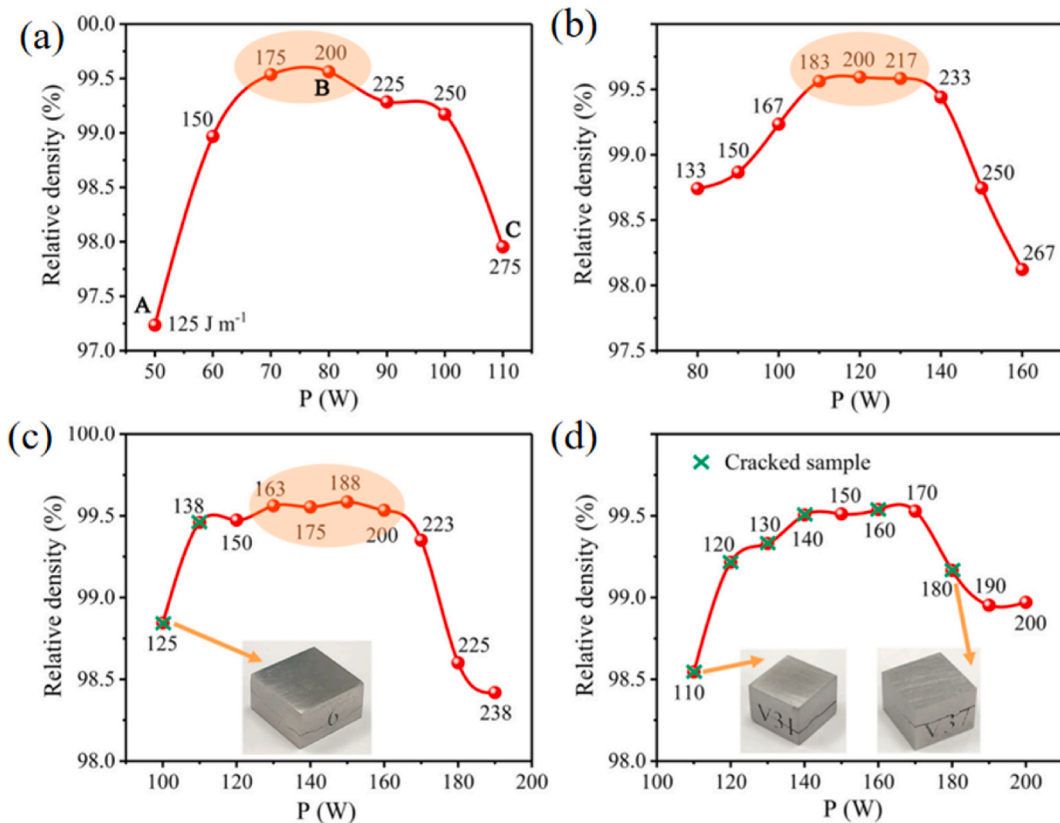


Fig. 9. Relationship between laser power and relative density for TMCs manufactured at different scanning rates (a) 400 mm/s, (b) 600 mm/s, (c) 800 mm/s, (d) 1000 mm/s; The insets in (c) and (d) display images of cracked samples [139].

adjusting the amount of reinforcing agent and improving the process parameters to create ultra-high strength TMCs with near-equiaxed grain shapes and nanoscale composition without fracture [125]. In summary, the development of reinforced phase microstructures is largely determined by the particle addition process parameters, with important consequences for material performance and application.

Studies have indicated that process parameters can play a crucial role in the mechanical properties and microstructure of composite materials. Improved strengthening mechanisms have been achieved, for instance, when Ti-based nanocomposites have been created and reinforced with TiB_w or TiC_p ceramic particles [107,150]. B₄C/Ti6Al4V composite produced by SLM increased Vickers microhardness by up to 45 % and compressive strength by 26 % [89]. Examined the use of SLM in the in-situ TiB₂/Ti6Al4V composites'

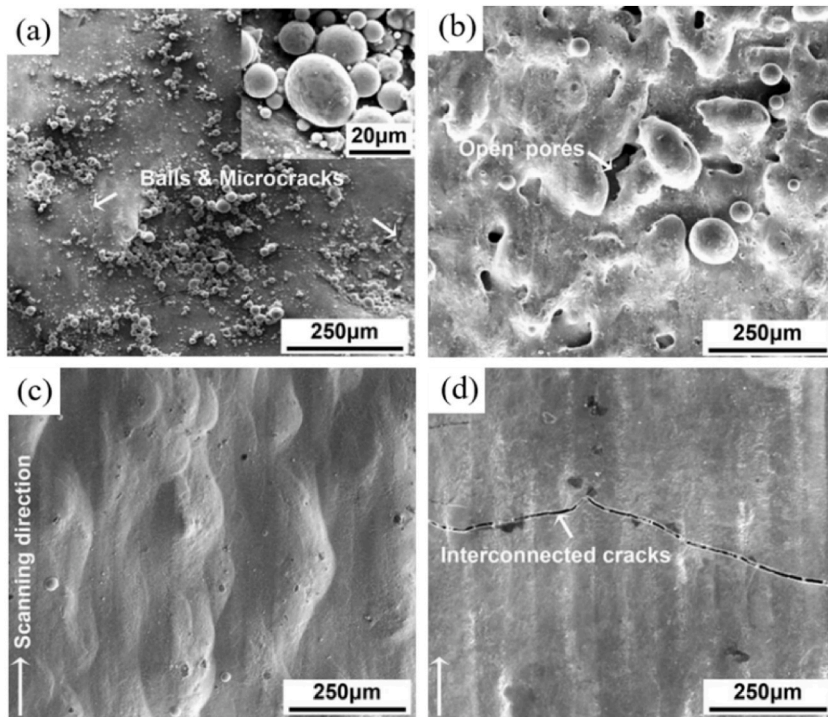


Fig. 10. Influence of powder scanning speeds on porosity (a) $v = 0.4$ m/s, $g = 2.5$ kJ/m, (b) $v = 0.3$ m/s, $g = 3.33$ kJ/m, (c) $v = 0.2$ m/s, $g = 5$ kJ/m, (d) $v = 0.1$ m/s, $g = 10$ kJ/m [81].

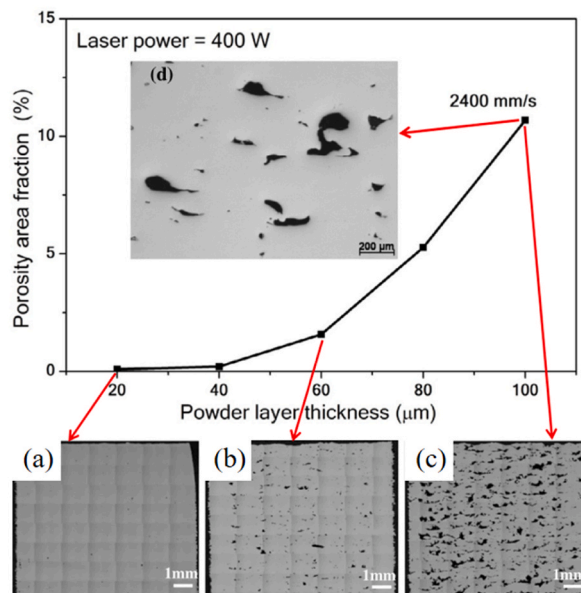


Fig. 11. Influence of powder layer thickness on porosity [155].

manufacturing, discovering parallel ribbon-like structures with sections that are TiB-rich and TiB-poor [149,151]. SLM has also been successfully used to create carbon nanotube-reinforced composites, which have relative densities of more than 99 % [152].

SLM has demonstrated potential in creating pure titanium powder and CrB₂ to create high-performance, tailored composite materials. However, when the relative density grows with increasing laser energy density, further work is required to improve the mechanical characteristics of these materials and optimize process parameters [153].

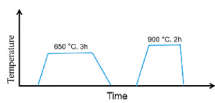
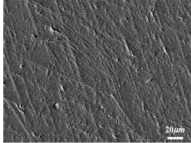
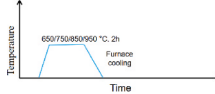
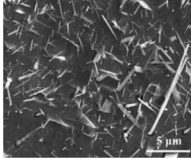
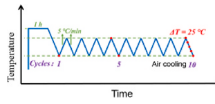
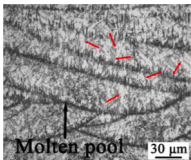
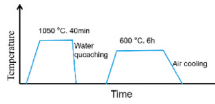
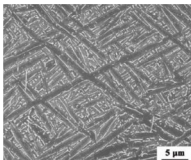
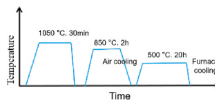
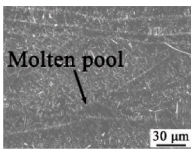
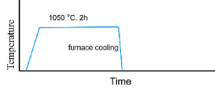
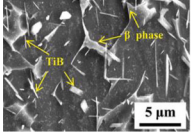
Components produced with the same energy density but various printing conditions might have varying degrees of porosity.

Researchers investigated Ti6Al4V and B₄C titanium-based nanocomposites with the same E_d but distinct printing conditions and discovered that the spheroidization effect and microcracks varied, and there were notable variations in the relative densities among the samples (Fig. 8) [107]. This implies that, within some parameter ranges, E_d is unable to effectively depict the link between print parameters and component melt pool shape. This indicates that there are still important variables that affect these fundamental constituents and that the effects of laser power, scan distance, and scan speed on melt pool shape are not the same. Incomplete melting of the powder material due to low laser power might result in flaws and a weaker printed object. Conversely, thermal stress and material deformation might result from high laser power's excessive heat generation (Fig. 9) [139].

Relevant research in the field of SLM technology indicates that individual process parameters, including laser power, scanning speed, powder layer thickness, and scanning spacing, are insufficient for evaluating the overall quality of produced titanium-based composite materials [53]. Therefore, for efficient and effective manufacturing, a more comprehensive strategy that considers numerous interdependent aspects is needed. According to reports, a scanning speed range of 100–400 mm/s is ideal for the SLM of titanium (Ti) and Ti-based metal composites. Speeds exceeding or falling below this range can lead to a decline in the composite material's performance (Fig. 10) [154]. This range is not without exceptions. The final product may also be affected by additional factors like the powder ratio and energy density (E_d) [106,149].

Another important factor in the material's creation during SLM is the thickness of the powder layer. A thinner powder layer results in higher energy density per unit volume, causing the powder to melt completely and improving surface quality. On the other hand, more unmelted powder particles and a lower density of the generated product are produced by a thicker powder layer because it has a lower energy density per unit volume (Fig. 11) [155].

Table 7
Current relevant literature on heat treatment of SLM titanium composites.

Material	Process	Microstructure	Ref.
Ti6Al4V			[165]
Ti6Al4V-TiB			[163]
Ti6Al4V-TiB			[168]
Ti6Al4V-TiB			[169]
Ti6Al4V-TiB			[170]
Ti6Al4V-B ₄ C			[171]

The size, stability, and behavior of the melt pool significantly impact the porosity of the final product. A larger melt pool may lead to increased porosity if it cools too quickly, trapping gas bubbles within the solidifying material. Stability is crucial because an unstable melt pool can cause turbulence, leading to irregular solidification and the formation of pores. The behavior of the melt pool, including its flow dynamics, influences the uniformity of material fusion; inadequate flow can result in a lack of fusion defects, while excessive penetration can cause keyhole porosity. These defects are intrinsically linked to the dynamics of the melt pool, affecting the overall porosity and quality of the final product [156,157]. Thus, it can be concluded that laser power and scan speed have the greatest effects on porosity [154]. Process variables can also have an impact on surface roughness. Higher scanning speeds can lead to Plateau-Rayleigh instability, which elongates melt pools and provides rougher surfaces, while lower energy densities can contribute to balling phenomena [158,159]. A crucial component is the SLM scan spacing, which is the distance between laser scans during each layer of laser scanning. The laser scan spacing significantly affects the surface quality of the product. However, there is currently limited research available in the literature [160,161].

In summary, these results suggest that optimizing process parameters for the SLM of titanium-based composite materials necessitates a holistic approach. Achieving high-density, low-porosity, and smooth-surfaced products requires considering a combination of factors, including powder layer thickness, laser power, scanning speed, energy density, and powder ratio. For instance, Du et al. (2021) employed a combination of machine learning, mechanical modeling, and experimental data to mitigate common defects and improve the mechanical properties of materials [162].

3.4. Influence of heat treatment

In recent years, extensive research has focused on the globularization of the α phase in SLM-processed Ti6Al4V alloy using heat treatments to enhance the mechanical properties and microstructure of the alloy [163,164]. The annealing temperature (800 °C–900 °C) was below but close to β transition temperature for Ti6Al4V. Lamellar and bimodal microstructures are the two main types found in conventionally treated Ti6Al4V. It is composed of interlayer β regions and alternating α layers [165]. After β homogenization (1080 °C, 0.5 h), the equiaxed α_p and β_t bimodal microstructure, which is a finely layered $\alpha+\beta$ combination, is renowned for having a favorable balance between strength and ductility [166]. When annealing above the β transus temperature (~ 1000 °C), it can result in age hardening and embrittlement, significantly increasing β grain size [167].

For SLM-processed TMCs, only a limited number of works on subsequent heat treatment have been reported. Table 7 summarizes

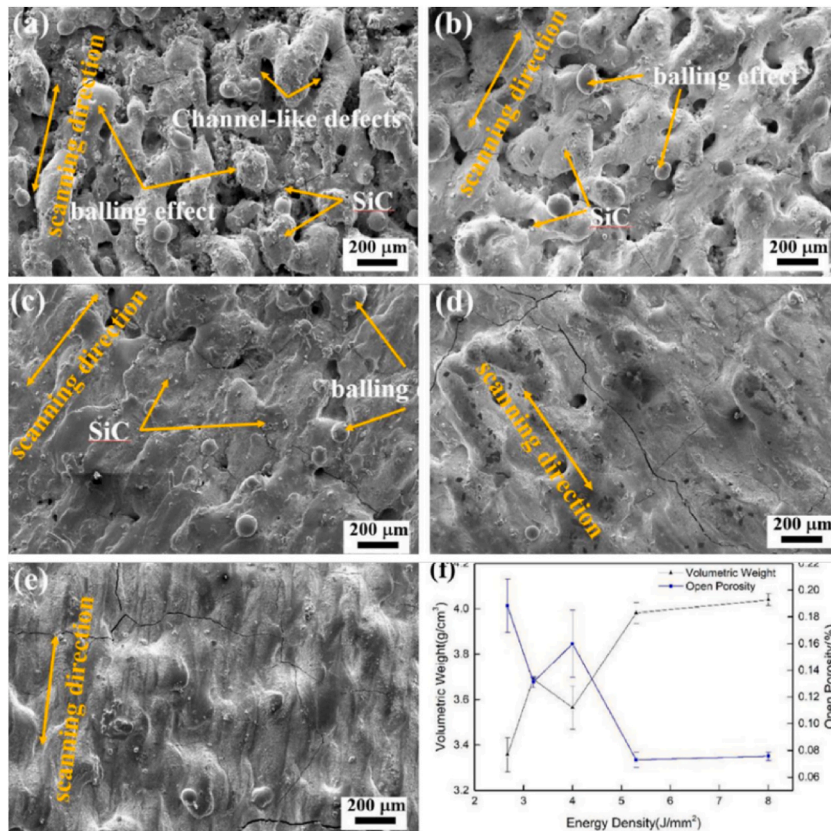


Fig. 12. Surface patterns of laser sintered samples at different scanning speeds (a) 320 W, 1200 mm/s, (b) 320 W, 1000 mm/s, (c) 320 W, 800 mm/s, (d) 320 W, 600 mm/s, (e) 320 W, 400 mm/s and (f) density and exposed porosity of multiple samples [183].

recent literature on SLM TMCs Researchers successfully adjusted the mechanical and microstructural properties of Ti6Al4V-TiB composites by chilling the samples in a furnace at varied temperatures.

The literature summarized in Table 7 reveals that several researchers have conducted in-depth studies on the microstructure of titanium-based composites produced by SLM and the impact of heat treatment on their properties. After aging and solubilization treatments, the microstructure of Ti6Al4V-TiB composites generated by SLM remained primarily lamellar α [169]. On the other hand, SLM-processed Ti6Al4V-5vol. %TiB composites that underwent air cooling following isothermal annealing developed a bilayer microstructure at 800 °C and 900 °C [163,171]. Moreover, these additional nucleation sites may facilitate the formation of globular α -phase at 950 °C and 1050 °C [163,171]. The creation of the bimodal microstructure β_t was hindered by the sluggish cooling of the furnace, which caused α_p to grow at the expense of parent β . Therefore, adequate rapid cooling is essential for the complete solidification process before final cooling, rather than solely depending on the nucleation effect of TiB [168,170]. To the best of our knowledge, there have been no reports of the formation of a bimodal microstructure in SLM-processed Ti-based composites [163,171].

Additionally, the high cooling rates inherent in the SLM process can result in a high level of residual stress within the components, leading to non-equilibrium and highly textured microstructures. This significantly reduces the machinability and mechanical properties of the components. In general, slower cooling rates are preferable. For instance, Zhou et al. (2022) designed a cooling scheme at 1 K/min. The cyclic thermal treatment (CTT) technique can effectively produce a bimodal microstructure in Ti6Al4V-5vol. %TiB composites produced by SLM. The CTT process involving thermal cycling between 875 and 975 °C resulted in significant changes in the proportions of α and β phases. Prior annealing of the β region at 1050 °C for 1 h was performed to facilitate liberalizations. The CTT-treated sample showed increased plasticity (12.3 %–27.3 %) with a slight reduction in yield strength (from 1743 MPa to 1392 MPa), making it suitable for structural applications [168].

These investigations illustrate that heat treatment methods, such as solid solution treatment and cyclic thermal processing,

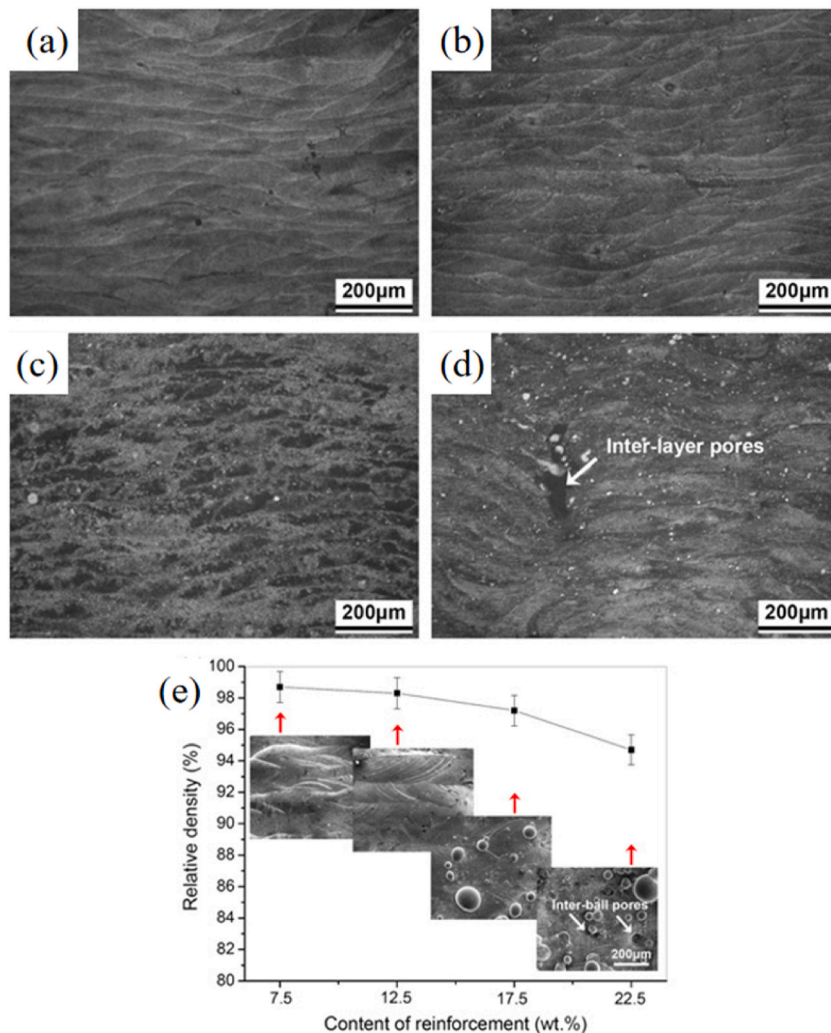


Fig. 13. The microstructure of TiC/Ti components subjected to SLM processing with (a) 7.5 wt%, (b) 12.5 wt%, (c) 17.5 wt%, (d) 22.5 wt%, (e) surface morphologies and densification rates of SLM parts containing TiC [83].

substantially influence the mechanical properties and microstructure of composite materials. These findings are pivotal in the development of heat treatment strategies designed to optimize the properties of composite materials for diverse applications [48]. In summary, heat treatment, mechanical milling, reinforcing phases, and SLM parameters each play a multifaceted role in shaping the microstructure of SLM-printed titanium matrix composites (TMCs). Mechanical milling improves powder distribution, hardness, and interfacial bonding. The distribution and characteristics of reinforcing phases significantly influence mechanical behavior. SLM parameters, including layer thickness and laser power, affect grain size and composite density. Heat treatment modifies the crystal structure and phase composition, thereby enhancing mechanical properties by mitigating residual stresses. Assessing and optimizing these variables is essential for improving the overall performance and quality of SLM-printed TMCs.

4. Defects

SLM is a highly effective technique for fabricating complex and precisely accurate titanium-based composite materials [49]. During the SLM process, the cooling conditions at the bottom of the melt pool predominantly occur within the columnar region of the grain refinement diagram. These conditions frequently result in grain elongation along the grain direction [172]. However, defects in the fabricated components are prevalent due to the sensitivity of titanium-based composites and the non-equilibrium solidification characteristics inherent to additive manufacturing [173]. Drawing from a recent review of the literature, this section aims to provide a comprehensive examination of the microstructural properties of titanium-based composites produced by SLM. This research considers several phenomena, including balling, the presence of small porosity defects, and cracking in the printed components.

4.1. Balling

Balling is a common problem with SLM metal components. The surface quality and densification of components are significantly affected by balling [174,175]. The formation of spherical aggregates on the surface of SLM metal components is referred to as balling [176,177]. Metal powder absorbs energy and rapidly melts when a high-intensity laser beam passes over it. The powder then shrinks into discontinuous spherical particles due to surface tension, gravity, and surrounding media, a process known as balling [49]. SLM spheres are divided into two categories: a larger, predominantly elliptical type with a diameter of 500 μm and a smaller, predominantly spherical type with a diameter of 10 μm . Poor wettability leads to the development of the first type of balling particle, which causes more severe balling in SLM; the second type of balling particle has no discernible effect on SLM sample performance [175]. The majority of research today is focused on the management of balling particles from an SLM processing standpoint, for example by modifying process parameters. It is thought that changing the process parameters may affect surface tension and flow stability, which in turn may alter the balling phenomenon [178]. For example, balling is severe when the energy density is below the optimum range. Balling improves as the energy density increases. The sample aperture shrinks but the surface roughness increases above the optimum range [179,180].

Changes in surface tension and viscosity have little effect on balling, whereas process parameters have a large effect on balling. In addition, process variables have a greater influence on SLM metal processes than material properties [181]. The smooth and dense

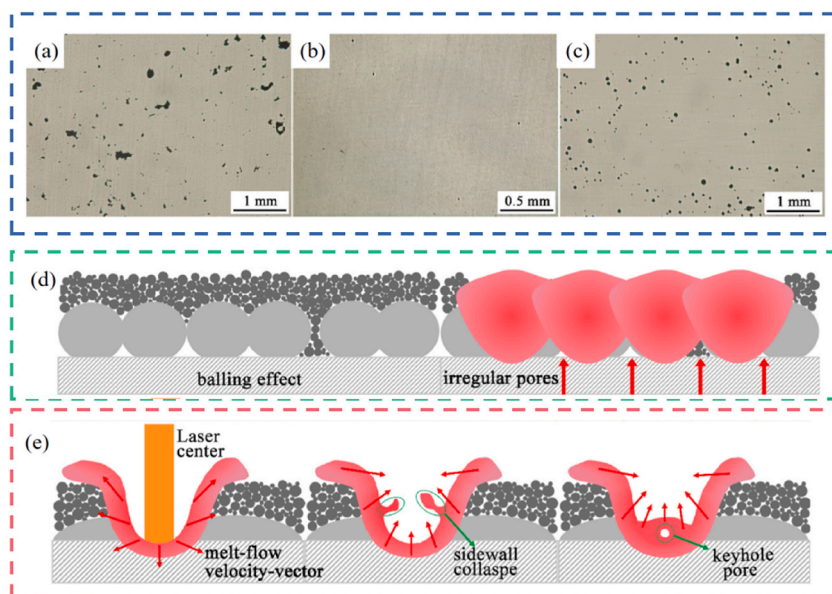


Fig. 14. The micropores in various TMCs samples (a) Ti6Al4V, (b) Ti6Al4V -TiB (2 vol %), (c) Ti6Al4V -TiB (5 vol %) as examples; schematic illustration of pore formation (d) irregular holes, (e) keyhole pores [139].

surface formed under relatively low scanning speeds (v) and the resulting high energy densities (E_d). At low E_d and higher v , large-sized balls appeared (Fig. 12b). This is mainly due to the extreme instability of the melt, caused by high melt viscosity at a comparatively low energy density. This causes balling, which reduces surface quality and densification behavior [182]. Meanwhile, increasing v tends to increase the local instability of the melt. To reach a balanced state, the unstable liquid paths split into several globular clusters. These results are comparable to those studied by Chen et al. (2020). The temperature of the melt pool is comparatively low due to the limited energy input (Fig. 12a–c). The trajectory of the molten material breaks and accumulates instead of spreading when the surface tension is high. The molten material builds up to form a rough surface with uneven pores and a balling phenomenon. The balling diminishes and the surface of the sample becomes smooth (Fig. 12d–f) [183].

The balling phenomenon is significantly influenced by the physical properties of the particles (Fig. 13a and b). Cross-sections of SLM components with 7.5 wt% and 12.5 wt% TiC shows a homogeneous microstructure consisting of metallurgical bonding layers without any layer porosity. As a result, the densification rate exceeds 98.3 % of the theoretical density. The cross-section shows a heterogeneous layered microstructure (Fig. 13c) with increasing TiC addition up to 17.5 wt%, and the SLM component density increases to 97.2 %. The balling effect in this case is responsible for the formation of several spheres on the surface with diameters ranging from 20 to 140 μm (Fig. 13e). A significant decrease in densification to 94.7 % occurs when the TiC addition is increased to 22.5 wt%. Layer porosity with diameters as small as 100 μm is seen in the cross-section (Fig. 13d) and ball clusters and interval pores form on the surface (Fig. 13e). The Marangoni force, which causes the TiC/Ti melt with higher TiC content to tend to flow radially inwards towards the center of the laser beam instead of spreading outwards at the lower surface, is the primary cause of this phenomenon (Fig. 13e) [83]. The other contributing factor is the limited rheological properties of the high melt viscosity resulting from the addition of high TiC content. Microstructure-reinforced TMCs show that defects such as balling can be influenced by particle size. At present, experiments are the principal method for observing balling phenomena, however, machine learning and finite element simulations are increasingly employed to predict balling defects [184]. For example, Raju et al. (2022) employed various machine learning algorithms to predict densification based on prior experimental results with different process parameters. Experimental validation demonstrated that the neural network-based model accurately predicted densification [157]. Ansari et al. (2022) developed a finite element model for SLM of AlSi10Mg to simulate and predict optimal processing parameters. The experimental results were consistent with the simulation predictions [185].

4.2. Porosity

A prevalent defect in all SLM components is porosity, which significantly affects their mechanical properties. Gases within the melt

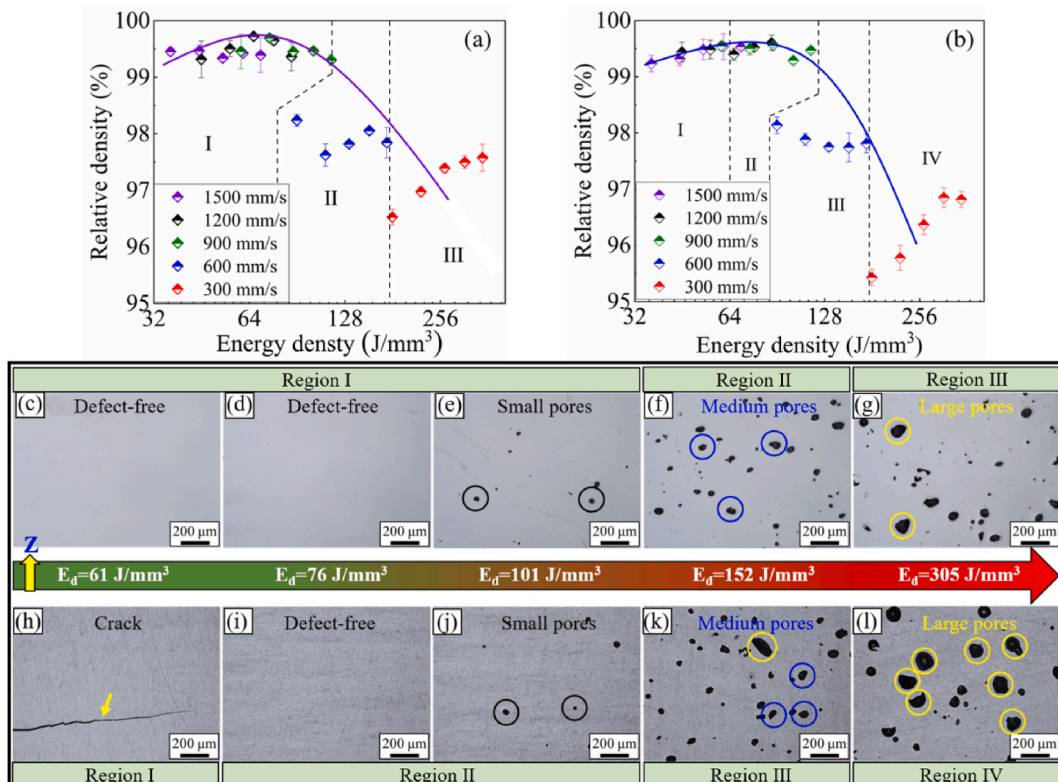


Fig. 15. Densification map: (a) SLM-ed Ti6Al4V; (b) SLM-ed 5%-TMCs. g: (c)–(g) SLM-ed Ti6Al4V; (h)–(l) SLM-ed TMCs [104].

pool play a critical role in the formation of porosity, particularly in TMCs that are easily vaporizable (Fig. 14d and e). Post-processing is generally less effective at reducing porosity compared to improving surface quality and addressing microstructural flaws [170]. Porosity in SLM components can be categorized into two types: metallurgical porosity, which results from the absorption of specific alloying elements (e.g., Mg) or ambient gases (e.g., N, O, or H) [43]; and parameter-based porosity, which primarily arises from process errors.

Fluid flow behavior studies have observed that as the surface temperature approaches the boiling point, the liquid is expelled from the center due to an exponential increase in back pressure perpendicular to the surface [66]. This phenomenon leads to the formation of a keyhole in the center of the melt. Multiple laser reflections within the keyhole accelerate the metal's absorption of the laser, causing metal evaporation and gas formation at the bottom of the keyhole. During solidification, porosity defects result from gas entrapment in the molten pool as the keyhole collapses [186]. Generally, variations in porosity can also arise from different amounts of reinforcement (Fig. 14a, b, c) [139].

Most studies on reducing porosity in SLM materials have concentrated on process parameters, with a particular emphasis on energy density. The two most significant factors affecting porosity levels are laser scan speed and laser power. High laser energy increases the absorption rate of the metal to the laser. When there is an inconsistency in cooling rates between the interior and exterior of the molten pool, bubbles may become trapped inside, forming closed pores. High laser energy also increases vapor pressure and recoil pressure, which forces the molten pool liquid to flow downward, resulting in pore formation [24,55]. Adjusting these parameters can enhance the flowability of the melt pool. As the Marangoni effect becomes active, liquid flow in the melt pool intensifies, increasing the rate of gas escape and reducing porosity defects. High laser energy density and low scan speed can induce vaporization by causing the melt pool to contract [187].

For instance, when energy density was increased from 0.2 to 0.267 kJ/m³, the degree of densification improved from 91.6 % to 95.7 %, reaching a maximum of 96.9 % at a higher energy density of 0.4 kJ/m³. Conversely, applying a relatively high energy density of 0.8 kJ/m³ resulted in a dramatic decrease in densification to 87.2 %. At a low energy density of 0.2 kJ/m³, the cross-sectional microstructure revealed numerous small interlayer pores with an average size of approximately 20 μm. No visible pores or cracks were observed in the relatively dense SLM layer when the energy density was increased to ≥0.267 kJ/m³ [105]. Samples of Ti6Al4V-2.5B₄C-2.5BN produced at an energy density of 41.9 J/mm³ exhibited slight fusion porosity, whereas the Ti6Al4V-2.5B₄C-2.5BN composite produced at 31.5 J/mm³ showed a higher porosity rate in the microstructure [188].

At the same energy density, more severe pore defects were found in the III and IV regions of SLM TMCs compared to SLM Ti6Al4V as shown in Fig. 15. In addition, the relative density (RD) decreased with increasing E_d due to the introduction of larger holes (Fig. 15a and b). The failure of powder dispersion was driven by large surface protuberances that accumulated with increasing sample height under high heat input, as evidenced by the opposite trend when E_d exceeded 180 J/mm³ for both materials. All samples exhibit interlayer cracking in this location, even though the E_d is high above 65 J/mm³ [104].

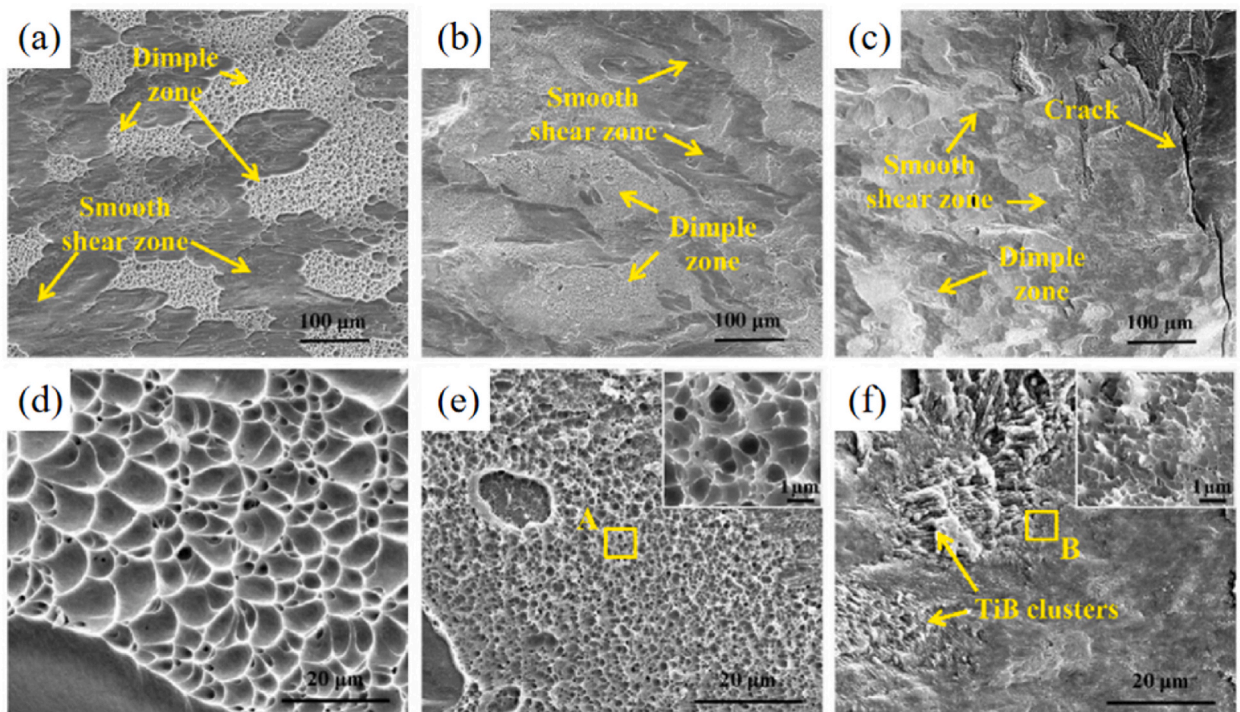


Fig. 16. The compressive samples' typical fracture surfaces at various magnifications (a, d) Ti6Al4V, (b, e) 0.5 wt% B₄C, (c, f) 1 wt% B₄C. At greater magnifications, the insets display intricate dimple morphologies [107].

As E_d increases, most samples in region II exhibit no cracks (Fig. 15i). Compared to SLM-ed Ti6Al4V synthesized under the same E_d conditions, a more severe drop in RD was observed in SLM-ed Ti6Al4V due to the presence of more severe pore defects in the III and IV regions of E_d TMCs (Fig. 15k and l). A work on TiC/Ti₅Si₃ produced by SLM revealed similar results [105].

Boron carbide (B₄C) particles are resistant to evaporation from the melt during the SLM process due to their extraordinarily high boiling point of 3500 °C. The formation of pores occurs because the liquid cannot effectively flow toward microscopic voids caused by the B₄C particles trapped in the melt. When the B₄C content is increased to 5 % by weight, there is a significant decrease in relative density, and macroscopic fissures emerge. Therefore, to improve the densification of (TiB + TiC)/Ti composites produced by SLM, it is essential to adjust the B₄C content [31].

4.3. Cracking

In addition, overheating and overcooling can occur due to the rapid melting and cooling of metal powders in SLM. This phenomenon is primarily caused by solidification shrinkage and internal tensions that develop during the SLM process [189]. Cracking is a major factor in material failure and notable performance deterioration [190,191].

The mechanism of thermal cracking can be attributed either to embrittlement, resulting from the inability of brittle hard phases to tolerate thermal stress, or to solidification deceleration, caused by the low melting point eutectic phase during rapid solidification, which weakens intergranular bonds. Similar to issues of spheroidization and porosity, optimizing critical process parameters is the most effective strategy for preventing cracking [43]. Similarly, The hydroxyapatite ratio was positively correlated with the increase in crack density, which increased from $1.5 \times 10^{-4} \mu\text{m}/\mu\text{m}^2$ to $2.7 \times 10^{-3} \mu\text{m}/\mu\text{m}^2$ [192]. The typical fracture surfaces of the Ti6Al4V and TMCs specimens were smooth shear surfaces and ductile indentations, as shown in Fig. 16. This indicates a mixed mode of brittle and ductile fracture. Larger dimple diameters generally indicate greater flexibility and resistance to local instability under the same fracture conditions [107].

By optimizing the SiC content and SLM process parameters, the production of in-situ Ti₅Si₃-reinforced titanium-based nanocomposites utilizing SLM resulted in considerable improvements in fracture propagation [124]. The densification rate is often reduced by the formation of spherical phenomena at low laser energy density combined with high scanning speed and by the generation of thermal cracks at excessive laser energy input [81].

Reducing the size of the ceramic particles can also significantly increase particle cracking [193]. Additional investigation has revealed that the addition of B in Ti6Al4V alloys tends to produce elongated needle-like TiB, whereas the addition of C produces large-sized TiC, which tends to fracture first when exposed to an external force [194]. As a result, altering the optimal process parameters and material composition design will address the cracking faults.

Since the powder exhibits a cyclic and unstable thermodynamic history, residual stresses inherently emerge during the melting and solidification in SLM due to the extraordinarily complex phase transition field. This has been one of the primary obstacles to the industrialization of SLM. In the SLM process, alloy components may undergo warping and cracking due to localized variations in thermoplastic properties, phase transformations, and microstructural inhomogeneity. These issues stem from the complex behavior of materials during high-temperature processing, including the development of thermal stresses, internal stresses resulting from phase changes, and heterogeneous microstructures. To mitigate these issues, it is imperative to optimize laser processing parameters, refine material formulations, and apply effective post-processing techniques to improve the overall performance and stability of the alloy components [109,195].

In summary, spherical stacking, pores, cracks, and residual stresses are frequently observed in TMCs fabricated via SLM. Excessive laser energy density leads to overheating, which impacts the microstructure by accelerating melting and material accumulation. Various conditions can cause pore defects, compromising material reliability. Due to rapid solidification, uneven shrinkage, and thermal stresses, cracking remains a prevalent issue. Rapid cooling generates residual stresses that undermine stability. Enhancing the microstructural integrity of TMCs necessitates careful control of temperature gradients, residual stresses, and material behavior during the SLM process.

5. Strengthening mechanisms

Titanium-based composites made using SLM have special qualities not present in materials made with other methods [70]. We can gain further insight into the mechanisms underlying the strengthening of these composites by examining the relationship between their overall characteristics and microstructure, as well as how their structures change [49]. Dislocation strengthening, load transfer

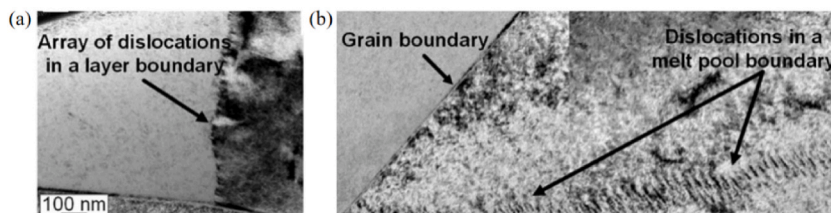


Fig. 17. (a) showing arrays of dislocations, (b) bright-field images of TiC/Ti6Al4V composites [138].

strengthening, Orowan strengthening, and fine grain strengthening owing to the Hall-Petch effect are the primary strengthening techniques used in titanium-based composites made by SLM [139]. This review intends to provide a comprehensive overview of SLM particle-reinforced metal matrix nanocomposites, focusing on the most recent research on their strengthening mechanisms [27].

5.1. Dislocation strengthening

The dislocation strengthening mechanism is crucial in the reinforcement of particle-reinforced titanium-based composites. The increased density of dislocations within the matrix results from localized plastic strain induced by the mismatch between the thermal expansion coefficients of the particles and the matrix [196]. The frequency of dislocation contacts during movement is increased due to the higher dislocation density, which impedes dislocation movement and prevents the matrix from continuously deforming plastically. As a result, the strength of the material increases. For example, in TiC/Ti6Al4V composites produced by SLM, high-density dislocations are close to the TiC/Ti contact [138]. Dislocation strengthening is observed in the graphene/matrix composite, with high dislocation density acting as an efficient strengthening mechanism. The increase in strength is caused by the coherent elastic strain transfer mechanism, which is described mathematically (Fig. 17a and b) [197–199].

$$\Delta\sigma_{CTE} = \sqrt{3}\beta Gb\sqrt{\rho_{CTE}} \quad (2)$$

$$\rho_{CTE} = \frac{B\Delta\alpha\Delta T\nu_p}{bd_p(1-\nu_p)} \quad (3)$$

Where β is the dislocation strengthening coefficient, G is the shear modulus of the Ti matrix and $\Delta\rho_{CTE}$ is the increase in strength (in MPa) due to dislocation strengthening. Where ρ_{CTE} is the dislocation density (4.3×10^4 MPa). The difference between the coefficients of thermal expansion of the matrix phase and the strengthening phase is denoted by $\Delta\alpha$ [200].

The purpose of this work is to investigate the effect of particle size and volume fraction on the strengthening stress of particle-reinforced metal matrix composites. The results show that a decrease in particle size and an increase in volume fraction cause more dislocations at the particle-metal matrix interface, which increases the strengthening stress [201,202]. On the other hand, for metal matrix composites supplemented with micron-sized particles, the strengthening stress induced by the change in thermal expansion coefficient at the interface position is quite minimal. In addition, particle agglomeration reduces the dislocation-induced strengthening stress, which reduces the yield strength of the composite. It is important to note that when subjected to external loading, uneven deformation occurs between the matrix and reinforcement phases due to their different elastic moduli. To maintain the coordination of the deformation, this non-uniform deformation creates a deformation gradient in the metal matrix, which induces the creation of geometrically necessary dislocations surrounding the reinforcement particles. The increase in strength of the composite material due to geometrically necessary dislocations can be represented as follows:

$$\Delta\sigma_{EM} = \sqrt{3}\alpha Gb\sqrt{\rho_{EM}} \quad (4)$$

Where α is a constant, usually taken as 0.5, ρ_{EM} is the dislocation density formed by a mismatch in elastic modulus, which can be expressed as [202].

$$\rho_{EM} = \frac{6\nu_p}{\pi d_p^2} \varepsilon \quad (5)$$

Where ε is strain, which is caused by work hardening.

5.2. Fine grain strengthening

An important element affecting the strength of titanium composites produced by SLM is the refinement of grain size by the addition of reinforcing particles. Grain growth can be inhibited by the aggregated particles acting as anchor points at grain boundaries. The Hall-Petch relationship states that finer reinforcing particles produce more internal grains and more tortuous grain boundaries. This makes them more effective at preventing dislocation motion, which causes dislocation pile-ups at grain boundaries and ultimately increases the strength and flexibility of the material. The yield strength in this case is represented by σ_y and the material constants are K_y and σ_0 . In addition, d represents the average grain size [196].

$$\sigma_y = \sigma_0 + \frac{K_y}{\sqrt{d}} \quad (6)$$

The size of the reinforcing phase affects the recrystallization and strength properties of laser-heated Ti-based composites. While larger reinforcing particles significantly increase recrystallization nucleation, smaller reinforcing particles can pin grain boundaries. While excessive B_4C inclusion can reduce the strength and ductility of Ti-based composites, TiC particles can minimize internal stresses in the Ti matrix and prevent grain formation [203]. Heterogeneous Si_4Ti_5 nucleation and TiC nanoparticles limit the formation of α (Al) grains in Al-Si-Mg-Ti/TiC materials produced by the SLM technique, thereby increasing tensile strength and elongation. TiB_2 particles can superimpose multiple strengthening mechanisms and increase the overall yield strength of the material when added to Ti-TiB composites [91,204].

5.3. Orowan strengthening

SLM process is capable of in-situ generation of small and dispersed reinforcing phases within the titanium matrix, effectively impeding dislocation movement, promoting dislocation pinning, and increasing the deformation resistance of the material. In SLM-formed particle-reinforced titanium-based composites, the addition of ceramic reinforcement is equivalent to the introduction of a large number of second-phase particles into a single base metal. The strengthening effect of non-deformable particles can be explained by the Orowan mechanism [17]. According to this mechanism, when a dislocation moves towards a hard-strength particle, it bypasses the particle and forms a dislocation loop near the particle. There is a relationship between the shear stress required for dislocation bypass and the distance between the disperse phase and the reinforcement particle [198,202].

$$\sigma_{Orowan} = M \frac{0.4G_m b}{\pi(1-\nu)^{\frac{1}{2}}} \frac{\ln\left(\frac{d}{b}\right)}{\lambda} \quad d = \sqrt{\frac{2}{3}}d \tag{7}$$

Table 8
Mechanical properties of particulate-reinforced TMCs fabricated by SLM.

Materials	E_d (J/mm ³)	E_r (GPa)	Wear rate (mm ³ /Nm)	HV (MPa)	Tensile strength (MPa)	σ_{us} (MPa)	σ_{ys} (MPa)	ϵ_f (%)	Ref.
CP-Ti	120	107	2.8×10^{-6}	261	757	582.39	499.05	19.5	[23, 31]
Ti-5wt.%TiC	142	–	–	–	914	–	–	18.3	
Ti-7.5 wt%TiC	120	–	2.6×10^{-7}	553	–	–	–	–	[76]
Ti-12.5 wt%TiC	120	–	2.3×10^{-7}	577	–	–	–	–	
Ti-15 wt%TiC	90–360	179–256	1.8×10^{-7} -7.0 $\times 10^{-7}$	487	–	–	–	–	
Ti-17.5 wt%TiC	120	–	3.75×10^{-7}	–	–	–	–	–	
Ti-22.5 wt%TiC	120	–	6.5×10^{-7}	412	–	–	–	–	
Ti-0wt.%TiB ₂	–	–	104.5×10^{-3}	258	–	–	–	–	[122]
Ti-2.5 wt%TiB ₂	40	–	91.26×10^{-3}	333	–	–	–	–	
Ti-5.0 wt%TiB ₂	–	–	82.51×10^{-3}	392	–	–	–	–	
Ti-7.5 wt%TiB ₂	–	–	70.76×10^{-3}	435	–	–	–	–	
Ti-5wt.%TiB ₂ (2 h milling)	–	–	–	–	779	–	–	–	[123]
Ti-5wt%TiB ₂ (4 h milling)	–	–	–	–	1103	–	–	–	
Ti-5wt.%TiB ₂	120–185	–	–	402	–	–	1103	–	[71]
Ti-1wt.%B ₄ C	–	127.69	–	275	–	945.99	761.77	26.37	[31]
Ti-2wt.%B ₄ C	49	114.42	–	320	–	834.14	744.66	4.75	
Ti-3wt.%B ₄ C	–	96.10	–	343	–	–	627.96	1.19	
Ti-5wt.%B ₄ C	–	–	–	424	–	–	–	0.56	
Ti-2wt.%CrB ₂	–	–	7.5×10^{-4} -13.3 $\times 10^{-4}$	320–380	–	–	–	–	[209]
Ti6Al4V-2.5 wt%SiC	400	–	1.42×10^{-4}	980.3	–	–	–	–	[105]
Ti6Al4V-1wt.%SiC	–	–	–	588	–	–	–	–	[124]
Ti6Al4V-2wt.%SiC	–	–	–	617	–	–	–	–	
Ti6Al4V-5wt.%SiC	–	231	–	706	–	–	2.39 GPa	–	
Ti-23.8 wt%SiC	80–320	–	1.42×10^{-4}	906–980	–	–	–	–	[105]
Ti-Si ₃ N ₄	167–666	–	6.84×10^{-5}	1083–1358	–	–	–	–	[48]
Ti-GNPs	–	–	–	503	–	–	–	–	[133]
Ti-AlN	70–140	–	–	919	–	–	–	–	[210]
Ti-2wt.%Re	80	–	–	956	961	–	956	1.0	[87]
Ti-4 wt.%Re	–	–	–	965	971	–	965	1.0	
Ti6Al4V-5vol. % TiC	152	–	–	–	1365.83	–	1257.40	1.27	[104]
Ti6Al4V-5vol. % TiC	101	–	–	–	1424.16	–	1284.29	1.47	
Ti6Al4V-5vol. % TiC	76	–	–	–	1538.98	–	1364.42	2.92	
Ti6Al4V-5vol. % TiC (850 °C)	–	–	–	–	–	1600	2230	18.8	[170]
Ti6Al4V -5vol. % TiC (900 °C)	104–187	–	–	–	–	1548	2211	20.7	
Ti6Al4V -5vol. % TiC (950 °C)	–	–	–	–	–	1486	2200	23	
Ti6Al4V -5vol. % TiC (975 °C)	–	–	–	–	–	1602	2176	17	
Ti6Al4V-5vol. %TiC furnace cooling (950 °C)	–	–	–	–	–	1395	2090	18.6	
Ti6Al4V -0.05 wt% B ₄ C	64.8	–	–	375.1	1225	–	–	14.17	[48,
Ti6Al4V -0.3 wt% B ₄ C	–	–	–	399.8	1207	–	–	7.71	151]
Ti6Al4V -0.5 wt% B ₄ C	–	–	–	410.1	1047	–	–	5.67	
Ti6Al4V -0wt.% Mo ₂ C	34.7	–	–	420.9	–	–	–	–	[62]
Ti6Al4V -1 wt.% Mo ₂ C	–	–	–	445.1	1383.7	–	–	7.0	
Ti6Al4V -2 wt.% Mo ₂ C	–	–	–	452.3	1499.2	–	–	4.2	
Ti6Al4V -3wt.% Mo ₂ C	–	–	–	368.4	–	–	–	–	
Ti6Al4V -LaB ₆	–	–	–	477.62	1337.1	–	–	5–6	[136]
Ti6Al4V -0.5 wt%GNS	–	–	–	–	1517	–	–	1.3	[211]

$$\gamma = d \sqrt{\frac{\pi}{4f - 1}} \tag{8}$$

$$G_m = \frac{E}{2(1 + \nu)} \tag{9}$$

Where M is the average orientation factor, and the face-centered cubic metal matrix is taken as 3.06, G_m is the shear modulus of the metal matrix, ν is the Poisson's ratio, E is the elastic modulus of the metal matrix, λ is enhanced particle spacing.

SLM technology has been successfully used to produce Al-Si-Mg-Ti/TiC material. The resulting material exhibits heterogeneous nucleation and growth restriction due to TiC nanoparticles, together with finely equiaxed α (Al) grains with nano-sized Si_4Ti_5 particles and Mg segregation along grain boundaries. The reported strengthening effect of the Orowan mechanism is partly explained by the rapid diffusion of Ti in the superheated Al liquid and its high chemical reactivity with Si during the solidification process [204].

Similarly, composite powder with good homogeneity and is made by combining graphene nanoplatelets (GNPs) with TC11 titanium alloy powder. Grain refinement, dislocation strengthening, Orowan strengthening, and load transfer strengthening are the reasons why the inclusion of GNPs greatly improved the mechanical properties of the composite, such as hardness, tensile strength, and fracture toughness [205].

5.4. Load-bearing strengthening

The transfer of external loads from the metallic matrix to the reinforcing phase, uniformly distributed among the reinforcing particles, is facilitated by the formation of a strong metallurgical bond between the two phases [206]. The Nardone-Prewo modified shear-lag model has been widely used in load transfer strengthening models related to the reinforcing phase. The basic idea of this concept is that loads propagate between the metallic matrix and the reinforcing phase interface, strengthening the metallic matrix through the presence of a strong interfacial bond. The yield strength of titanium composites can be expressed in this model as follows [74,207].

$$\sigma_{yc} = \sigma_{ym} \left[0.5V_m \left(2 + \frac{1}{d} \right) + (1 - V_w) \right] \tag{10}$$

$$\sigma_{yc} = \sigma_{ym} V_p \left[1 + \frac{(L + t)}{4L} \right] + \sigma_{ym} (1 - V_p) \tag{11}$$

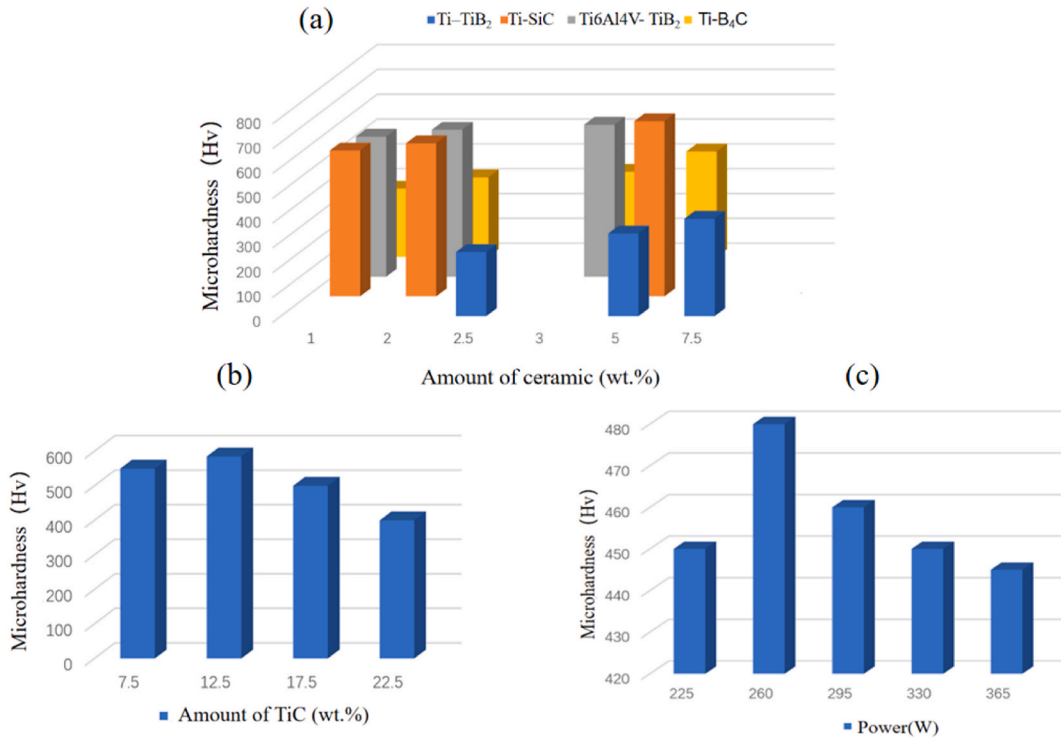


Fig. 18. (a) Effect of reinforcement content on microhardness [31,122,124,151]; (b) Effect of excessive addition of content on microhardness [83]; (c) The effect of laser power on the microhardness of LaB₆/Ti6Al4V composite parts processed by SLM [136].

In the context of composite materials, the yield strength of the material (σ_{yc}) is a critical parameter that characterizes its mechanical properties. In the case of isotropic particles, this parameter can be expressed as a function of the yield strength of the unreinforced matrix (σ_{ym}), as well as the volume fraction (V_W), length (L), and diameter (d) of the particles, along with the volume fraction of the particles themselves (V_p). Additionally, for particles oriented perpendicular to the loading direction, the length of the particles (L) plays a key role in determining the overall mechanical response of the composite. Conversely, for particles oriented parallel to the loading direction, the aspect ratio of the particles (A) must also be considered alongside their length (t) to accurately characterize the composite's mechanical behavior [27].

$$\sigma_{yc} = 0.5\sigma_{ym}V_p \tag{12}$$

The linear relationship between composite strength and reinforcing phase volume fraction fails to account for critical factors like matrix and reinforcing phase properties, reducing the accuracy of yield strength predictions. A deeper understanding of reinforcement mechanisms and the macro-micro relationship is essential, highlighting the need for further research on parameter optimization and strengthening mechanisms. Investigating interfaces, phases, crystal grain structures, and post-processing applications is crucial for improving titanium-based composite performance and realizing its full potential. Bridging these knowledge gaps will significantly advance composite material technology.

6. Overall performances

SLM has the potential to be an effective technique for creating titanium-based composites with enhanced mechanical properties [108]. The composition and microstructure of the matrix, as well as the size, content, and interaction between the reinforcing particles and the matrix, significantly influence the performance of these composites. Compared to traditional mechanical alloying methods, SLM offers the advantage of incorporating a higher volume of reinforcing particles into the material [208]. Consequently, titanium-based composites exhibit notable improvements in strength and hardness but also reduced tensile ductility and fracture toughness. Because of these composites' enhanced resistance to corrosion and wear, they are also a popular option for many industrial applications. The mechanical characteristics of the chosen particle-reinforced TMCs made using SLM are displayed in Table 8 [61,71].

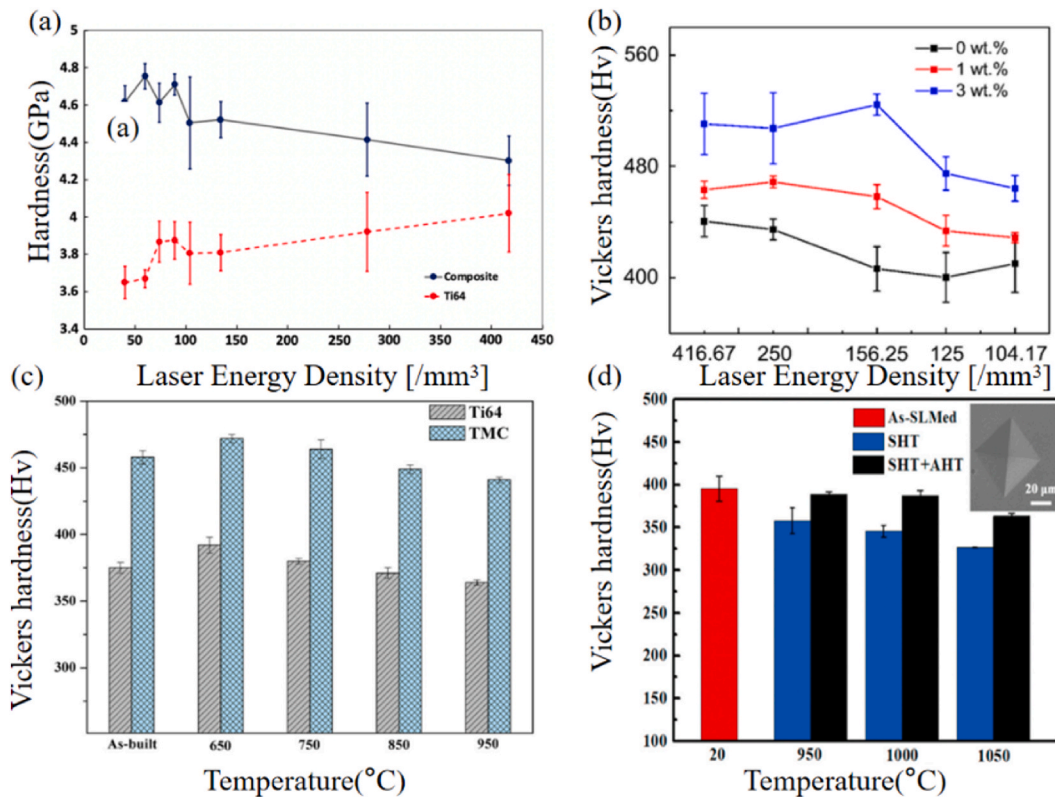


Fig. 19. Part hardness versus laser energy density (a) linear (b) laser energy density and general trend as energy input is increased [31,149,152], (c) and (d) Vickers hardness values of heat-treated SLM under different conditions [163,169].

6.1. Hardness

The milling time and particle size significantly impact the strength of composites. Within the field of SLM, nanoparticles are utilized to inhibit grain growth, facilitating structural fine-tuning and enhancing the microhardness of titanium-based composite materials [212]. The microhardness values of various titanium-based composites fabricated via SLM, as shown in Table 8, exhibit notable improvements over pure titanium. When B₄C particles are incorporated, in-situ formation of needle-shaped and whisker-shaped TiB and particle-shaped TiC occurs. These products serve as α -phase nucleation sites, promoting grain refinement and reinforcing the fine-grain structure.

Higher B₄C concentrations, however, have been shown to promote the aggregation of in-situ reaction products, which reduces hardness [48]. In SLM GNPs/Ti composites, TiC and residual GNPs are uniformly spread across the Ti matrix, and the inclusion of GNPs impedes grain formation, resulting in a decrease in grain size and an augmentation of the fine-grain structure's effect [213]. Furthermore, the hardness of composites based on titanium is enhanced by the addition of rare metals [87]. According to certain research, grinding composite materials at the appropriate moment can increase their strength [72].

The addition of reinforcing elements to ceramic matrices usually causes the microhardness to rise [62,116,214]. The reduction in matrix particle size with increasing concentrations of reinforcement (Fig. 18a) and the hard phase contribution of the reinforcement are credited for this result [31,122,124,151].

However, an excessive addition of the reinforcement phase can lead to a decrease in the hardness of the composite material, For example, the addition of 22.5 wt% TiC notably decreases the hardness due to the net-like distribution and dendritic morphology of TiC reinforcement, which leads to coarsening of the grain size and weakening of the nanostructure of the composite material (Fig. 18b) [122]. Similarly, the nanoneedle-shaped T particles induced high hardness, resulting in the hardening effect and ultimately enhancing the hardness of titanium-based composite materials [151]. Moreover, the synergistic effects of variations in grain size and the different morphologies and distributions of TiB phases initially increase, followed by a subsequent decrease in microhardness due to the increase

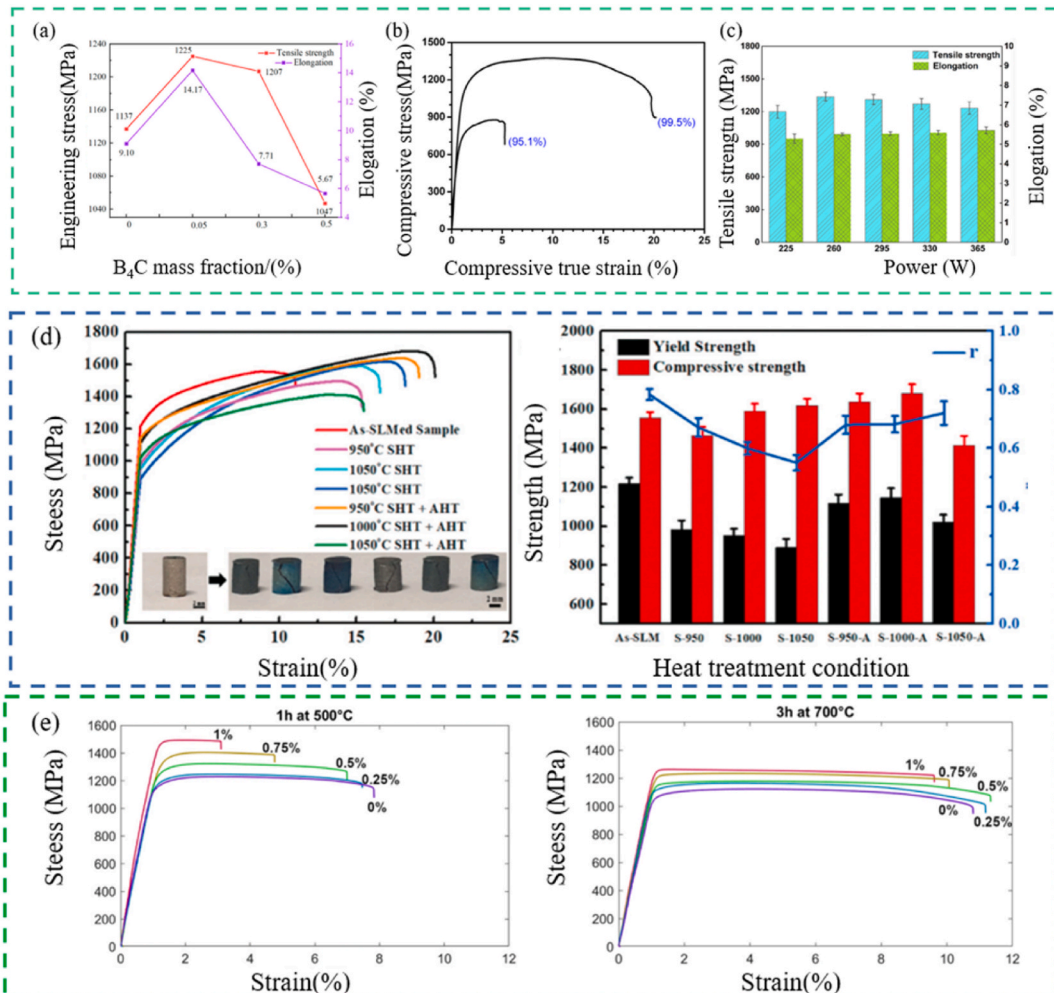


Fig. 20. Properties of composite samples at different conditions [48,123,136,169,219].

in energy density. These findings demonstrate the importance of careful consideration of the type, concentration, and morphology of the reinforcement phase for achieving optimal hardness in ceramic matrix composites [149].

The microhardness of SLM titanium-based composite materials is influenced by the SLM process parameters [54]. The variation in microhardness of in-situ LaB₆/Ti6Al4V composites prepared under different laser powers directly affects the energy density (Fig. 18c) [136]. Generally, below the optimal laser process parameters, the microhardness increases with an increase in laser process parameters [106]. However, due to the synergistic influence of grain size and TiB phase shape and distribution, the microhardness declines with a rise in laser process parameters once a specific value is exceeded. Relevant research has confirmed similar findings [215]. Nevertheless, as the energy density increases, the trend of microhardness variation for TiB/Ti6Al4V composites differs from that of Ti6Al4V specimens. The microhardness value of Ti6Al4V specimens decreases with a decrease in energy density, which is consistent with previous research findings (Table 8). The main reason for this is the significant decrease in microhardness due to the significant growth and coarsening of the in-situ phase as the laser power is increased [215,216].

The impact of laser energy density on the hardness of selectively laser-melted reinforced titanium composites has been investigated [54]. In cases of insufficient energy density, a substantial melted pool failed to form, resulting in a gradient structure that was partially melted, partially solidified, and porous (Fig. 19a). Elevated energy density, however, induced a higher temperature gradient, reducing porosity and increasing density. This transition from α to α' Ti contributed to heightened composite hardness [209]. Excessive energy, on the other hand, destabilized the melt pool, elevating porosity and ultimately reducing hardness (Fig. 19b) [152]. This nuanced understanding provides valuable insights into optimizing energy parameters for enhanced composite properties, essential for the advancement of manufacturing techniques in titanium composites.

The use of scanning techniques in SLM can result in uneven particle distribution and anisotropy in the microstructure of the generated material [147]. Studies on the Ti6Al4V alloy have shown that, despite the lack of research on composite materials, SLM-produced samples with a 0° scanning approach exhibit the most pronounced anisotropy. The top surface has a microhardness approximately 30 % higher than the front surface, and the first columnar crystals on the front surface (158–173 μm) are approximately 1.8–3.2 times larger than those on the top surface (54–88 μm) [217]. The effect of heat concentration on the properties of GO/Ti6Al4V nanocomposites produced by SLM using numerical simulations of four different scanning techniques is investigated. Their results showed that of all the samples studied, those produced using the C-scanning approach performed best [218].

It has been shown that the strength of composites is influenced by the type of heat treatment [219]. The relevant current literature on the heat treatment of SLM titanium composites is summarized in Table 8. Despite this, the hardness values of the heat-treated TMCs specimens were greater than those of the corresponding Ti6Al4V specimens, suggesting that the in-situ produced TiB ceramics had a significant strengthening effect (Fig. 19c) [163]. This could be due to certain α' phases breaking down in-situ into smaller α -Ti grains. This is consistent with findings from previous research on Ti6Al4V alloys produced by heat-treated stress-relieved SLM [220].

Grain coarsening causes hardness to decrease as the heat treatment temperature increases. The hardness growth trend of TMCs is comparable to that of Ti6Al4V alloy (Fig. 19d). However, heat treatment of these composites should not be carried out at temperatures that are too high in solution [163,169].

6.2. Tensile properties

High-strength structural materials produced by additive manufacturing are increasingly noted for their ability to create complex components, especially in the aerospace and transportation industries [221]. Studies have shown that incorporating ceramic phases into titanium alloys enhances their strength but reduces their ductility. Recent advancements in SLM technology have significantly

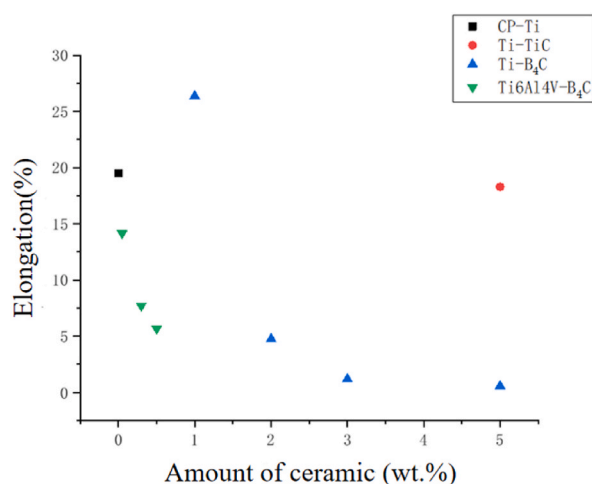


Fig. 21. Graphical summary of results from several studies on the relationship between strain and ceramic volume fraction of SLM-fabricated particle-reinforced TMCs [23,31,48,76].

increased the strength of titanium-based composites. For instance, CP-Ti nanocomposites produced by SLM exhibit higher yield strength compared to pure CP-Ti, with an elongation of $19.57 \pm 1.8 \%$ and a compressive strength of approximately 555 MPa [76]. SLM titanium-based composites are generally stronger but exhibit reduced ductility. TiB + TiC reinforcement enhances the strength of the titanium matrix but significantly reduces its ductility, as observed in the Ti-1 wt.% B₄C composite, which shows a tensile strength of 762 MPa but a reduction in ductility from 26.4 % to 0.6 % upon adding 1 wt% B₄C powder (Fig. 20a) [31,48].

Reinforcement content significantly affects both the tensile strength and elongation of composites. The in-situ formation of ultrafine TiC particles and local reactions with GNSs primarily account for the excellent mechanical properties of SLM GNSs/Ti composites (Table 8). The application of SLM technology has introduced new opportunities for improving the mechanical properties of titanium-based composites, though adding ceramic phases requires careful management of the trade-off between strength and ductility [211]. Additionally, nanoscale TiB whiskers provide a second-phase strengthening effect, leading to Ti grain refinement and enhanced strength. Solid-solution strengthening from interstitial carbon in the titanium matrix also contributes to increased strength, while nanoscale granular TiC particles further enhance tensile properties [107,222].

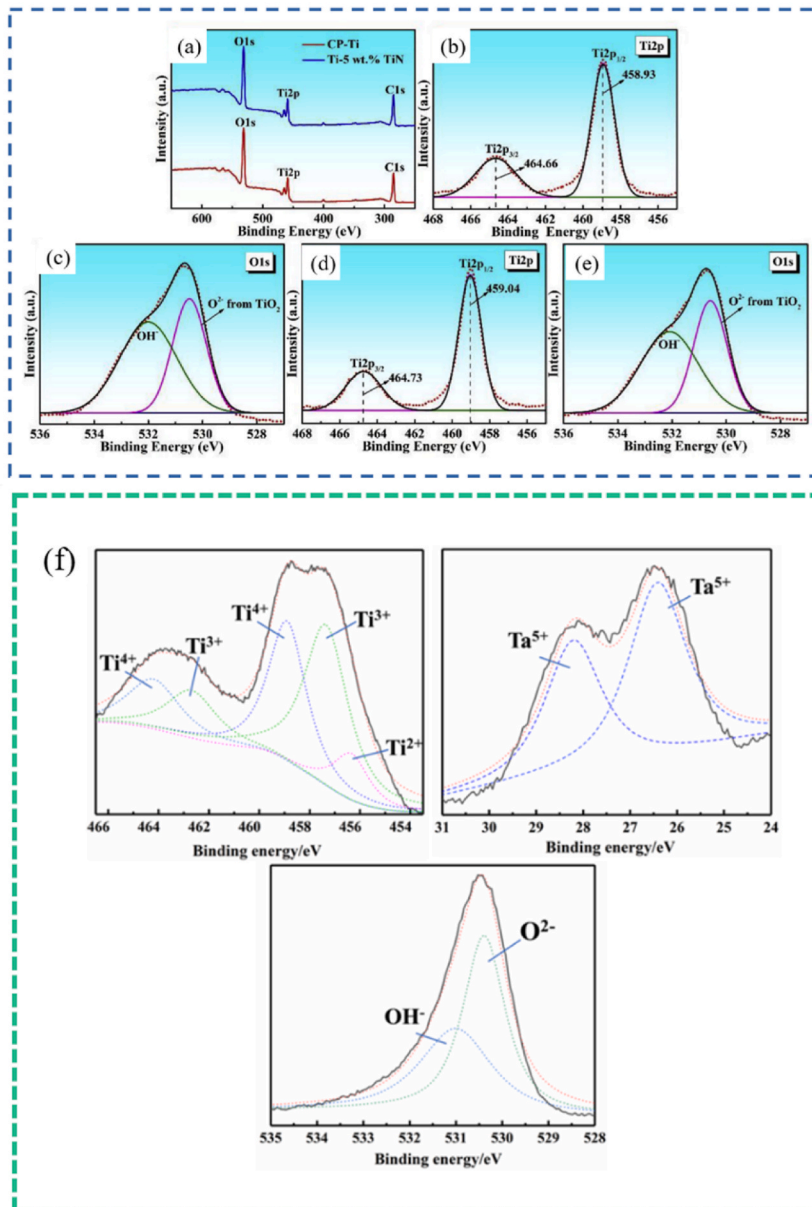


Fig. 22. XPS spectrum of passivation film on the surface of the samples (a) CP-Ti and Ti-5 wt.% TiN, (b) Ti2p spectrum in CP-Ti, (c) O1s spectrum in CP-Ti, (d) Ti2p spectrum in Ti-5 wt.% TiN composite, (e) O1s spectrum in Ti-5 wt.% TiN composite [234]; SLM-processed Ti-25Ta alloy for Ti 2p, Ta 4f and O1s [237].

Milling time during powder preparation is a key factor influencing grain size (Fig. 20b). Studies indicate that TMCs prepared from powders ground for 2 h versus 4 h exhibit different shapes and densities. The latter shows higher porosity and lower relative density but increased ultimate strength. Excessive reinforcement may lead to spheroidization, which decreases material strength [123]. Achieving optimal TMCs requires careful consideration of the reinforcing agent's properties, grain refinement, and other relevant factors. For example, incorporating nanoscale BN particles promotes grain refinement, creating ultrafine-grained structures that improve both strength and ductility. Similarly, TiB nanocrystalline whisker-reinforced TMCs exhibit high strength and favorable ductility [126].

Moreover, processing conditions significantly impact the tensile properties of Ti-based composites [223]. Higher laser power increases melt temperature and heat input, thereby enhancing material strength. Conversely, excessive laser power can cause localized overheating, leading to cracks and other defects that weaken the material (Fig. 20c) [136]. Increasing scan speed reduces heat absorption time, accelerates cooling rates, decreases grain size, and strengthens the material [224]. However, excessively high scanning speeds can lead to uneven melt pool formation, resulting in defects and reduced strength [48,212]. Optimal energy density ensures a fully melted pool and uniform distribution, thereby enhancing material strength. Excessive energy density may cause insufficient

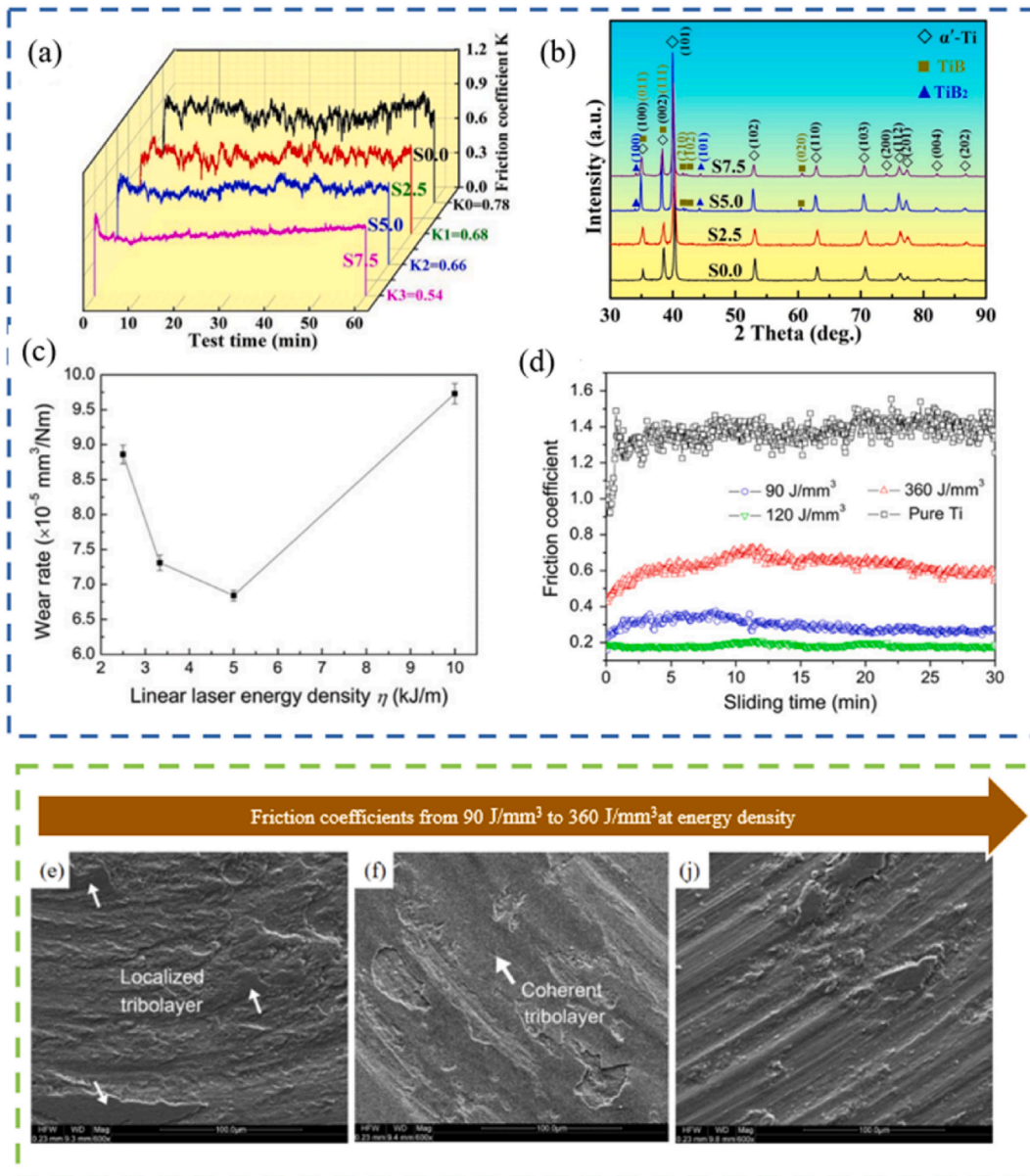


Fig. 23. Composite wear properties under conditions (a, b) different reinforcements content [122], (c) Friction coefficients of SLM-processed Ti and TiC/Ti parts at different energy densities [124], (e) $E_d = 90 \text{ J/mm}^3$, (f) $E_d = 120 \text{ J/mm}^3$, (j) $E_d = 360 \text{ J/mm}^3$ [84].

melting, leading to porosity and inclusions that reduce material strength, while insufficient energy density can result in a small melt pool, instability, and decreased material strength [104].

Heat treatment has an important effect on the tensile properties of selective laser-melted TMCs (Table 8) [225]. Annealing, a prevalent heat treatment method, plays a crucial role in enhancing the strength of TMCs [226]. By heating the material to a specific temperature and subsequently cooling it slowly, internal stresses are relieved, and crystal rearrangement is promoted, which improves crystallinity and material strength (Fig. 20d). Additionally, annealing enhances the material's hardness, plasticity, wear resistance, and toughness [170]. Another important heat treatment method for some TMCs is solid solution treatment [227]. This involves heating the material to its solution temperature, allowing the solid solution elements to dissolve into the titanium matrix, and then maintaining this temperature for a suitable duration to form a uniform solid solution [228]. Solution annealing can increase hardness, strength, and corrosion resistance. However, careful control of temperature and time during this process is essential to prevent excessive grain growth and the precipitation of solution elements, which could adversely affect the material's strength and properties. Additionally, the selection of appropriate heat treatment time is a critical factor (Fig. 20e) [168–170].

Elongation, a key mechanical characteristic of particle-reinforced TMCs, is extensively evaluated during tensile testing [23]. This metric is often used to assess the plasticity of engineering materials [48]. Ceramic particles, being brittle and having limited malleability, influence the elongation behavior. When stress concentrations occur, a plastic zone forms at the crack tip, blunting the fissure and inducing ductile behavior [76]. As illustrated in Fig. 21, elongation at fracture typically decreases with increasing ceramic volume fraction [48]. This reduction is attributed to the increased likelihood of ceramic particles acting as crack initiation sites, leading to premature failure and reduced elongation [55]. In addition, considerable efforts have been made to improve the elongation at fracture [104]. Efforts to enhance elongation at fracture have focused on heat treatment and process parameter optimization. For instance, optimizing parameters such as energy density has been shown to improve elongation at fracture in TiC/Ti6Al4V composites [170].

However, achieving high strength in the Ti matrix does not necessarily mean compromising its ductility [36]. In some cases, both strength and ductility can be enhanced simultaneously [229]. For example, Ti-based composites reinforced with TiC and TiB have been produced with refined structures that effectively suppress microcracks and improve both strength and ductility [148].

Overall, careful consideration of some variables such as reinforcement properties, grain refinement, and processing techniques is required to achieve the appropriate mechanical properties of TMCs. It is conceivable that further research could produce TMCs with high strength and ductility, making them suitable for a range of industrial applications.

6.3. Corrosion

Titanium-based composites are widely used in marine and aerospace industries for their superior strength-to-weight ratio and corrosion resistance [230]. Manufactured typically via SLM, these composites are the focus of research aimed at improving corrosion and wear resistance [231,232].

One approach involves incorporating nanoparticles into the titanium matrix to enhance mechanical properties [233]. TiN particles added to the Ti-5wt% composite enhance corrosion resistance by forming a protective TiO₂ layer on the surface (Fig. 22a–e). A stable passivation layer on Ti-2.5TiN can be achieved with a finer grain size in the δ -TiN phase and higher relative density [234,235]. Incorporating elements like tantalum (Ta) into titanium alloys is another effective method [236]. The in-situ production of Ti-Ta alloys by SLM, involving grain refinement, solid solution strengthening, and formation of TiO, Ti₂O₃, and Ta₂O₅, improves corrosion resistance (Fig. 22f) [237]. Surface modifications, such as hydrofluoric acid (HF) etching, can also improve the corrosion resistance of SLM-produced titanium alloy [231].

SLM is a viable technique for producing titanium-based composites with enhanced mechanical and corrosion properties. Further research is needed to optimize processing parameters and post-treatment processes to fully realize their potential for various applications.

6.4. Wear resistance

The remarkable mechanical and physical properties of ceramic particle-reinforced composites have garnered growing attention in recent years [238]. Reinforcing particles facilitate microstructural refinement and enhancement, thereby improving the wear resistance of composites (Fig. 23a and b) [122].

Energy density significantly influences the wear of selectively laser-melted TMCs [239]. Energy density critically affects the melting and solidification of the material surface during the SLM process. Low energy density can cause partial, shallow melting, leading to surface defects such as holes and cracks, which reduce the wear resistance of the materials (Fig. 23c) [124]. High energy density can lead to excessive melting and rapid cooling, causing large grain sizes and an uneven structure that degrades wear properties (Fig. 23d) [240]. Wear mechanisms are closely related to energy density (Fig. 23d). Ti-based composites melted with a selective laser at high energy densities can form a glassy or amorphous structure, which generally exhibits higher hardness and wear resistance (Fig. 23f–j) [241]. At low energy densities, the material forms a crystalline structure with larger grains and poorer wear properties (Fig. 23e) [242]. To improve wear properties, controlling the microstructure and physical properties through appropriate energy density management is essential [105].

Following an in-situ reaction between TiB₂ and Ti, TiB grains are formed. The formation of α' martensite and the addition of TiB₂ can induce fine grain strengthening in SLM-produced composites (Fig. 24a, b, c). This results in increased wear resistance, with higher TiB₂ contents leading to the formation of protective zones [122]. Similarly, reinforcing particles significantly enhance the wear resistance of

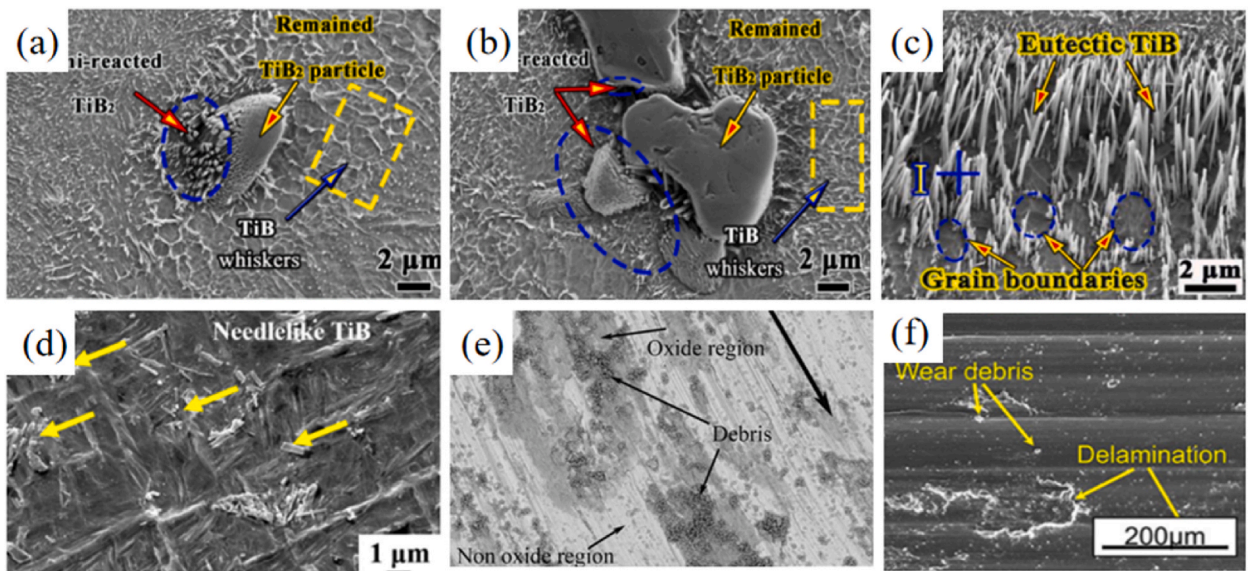


Fig. 24. Addition of reinforcing particles changes the schematic diagram of the composite structure [31,48,76,151].

alloys, with hardness and grain refinement contributing to improved wear resistance [151]. Incorporating TiB_2 into Ti6Al4V resulted in the complete transformation of TiB_2 into the desired nanoscale TiB phase and near- α phase. This resulted in the formation of a composite material with parallel strip structures, significantly enhancing wear resistance (Fig. 24d) [81]. A protective oxide layer was also observed, further enhancing the wear resistance of the composite material (Fig. 24e) [209]. The uniform distribution of the phase within the matrix enhances microhardness, further improving wear resistance [243]. Overall, the addition of TiB_2 particles to titanium-based composites significantly enhances their wear resistance through microstructural refinement, strengthening effects, and protective mechanisms (Fig. 24f) [149].

Recently, there has been increasing interest in the development of high-strength and high-ductility composite materials [244]. One promising approach is to incorporate nanoparticles into the matrix material to trigger nucleation events and induce grain refinement [245]. For example, researchers investigated the reinforcement and toughness of Ti-based composites using nanoscale BN particles. As TiB forms, it provides nucleation sites and creates ultrafine grain structures, maintaining up to 10 % tensile ductility [148]. Similarly, Yang et al. (2022) employed laser melting to reinforce Ti6Al4V composites with nanoscale SiC whiskers, resulting in a 19.4 % increase in ultimate tensile strength while retaining good ductility, primarily due to grain refinement [140,213]. These studies demonstrate the potential of using nanoparticles to enhance the mechanical properties of composite materials through grain refinement and nucleation events.

The heat treatment behavior, fatigue performance, and tribological properties of titanium-based composites forged via SLM [246]. The research findings establish that annealing prompts a complete phase transformation of pure Ti6Al4V alloy into lamellar α phase and spherical β phase, and that incorporating graphene notably bolsters the mechanical properties of the SLM-processed titanium-based composites [164,171]. Additionally, the study highlights that material properties and porous structure have a significant bearing on fatigue crack initiation time and fatigue life, but microstructure refinement has a marked impact on the development of tribological properties. These outcomes furnish valuable insights for optimizing the performance of SLM titanium-based composites [8, 72].

In summary, the mechanisms of hardness in SLM-treated TMCs are not yet fully understood, underscoring the need for comprehensive research to optimize these materials on fracture mechanics in Ti-based composites is currently limited, underscoring the need for further investigation to deepen understanding and optimize the design of TMCs for improved toughness. Beyond hardness, it is essential to study fatigue properties, high-temperature hardness, and corrosion resistance in SLM-treated Ti-based composites for practical applications. Additionally, adopting post-processing methods to enhance surface quality and developing effective techniques are crucial for ensuring the production of high-quality components. Acknowledging the current limitations in research highlights the ample opportunities for further exploration in these critical areas, which will contribute to the advancement and practical application of SLM-prepared TMCs.

7. Conclusions

This study offers an in-depth examination of the microstructure, mechanical properties, and wear behavior of ceramic particle-reinforced TMCs produced by SLM. Results indicate that the performance of SLM-produced particle-reinforced TMCs is significantly affected by the type of ceramic particles, related to their intrinsic properties. A homogeneous dispersion of ceramic particles is crucial for achieving a synergistic combination of strength and flexibility in these TMCs. Altering the spatial distribution of ceramic

particles in the titanium matrix can enhance performance. SLT process parameters strongly influence the microstructure and mechanical properties of particle-reinforced TMCs, with performance further improved by optimizing the interfacial bonding between ceramic particles and the titanium matrix. This work offers a detailed analysis of mechanisms improving mechanical properties, emphasizing Orowan strengthening, load transfer effects, and grain refinement. Future studies should investigate additional factors and develop theoretical models to elucidate these mechanisms. Further research will enhance understanding of particle-reinforced TMCs performance, providing better theoretical guidance for automotive, aerospace, and other applications. Extensive research confirms the unique properties of particle-reinforced TMCs as advanced materials suitable for diverse applications. However, further work is needed to optimize these materials for commercial use.

The size of reinforcing particles is a critical factor affecting the mechanical properties of particle-reinforced TMCs. Nanometer-sized particles show superior yield strength, tensile strength, and ductility compared to micrometer-sized particles, though particle aggregation can cause premature material fracture. Developing multi-scale particle-reinforced TMCs holds promise for high-performance materials.

Particle-reinforced composites are highly engineered due to their complex interactions and precise design requirements. Factors such as matrix alloy composition and reinforcement particle size, morphology, and type significantly influence performance, formability, and processability. Ongoing studies have focused on deformation behavior, but results have been mainly anecdotal. Future work should create a deformation and processing database and develop simulation methods to model microstructural changes during deformation and accelerating development.

Addressing technological bottlenecks requires focusing on processing and controlling microstructure, laying the foundation for practical applications. Load transfer strengthening, achieved by introducing reinforcing particles into the matrix, is a direct form of reinforcement. Controlling phase transformation behavior during SLM by adjusting parameters such as material composition, heating rate, and cooling rate is essential for optimizing crystal structure and microstructure. Research should focus on the formation mechanisms of grain boundaries, dislocations, and twinning, and controlling their distribution and morphology to enhance performance. Additionally, applying multi-scale modeling and simulation techniques to understand microstructural changes, phase transformations, and texture during SLM is key, involving solidification, solid-state transformations, and accurate simulation models for predicting properties.

CRediT authorship contribution statement

Jun Fang: Writing – review & editing, Writing – original draft, Formal analysis, Data curation, Conceptualization. **Yong Chai Tan:** Writing – review & editing, Methodology. **Vin Cent Tai:** Writing – original draft, Methodology, Investigation. **Shamini Janasekaran:** Methodology. **Chia Ching Kee:** Formal analysis. **Dongsheng Wang:** Methodology, Investigation, Funding acquisition. **Youwen Yang:** Writing – original draft, Conceptualization.

Ethics declaration

Informed consent was not required for this study, and no reason for ethical vetting was found since a review of previously published material has been made.

Data availability

Data will be made available on request.

Declaration of competing interest

The authors declare that they have no competing financial interests that could have influenced the work reported in this paper.

Acknowledgments

Funding: This work was supported by the Tongling University Scientific Research Project [2023tlxyz02, 2023tlxydxs092]; The University Synergy Innovation Program of Anhui Province [GXXT-2023-025, GXXT-2023-026]; and the Anhui University Scientific Research Project, China [2308085ME171].

References

- [1] Q. Zhao, Q. Sun, S. Xin, Y. Chen, C. Wu, H. Wang, J. Xu, M. Wan, W. Zeng, Y. Zhao, High-strength titanium alloys for aerospace engineering applications: a review on melting-forging process, *Mater. Sci. Eng. A* 845 (2022) 143260, <https://doi.org/10.1016/j.msea.2022.143260>.
- [2] T.S. Tshephe, S.O. Akinwamide, E. Olevsky, P.A. Olubambi, Additive manufacturing of titanium-based alloys- A review of methods, properties, challenges, and prospects, *Heliyon* 8 (2022) e09041, <https://doi.org/10.1016/j.heliyon.2022.e09041>.
- [3] X. Liu, P. Chu, C. Ding, Surface modification of titanium, titanium alloys, and related materials for biomedical applications, *Mater. Sci. Eng. R Rep.* 47 (2004) 49–121, <https://doi.org/10.1016/j.mser.2004.11.001>.
- [4] M. Kaur, K. Singh, Review on titanium and titanium based alloys as biomaterials for orthopaedic applications, *Mater. Sci. Eng. C* 102 (2019) 844–862, <https://doi.org/10.1016/j.msec.2019.04.064>.

- [5] F. Yu, Y. Zhang, C. Kong, H. Yu, High strength and toughness of Ti-6Al-4V sheets via cryorolling and short-period annealing, *Mater. Sci. Eng. A* 854 (2022) 143766, <https://doi.org/10.1016/j.msea.2022.143766>.
- [6] A. Hemmasian Etefagh, C. Zeng, S. Guo, J. Raush, Corrosion behavior of additively manufactured Ti-6Al-4V parts and the effect of post annealing, *Addit. Manuf.* 28 (2019) 252–258, <https://doi.org/10.1016/j.addma.2019.05.011>.
- [7] Y. Sun, G. Luo, J. Zhang, C. Wu, J. Li, Q. Shen, L. Zhang, Phase transition, microstructure and mechanical properties of TC4 titanium alloy prepared by plasma activated sintering, *J. Alloys Compd.* 741 (2018) 918–926, <https://doi.org/10.1016/j.jallcom.2018.01.197>.
- [8] Y.J. Liu, D.C. Ren, S.J. Li, H. Wang, L.C. Zhang, T.B. Sercombe, Enhanced fatigue characteristics of a topology-optimized porous titanium structure produced by selective laser melting, *Addit. Manuf.* 32 (2020) 101060, <https://doi.org/10.1016/j.addma.2020.101060>.
- [9] B. Sengupta, S. Shekhar, K.N. Kulkarni, A novel ultra-high strength and low-cost as-cast titanium alloy, *Mater. Sci. Eng. A* 696 (2017) 478–481, <https://doi.org/10.1016/j.msea.2017.04.106>.
- [10] M.C. Spataru, M. Butnaru, A.V. Sandu, V. Vulpe, M.D. Vlad, M.S. Baltatu, V. Geanta, I. Voiculescu, P. Vizureanu, C. Solcan, In-depth assessment of new Ti-based biocompatible materials, *Mater. Chem. Phys.* 258 (2021) 123959, <https://doi.org/10.1016/j.matchemphys.2020.123959>.
- [11] D. Banerjee, J.C. Williams, Perspectives on titanium science and technology, *Acta Mater.* 61 (2013) 844–879, <https://doi.org/10.1016/j.actamat.2012.10.043>.
- [12] K. Morsi, V.V. Patel, Processing and properties of titanium–titanium boride (TiB_w) matrix composites—a review, *J. Mater. Sci.* 42 (2007) 2037–2047, <https://doi.org/10.1007/s10853-006-0776-2>.
- [13] C. Xia, X. Ma, X. Zhang, K. Li, J. Tan, Y. Qiao, X. Liu, Enhanced physicochemical and biological properties of C/Cu dual ions implanted medical titanium, *Bioact. Mater.* 5 (2020) 377–386, <https://doi.org/10.1016/j.bioactmat.2020.02.017>.
- [14] Q. Guo, H. Hou, K. Wang, M. Li, P.K. Liaw, Y. Zhao, Coalescence of Al_{0.3}CoCrFeNi polycrystalline high-entropy alloy in hot-pressed sintering: a molecular dynamics and phase-field study, *npj Comput. Mater.* 9 (2023) 185, <https://doi.org/10.1038/s41524-023-01139-9>.
- [15] X. Tian, Y. Zhao, T. Gu, Y. Guo, F. Xu, H. Hou, Cooperative effect of strength and ductility processed by thermomechanical treatment for Cu–Al–Ni alloy, *Mater. Sci. Eng. A* 849 (2022) 143485, <https://doi.org/10.1016/j.msea.2022.143485>.
- [16] E. Fereiduni, A. Ghasemi, M. Elbestawi, Selective laser melting of aluminum and titanium matrix composites: recent progress and potential applications in the aerospace industry, *Aerospace* 7 (2020) 77, <https://doi.org/10.3390/aerospace7060077>.
- [17] M.D. Hayat, H. Singh, Z. He, P. Cao, Titanium metal matrix composites: an overview, *Compos. Part Appl. Sci. Manuf.* 121 (2019) 418–438, <https://doi.org/10.1016/j.compositesa.2019.04.005>.
- [18] H. Ding, P. Gong, W. Chen, Z. Peng, H. Bu, M. Zhang, X. Tang, J. Jin, L. Deng, G. Xie, X. Wang, K. Yao, J. Schroers, Achieving strength-ductility synergy in metallic glasses via electric current-enhanced structural fluctuations, *Int. J. Plast.* 169 (2023) 103711, <https://doi.org/10.1016/j.ijplas.2023.103711>.
- [19] M. Ebrahimi, Q. Wang, S. Attarilar, A comprehensive review of magnesium-based alloys and composites processed by cyclic extrusion compression and the related techniques, *Prog. Mater. Sci.* 131 (2023) 101016, <https://doi.org/10.1016/j.pmatsci.2022.101016>.
- [20] G. Qiao, B. Zhang, Q. Bai, Y. Gao, W. Du, Y. Zhang, Machinability of TiC-reinforced titanium matrix composites fabricated by additive manufacturing, *J. Manuf. Process.* 76 (2022) 412–418, <https://doi.org/10.1016/j.jmapro.2022.02.033>.
- [21] J.X. Fang, S.B. Li, S.Y. Dong, Y.J. Wang, H.S. Huang, Y.L. Jiang, B. Liu, Effects of phase transition temperature and preheating on residual stress in multi-pass & multi-layer laser metal deposition, *J. Alloys Compd.* 792 (2019) 928–937, <https://doi.org/10.1016/j.jallcom.2019.04.104>.
- [22] J. Wang, Z. Pan, Y. Wang, L. Wang, L. Su, D. Cuiuri, Y. Zhao, H. Li, Evolution of crystallographic orientation, precipitation, phase transformation and mechanical properties realized by enhancing deposition current for dual-wire arc additive manufactured Ni-rich NiTi alloy, *Addit. Manuf.* 34 (2020) 101240, <https://doi.org/10.1016/j.addma.2020.101240>.
- [23] H. Attar, S. Ehtemam-Haghighi, D. Kent, M.S. Dargusch, Recent developments and opportunities in additive manufacturing of titanium-based matrix composites: a review, *Int. J. Mach. Tools Manuf.* 133 (2018) 85–102, <https://doi.org/10.1016/j.ijmactools.2018.06.003>.
- [24] W.H. Yu, S.L. Sing, C.K. Chua, C.N. Kuo, X.L. Tian, Particle-reinforced metal matrix nanocomposites fabricated by selective laser melting: a state of the art review, *Prog. Mater. Sci.* 104 (2019) 330–379, <https://doi.org/10.1016/j.pmatsci.2019.04.006>.
- [25] Y. Fang, M.-K. Kim, Y. Zhang, Z. Duan, Q. Yuan, J. Suhr, Particulate-reinforced iron-based metal matrix composites fabricated by selective laser melting: a systematic review, *J. Manuf. Process.* 74 (2022) 592–639, <https://doi.org/10.1016/j.jmapro.2021.12.018>.
- [26] S. Das, Physical aspects of process control in selective laser sintering of metals, *Adv. Eng. Mater.* 5 (2003) 701–711, <https://doi.org/10.1002/adem.200310099>.
- [27] W.H. Yu, S.L. Sing, C.K. Chua, C.N. Kuo, X.L. Tian, Particle-reinforced metal matrix nanocomposites fabricated by selective laser melting: a state of the art review, *Prog. Mater. Sci.* 104 (2019) 330–379, <https://doi.org/10.1016/j.pmatsci.2019.04.006>.
- [28] Z. Fang, B. Ma, E. Liang, Y. Jia, S. Guan, Interaction regularity of biomolecules on Mg and Mg-based alloy surfaces: a first-principles study, *Coatings* 14 (2023) 25, <https://doi.org/10.3390/coatings14010025>.
- [29] L. Chen, Y. Zhao, J. Jing, H. Hou, Microstructural evolution in graphene nanoplatelets reinforced magnesium matrix composites fabricated through thixomolding process, *J. Alloys Compd.* 940 (2023) 168824, <https://doi.org/10.1016/j.jallcom.2023.168824>.
- [30] Y. Xiao, C. Song, Z. Liu, L. Liu, H. Zhou, D. Wang, Y. Yang, In-situ additive manufacturing of high strength yet ductility titanium composites with gradient layered structure using N₂, *Int. J. Extreme Manuf.* 6 (2024) 035001, <https://doi.org/10.1088/2631-7990/ad2602>.
- [31] C. Han, R. Babicheva, J.D.Q. Chua, U. Ramamurthy, S.B. Tor, C.-N. Sun, K. Zhou, Microstructure and mechanical properties of (TiB+TiC)/Ti composites fabricated in situ via selective laser melting of Ti and B₄C powders, *Addit. Manuf.* 36 (2020) 101466, <https://doi.org/10.1016/j.addma.2020.101466>.
- [32] B. AlMangour, D. Grzesiak, J. Cheng, Y. Ertas, Thermal behavior of the molten pool, microstructural evolution, and tribological performance during selective laser melting of TiC/316L stainless steel nanocomposites: experimental and simulation methods, *J. Mater. Process. Technol.* 257 (2018) 288–301, <https://doi.org/10.1016/j.jmatprotec.2018.01.028>.
- [33] S. Wang, X. Chen, K. Luo, H. Zhou, R. Li, P. He, K.-W. Paik, S. Zhang, The design of low-temperature solder alloys and the comparison of mechanical performance of solder joints on ENIG and ENEPIG interface, *J. Mater. Res. Technol.* 27 (2023) 5332–5339, <https://doi.org/10.1016/j.jmrt.2023.11.066>.
- [34] J.X. Fang, G.Z. Ma, H.L. Tian, S.B. Li, H.S. Huang, Y. Liu, Y.L. Jiang, B. Liu, Transformation-induced strain of a low transformation temperature alloy with high hardness during laser metal deposition, *J. Manuf. Process.* 68 (2021) 1585–1595, <https://doi.org/10.1016/j.jmapro.2021.06.066>.
- [35] N.E. Putra, M.J. Mirzaali, I. Apachitei, J. Zhou, A.A. Zadpoor, Multi-material additive manufacturing technologies for Ti-, Mg-, and Fe-based biomaterials for bone substitution, *Acta Biomater.* 109 (2020) 1–20, <https://doi.org/10.1016/j.actbio.2020.03.037>.
- [36] C. Tan, R. Li, J. Su, D. Du, Y. Du, B. Attard, Y. Chew, H. Zhang, E.J. Lavernia, Y. Fautrelle, J. Teng, A. Dong, Review on field assisted metal additive manufacturing, *Int. J. Mach. Tools Manuf.* 189 (2023) 104032, <https://doi.org/10.1016/j.ijmactools.2023.104032>.
- [37] C. Han, Q. Fang, Y. Shi, S.B. Tor, C.K. Chua, K. Zhou, Recent advances on high-entropy alloys for 3D printing, *Adv. Mater.* 32 (2020) 1903855, <https://doi.org/10.1002/adma.201903855>.
- [38] Y. Kim, H. Yuk, R. Zhao, S.A. Chester, X. Zhao, Printing ferromagnetic domains for untethered fast-transforming soft materials, *Nature* 558 (2018) 274–279, <https://doi.org/10.1038/s41586-018-0185-0>.
- [39] G. Xue, L. Ke, H. Zhu, H. Liao, J. Zhu, X. Zeng, Influence of processing parameters on selective laser melted SiC_p/AlSi10Mg composites: densification, microstructure and mechanical properties, *Mater. Sci. Eng. A* 764 (2019) 138155, <https://doi.org/10.1016/j.msea.2019.138155>.
- [40] A. Al Noman, B.K. Kumar, T. Dickens, Field assisted additive manufacturing for polymers and metals: materials and methods, *Virtual Phys. Prototyp.* 18 (2023) e2256707, <https://doi.org/10.1080/17452759.2023.2256707>.
- [41] A. Razavykia, E. Brusa, C. Delprete, R. Yavari, An overview of additive manufacturing technologies—a review to technical synthesis in numerical study of selective laser melting, *Materials* 13 (2020) 3895, <https://doi.org/10.3390/ma13173895>.
- [42] B. Gao, H. Zhao, L. Peng, Z. Sun, A review of research progress in selective laser melting (SLM), *Micromachines* 14 (2022) 57, <https://doi.org/10.3390/mi14010057>.
- [43] C. Galy, E. Le Guen, E. Lacoste, C. Arvieu, Main defects observed in aluminum alloy parts produced by SLM: from causes to consequences, *Addit. Manuf.* 22 (2018) 165–175, <https://doi.org/10.1016/j.addma.2018.05.005>.

- [44] K.D. Traxel, A. Bandyopadhyay, Influence of in situ ceramic reinforcement towards tailoring titanium matrix composites using laser-based additive manufacturing, *Addit. Manuf.* 31 (2020) 101004, <https://doi.org/10.1016/j.addma.2019.101004>.
- [45] S. Wen, H. Hu, Y. Zhou, Z. Chen, Q. Wei, Y. Shi, Enhanced hardness and wear property of S136 mould steel with nano-TiB₂ composites fabricated by selective laser melting method, *Appl. Surf. Sci.* 457 (2018) 11–20, <https://doi.org/10.1016/j.apsusc.2018.06.220>.
- [46] X. Song, Y. Zhang, Progress of high-entropy alloys prepared using selective laser melting, *Sci. China Mater.* 66 (2023) 4165–4181, <https://doi.org/10.1007/s40843-023-2578-5>.
- [47] S. Dadbaksh, R. Mertens, L. Hao, J. Van Humbeeck, J. Kruth, Selective laser melting to manufacture “in situ” metal matrix composites: a review, *Adv. Eng. Mater.* 21 (2019) 1801244, <https://doi.org/10.1002/adem.201801244>.
- [48] S. Guo, Y. Li, J. Gu, J. Liu, Y. Peng, P. Wang, Q. Zhou, K. Wang, Microstructure and mechanical properties of Ti6Al4V/B4C titanium matrix composite fabricated by selective laser melting (SLM), *J. Mater. Res. Technol.* 23 (2023) 1934–1946, <https://doi.org/10.1016/j.jmrt.2023.01.126>.
- [49] K. Li, C. Ji, S. Bai, B. Jiang, F. Pan, Selective laser melting of magnesium alloys: necessity, formability, performance, optimization and applications, *J. Mater. Sci. Technol.* 154 (2023) 65–93, <https://doi.org/10.1016/j.jmst.2022.12.053>.
- [50] J. Gunasekaran, P. Sevvell, I. John Solomon, Metallic materials fabrication by selective laser melting: a review, *Mater. Today Proc.* 37 (2021) 252–256, <https://doi.org/10.1016/j.matpr.2020.05.162>.
- [51] H. Shipley, D. McDonnell, M. Culleton, R. Coull, R. Lupoi, G. O'Donnell, D. Trimble, Optimisation of process parameters to address fundamental challenges during selective laser melting of Ti-6Al-4V: a review, *Int. J. Mach. Tools Manuf.* 128 (2018) 1–20, <https://doi.org/10.1016/j.ijmactools.2018.01.003>.
- [52] X. Mao, L. Dong, Y. Zhang, S. Qin, G. Sun, L. Wang, Y. Zhang, Superior strength-ductility combination in TiC/TC4 composites via in situ construction Ti₂Cu nanoparticles, *Carbon* 219 (2024) 118805, <https://doi.org/10.1016/j.carbon.2024.118805>.
- [53] M.E. Korkmaz, M.K. Gupta, S. Waqar, M. Kuntoglu, G.M. Krolczyk, R.W. Maruda, D.Yu Pimenov, A short review on thermal treatments of Titanium & Nickel based alloys processed by selective laser melting, *J. Mater. Res. Technol.* 16 (2022) 1090–1101, <https://doi.org/10.1016/j.jmrt.2021.12.061>.
- [54] R. Nandhakumar, K. Venkatesan, A process parameters review on selective laser melting-based additive manufacturing of single and multi-material: microstructure, physical properties, tribological, and surface roughness, *Mater. Today Commun.* 35 (2023) 105538, <https://doi.org/10.1016/j.mtcomm.2023.105538>.
- [55] P. Wang, J. Eckert, K. Prashanth, M. Wu, I. Kaban, L. Xi, S. Scudino, A review of particulate-reinforced aluminum matrix composites fabricated by selective laser melting, *Trans. Nonferrous Met. Soc. China* 30 (2020) 2001–2034, [https://doi.org/10.1016/S1003-6326\(20\)65357-2](https://doi.org/10.1016/S1003-6326(20)65357-2).
- [56] Y. Li, D. Gu, Thermal behavior during selective laser melting of commercially pure titanium powder: numerical simulation and experimental study, *Addit. Manuf.* 1–4 (2014) 99–109, <https://doi.org/10.1016/j.addma.2014.09.001>.
- [57] Q. Yan, B. Chen, N. Kang, X. Lin, S. Lv, K. Kondoh, S. Li, J.S. Li, Comparison study on microstructure and mechanical properties of Ti-6Al-4V alloys fabricated by powder-based selective-laser-melting and sintering methods, *Mater. Charact.* 164 (2020) 110358, <https://doi.org/10.1016/j.matchar.2020.110358>.
- [58] C. Cosma, I. Drstvensek, P. Berce, S. Prunean, S. Legutko, C. Popa, N. Bal, Physical-mechanical characteristics and microstructure of Ti6Al7Nb lattice structures manufactured by selective laser melting, *Materials* 13 (2020) 4123, <https://doi.org/10.3390/ma13184123>.
- [59] E.M. Sefene, State-of-the-art of selective laser melting process: a comprehensive review, *J. Manuf. Syst.* 63 (2022) 250–274, <https://doi.org/10.1016/j.jmsy.2022.04.002>.
- [60] M.H. Mosallanejad, A. Abdi, F. Karpasand, N. Nassiri, L. Iuliano, A. Saboori, Additive manufacturing of titanium alloys: processability, properties, and applications, *Adv. Eng. Mater.* 25 (2023) 2301122, <https://doi.org/10.1002/adem.202301122>.
- [61] L.-C. Zhang, H. Attar, Selective laser melting of titanium alloys and titanium matrix composites for biomedical applications: a review: selective laser melting of titanium alloys, *Adv. Eng. Mater.* 18 (2016) 463–475, <https://doi.org/10.1002/adem.201500419>.
- [62] C. Cai, J.C.D. Qiu, T.W. Shian, C. Han, T. Liu, L.B. Kong, N. Srikanth, C.-N. Sun, K. Zhou, Laser powder bed fusion of Mo₂C/Ti-6Al-4V composites with alternately laminated α/β phases for enhanced mechanical properties, *Addit. Manuf.* 46 (2021) 102134, <https://doi.org/10.1016/j.addma.2021.102134>.
- [63] J. Xu, J. Zhang, Y. Shi, J. Tang, D. Huang, M. Yan, M.S. Dargusch, Surface modification of biomedical Ti and Ti alloys: a review on current advances, *Materials* 15 (2022) 1749, <https://doi.org/10.3390/ma15051749>.
- [64] N. Singh, S. Acharya, K.G. Prashanth, K. Chatterjee, S. Suwas, Ti6Al7Nb-based TiB-reinforced composites by selective laser melting, *J. Mater. Res.* 36 (2021) 3691–3700, <https://doi.org/10.1557/s43578-021-00238-x>.
- [65] Z. Liu, B. He, T. Lyu, Y. Zou, A review on additive manufacturing of titanium alloys for aerospace applications: directed energy deposition and beyond Ti-6Al-4V, *JOM* 73 (2021) 1804–1818, <https://doi.org/10.1007/s11837-021-04670-6>.
- [66] A.K. Singla, M. Banerjee, A. Sharma, J. Singh, A. Bansal, M.K. Gupta, N. Khanna, A.S. Shahi, D.K. Goyal, Selective laser melting of Ti6Al4V alloy: process parameters, defects and post-treatments, *J. Manuf. Process.* 64 (2021) 161–187, <https://doi.org/10.1016/j.jmapro.2021.01.009>.
- [67] A. Mahajan, G. Singh, S. Devgan, Additive manufacturing of metallic biomaterials: a concise review, *Arch. Civ. Mech. Eng.* 23 (2023) 187, <https://doi.org/10.1007/s43452-023-00730-7>.
- [68] G. Li, S. Chandra, R.A. Rahman Rashid, S. Palanisamy, S. Ding, Machinability of additively manufactured titanium alloys: a comprehensive review, *J. Manuf. Process.* 75 (2022) 72–99, <https://doi.org/10.1016/j.jmapro.2022.01.007>.
- [69] E.O. Olakanmi, R.F. Cochrane, K.W. Dalgarno, A review on selective laser sintering/melting (SLS/SLM) of aluminium alloy powders: processing, microstructure, and properties, *Prog. Mater. Sci.* 74 (2015) 401–477, <https://doi.org/10.1016/j.pmatsci.2015.03.002>.
- [70] J. Gunasekaran, P. Sevvell, I. John Solomon, P. Tanushkumar, A brief review on the manufacturing of metal components using selective laser melting, *Mater. Today Proc.* 64 (2022) 173–180, <https://doi.org/10.1016/j.matpr.2022.04.213>.
- [71] H. Attar, M. Bönisch, M. Calin, L.-C. Zhang, S. Scudino, J. Eckert, Selective laser melting of in situ titanium–titanium boride composites: processing, microstructure and mechanical properties, *Acta Mater.* 76 (2014) 13–22, <https://doi.org/10.1016/j.actamat.2014.05.022>.
- [72] K. Lin, Y. Fang, D. Gu, Q. Ge, J. Zhuang, L. Xi, Selective laser melting of graphene reinforced titanium matrix composites: powder preparation and its formability, *Adv. Powder Technol.* 32 (2021) 1426–1437, <https://doi.org/10.1016/j.apt.2021.03.003>.
- [73] S. Sun, Q. Teng, Y. Xie, T. Liu, R. Ma, J. Bai, C. Cai, Q. Wei, Two-step heat treatment for laser powder bed fusion of a nickel-based superalloy with simultaneously enhanced tensile strength and ductility, *Addit. Manuf.* 46 (2021) 102168, <https://doi.org/10.1016/j.addma.2021.102168>.
- [74] Y. Jiao, L. Huang, L. Geng, Progress on discontinuously reinforced titanium matrix composites, *J. Alloys Compd.* 767 (2018) 1196–1215, <https://doi.org/10.1016/j.jallcom.2018.07.100>.
- [75] S.O. Jeje, M.B. Shongwe, A.L. Rominiyi, P.A. Olubambi, Spark plasma sintering of titanium matrix composite—a review, *Int. J. Adv. Manuf. Technol.* 117 (2021) 2529–2544, <https://doi.org/10.1007/s00170-021-07840-7>.
- [76] B. He, K. Chang, W. Wu, C. Zhang, The formation mechanism of TiC reinforcement and improved tensile strength in additive manufactured Ti matrix nanocomposite, *Vacuum* 143 (2017) 23–27, <https://doi.org/10.1016/j.vacuum.2017.05.029>.
- [77] Ş. Karabulut, H. Karakoç, R. Çitak, Influence of B₄C particle reinforcement on mechanical and machining properties of Al6061/B₄C composites, *Compos. Part B Eng.* 101 (2016) 87–98, <https://doi.org/10.1016/j.compositesb.2016.07.006>.
- [78] H. Attar, L. Löber, A. Funk, M. Calin, L.C. Zhang, K.G. Prashanth, S. Scudino, Y.S. Zhang, J. Eckert, Mechanical behavior of porous commercially pure Ti and Ti-TiB composite materials manufactured by selective laser melting, *Mater. Sci. Eng. A* 625 (2015) 350–356, <https://doi.org/10.1016/j.msea.2014.12.036>.
- [79] H. Wu, Y. Han, G. Huang, N. Zong, J. Mao, H. Shi, W. Lu, Configuration of new fiber-like structure driven high matching of strength-ductility in TiB reinforced titanium matrix composites, *Compos. Part B Eng.* 231 (2022) 109564, <https://doi.org/10.1016/j.compositesb.2021.109564>.
- [80] H.-Y. Yang, Z. Wang, L.-Y. Chen, S.-L. Shu, F. Qiu, L.-C. Zhang, Interface formation and bonding control in high-volume-fraction (TiC+TiB₂)/Al composites and their roles in enhancing properties, *Compos. Part B Eng.* 209 (2021) 108605, <https://doi.org/10.1016/j.compositesb.2021.108605>.
- [81] D. Gu, C. Hong, G. Meng, Densification, microstructure, and wear property of in situ titanium nitride-reinforced titanium silicide matrix composites prepared by a novel selective laser melting process, *Metall. Mater. Trans. A* 43 (2012) 697–708, <https://doi.org/10.1007/s11661-011-0876-8>.
- [82] R. Sitek, M. Szustecki, L. Zrodowski, B. Wysocki, J. Jaroszewicz, P. Wisniewski, J. Mizera, Analysis of microstructure and properties of a Ti–AlN composite produced by selective laser melting, *Materials* 13 (2020) 2218, <https://doi.org/10.3390/ma13102218>.

- [83] D. Gu, G. Meng, C. Li, W. Meiners, R. Poprawe, Selective laser melting of TiC/Ti bulk nanocomposites: influence of nanoscale reinforcement, *Scr. Mater.* 67 (2012) 185–188, <https://doi.org/10.1016/j.scriptamat.2012.04.013>.
- [84] D. Gu, Y.-C. Hagedorn, W. Meiners, K. Wissenbach, R. Poprawe, Nanocrystalline TiC reinforced Ti matrix bulk-form nanocomposites by Selective Laser Melting (SLM): densification, growth mechanism and wear behavior, *Compos. Sci. Technol.* 71 (2011) 1612–1620, <https://doi.org/10.1016/j.compscitech.2011.07.010>.
- [85] L. Xi, Q. Lu, R. Wang, L. Feng, Effect of carbon nanotubes on the microstructure and tribological properties of in situ synthesized MWCNTs/Ti6Al4V composites fabricated by Selective laser melting, *Opt. Laser Technol.* 153 (2022) 108176, <https://doi.org/10.1016/j.optlastec.2022.108176>.
- [86] X. Guo, L. Wang, M. Wang, J. Qin, D. Zhang, W. Lu, Effects of degree of deformation on the microstructure, mechanical properties and texture of hybrid-reinforced titanium matrix composites, *Acta Mater.* 60 (2012) 2656–2667, <https://doi.org/10.1016/j.actamat.2012.01.032>.
- [87] K. Majchrowicz, Z. Pakielna, T. Brynk, B. Romelczyk-Baishya, M. Płocińska, T. Kurzynowski, E. Chlebus, Microstructure and mechanical properties of Ti–Re alloys manufactured by selective laser melting, *Mater. Sci. Eng. A* 765 (2019) 138290, <https://doi.org/10.1016/j.msea.2019.138290>.
- [88] H. Qiu, X. Li, C. Pan, J. Fan, S. Qu, Effect of Mo₂C addition on the formation of core-rim structure and mechanical properties of Ti (C, N)-WC-Mo₂C- (Ni, Co) cermet, *J. Mater. Res. Technol.* 25 (2023) 750–762, <https://doi.org/10.1016/j.jmrt.2023.05.224>.
- [89] E. Fereiduni, A. Ghasemi, M. Elbestawi, Selective laser melting of hybrid ex-situ/in-situ reinforced titanium matrix composites: laser/powder interaction, reinforcement formation mechanism, and non-equilibrium microstructural evolutions, *Mater. Des.* 184 (2019) 108185, <https://doi.org/10.1016/j.matdes.2019.108185>.
- [90] Y. Pan, W. Li, X. Lu, M.D. Hayat, L. Yin, W. Song, X. Qu, P. Cao, Microstructure and tribological properties of titanium matrix composites reinforced with in situ synthesized TiC particles, *Mater. Charact.* 170 (2020) 110633, <https://doi.org/10.1016/j.matchar.2020.110633>.
- [91] Y. Dong, Y. Li, T. Ebel, M. Yan, Cost-affordable, high-performance Ti–TiB composite for selective laser melting additive manufacturing, *J. Mater. Res.* 35 (2020) 1922–1935, <https://doi.org/10.1557/jmr.2019.389>.
- [92] D. Gu, H. Wang, G. Zhang, Selective laser melting additive manufacturing of Ti-based nanocomposites: the role of nanopowder, *Metall. Mater. Trans. A* 45 (2014) 464–476, <https://doi.org/10.1007/s11661-013-1968-4>.
- [93] P. Shojaei, R. Scazzosi, M. Trabia, B. O'Toole, M. Giglio, X. Zhang, Y. Liao, A. Manes, An approach for material model identification of a composite coating using micro-indentation and multi-scale simulations, *Coatings* 12 (2022) 92, <https://doi.org/10.3390/coatings12010092>.
- [94] Q. Chen, H. Geng, H. Zhang, X. Li, G. Chen, Microstructure and mechanical properties of in situ TiB₂/TiAl₃/2024Al composite subjected to multidirectional forging, *J. Mater. Res. Technol.* 21 (2022) 2827–2840, <https://doi.org/10.1016/j.jmrt.2022.10.098>.
- [95] M. Fattahi, S.A. Delbari, A. Sabahi Namini, Z. Ahmadi, M. Azadbeh, M. Shahedi Asl, Characterization of triplet Ti–TiB–TiC composites: comparison of in-situ formation and ex-situ addition of TiC, *Ceram. Int.* 46 (2020) 11726–11734, <https://doi.org/10.1016/j.ceramint.2020.01.204>.
- [96] A. Wang, J. Wang, F. Yang, T. Wen, H. Yang, S. Ji, Improved strength–ductility synergy of a CoCrNi medium-entropy alloy by ex situ TiN nanoparticles, *Adv. Eng. Mater.* 25 (2023) 2200939, <https://doi.org/10.1002/adem.202200939>.
- [97] L. Liu, J. Xu, P. Munroe, Z.-H. Xie, Microstructure, mechanical and electrochemical properties of in situ synthesized TiC reinforced Ti₅Si₃ nanocomposite coatings on Ti–6Al–4V substrates, *Electrochim. Acta* 115 (2014) 86–95, <https://doi.org/10.1016/j.electacta.2013.10.138>.
- [98] H. Attar, M. Bönisch, M. Calin, L.C. Zhang, K. Zhuravleva, A. Funk, S. Scudino, C. Yang, J. Eckert, Comparative study of microstructures and mechanical properties of in situ Ti–TiB composites produced by selective laser melting, powder metallurgy, and casting technologies, *J. Mater. Res.* 29 (2014) 1941–1950, <https://doi.org/10.1557/jmr.2014.122>.
- [99] Y. Jiao, L. Huang, L. Geng, Progress on discontinuously reinforced titanium matrix composites, *J. Alloys Compd.* 767 (2018) 1196–1215, <https://doi.org/10.1016/j.jallcom.2018.07.100>.
- [100] M. Li, X. Wu, Y. Yang, Q. Wei, C. Yan, C. Cai, J. Liu, W. Li, Y. Shi, TiAl/RGO (reduced graphene oxide) bulk composites with refined microstructure and enhanced nanohardness fabricated by selective laser melting (SLM), *Mater. Charact.* 143 (2018) 197–205, <https://doi.org/10.1016/j.matchar.2018.05.040>.
- [101] T.A. Mukalay, J.A. Trimble, K. Mpofo, R. Muvunzi, A systematic review of process uncertainty in Ti6Al4V-selective laser melting, *CIRP J. Manuf. Sci. Technol.* 36 (2022) 185–212, <https://doi.org/10.1016/j.cirpj.2021.12.005>.
- [102] E. Tiferet, O. Rivin, M. Ganor, H. Etedgui, O. Ozeri, E.N. Caspi, O. Yeheskel, Structural investigation of selective laser melting and electron beam melting of Ti–6Al–4V using neutron diffraction, *Addit. Manuf.* 10 (2016) 43–46, <https://doi.org/10.1016/j.addma.2016.02.001>.
- [103] M. Tang, L. Zhang, N. Zhang, Microstructural evolution, mechanical and tribological properties of TiC/Ti6Al4V composites with unique microstructure prepared by SLM, *Mater. Sci. Eng. A* 814 (2021) 141187, <https://doi.org/10.1016/j.msea.2021.141187>.
- [104] Q. Jiang, S. Li, S. Guo, M. Fu, B. Zhang, Comparative study on process-structure-property relationships of TiC/Ti6Al4V and Ti6Al4V by selective laser melting, *Int. J. Mech. Sci.* 241 (2023) 107963, <https://doi.org/10.1016/j.ijmecsci.2022.107963>.
- [105] D. Gu, Y.-C. Hagedorn, W. Meiners, K. Wissenbach, R. Poprawe, Selective Laser Melting of in-situ TiC/Ti₅Si₃ composites with novel reinforcement architecture and elevated performance, *Surf. Coat. Technol.* 205 (2011) 3285–3292, <https://doi.org/10.1016/j.surfcoat.2010.11.051>.
- [106] L. Liu, T. Minasyan, R. Ivanov, S. Aydinyan, I. Hussainova, Selective laser melting of TiB₂-Ti composite with high content of ceramic phase, *Ceram. Int.* 46 (2020) 21128–21135, <https://doi.org/10.1016/j.ceramint.2020.05.189>.
- [107] H. Li, Z. Yang, D. Cai, D. Jia, Y. Zhou, Microstructure evolution and mechanical properties of selective laser melted bulk-form titanium matrix nanocomposites with minor B₄C additions, *Mater. Des.* 185 (2020) 108245, <https://doi.org/10.1016/j.matdes.2019.108245>.
- [108] B. Zhang, Y. Li, Q. Bai, Defect Formation mechanisms in selective laser melting: a review, *Chin. J. Mech. Eng.* 30 (2017) 515–527, <https://doi.org/10.1007/s10033-017-0121-5>.
- [109] B. Liu, G. Fang, L. Lei, X. Yan, Predicting the porosity defects in selective laser melting (SLM) by molten pool geometry, *Int. J. Mech. Sci.* 228 (2022) 107478, <https://doi.org/10.1016/j.ijmecsci.2022.107478>.
- [110] O.H. Famodimu, M. Stanford, C.F. Oduoza, L. Zhang, Effect of process parameters on the density and porosity of laser melted AlSi10Mg/SiC metal matrix composite, *Front. Mech. Eng.* 13 (2018) 520–527, <https://doi.org/10.1007/s11465-018-0521-y>.
- [111] W.R. Kim, G.B. Bang, O. Kwon, K.-H. Jung, H.-K. Park, G.-H. Kim, H.-T. Jeong, H.G. Kim, Fabrication of porous pure titanium via selective laser melting under low-energy-density process conditions, *Mater. Des.* 195 (2020) 109035, <https://doi.org/10.1016/j.matdes.2020.109035>.
- [112] X.P. Li, J. Van Humbeek, J.P. Kruth, Selective laser melting of weak-textured commercially pure titanium with high strength and ductility: a study from laser power perspective, *Mater. Des.* 116 (2017) 352–358, <https://doi.org/10.1016/j.matdes.2016.12.019>.
- [113] H. Attar, M. Calin, L.C. Zhang, S. Scudino, J. Eckert, Manufacture by selective laser melting and mechanical behavior of commercially pure titanium, *Mater. Sci. Eng. A* 593 (2014) 170–177, <https://doi.org/10.1016/j.msea.2013.11.038>.
- [114] R. Wang, D. Gu, G. Huang, K. Shi, L. Yuan, H. Zhang, Multilayered gradient titanium-matrix composites fabricated by multi-material laser powder bed fusion using metallized ceramic: forming characteristics, microstructure evolution, and multifunctional properties, *Addit. Manuf.* 62 (2023) 103407, <https://doi.org/10.1016/j.addma.2023.103407>.
- [115] D. Grossin, A. Montón, P. Navarrete-Segado, E. Özmen, G. Urruth, F. Maury, D. Maury, C. Frances, M. Tourbin, P. Lenormand, G. Bertrand, A review of additive manufacturing of ceramics by powder bed selective laser processing (sintering/melting): calcium phosphate, silicon carbide, zirconia, alumina, and their composites, *Open Ceram* 5 (2021) 100073, <https://doi.org/10.1016/j.oceram.2021.100073>.
- [116] C. Gao, W. Wu, J. Shi, Z. Xiao, A.H. Akbarzadeh, Simultaneous enhancement of strength, ductility, and hardness of TiN/AlSi10Mg nanocomposites via selective laser melting, *Addit. Manuf.* 34 (2020) 101378, <https://doi.org/10.1016/j.addma.2020.101378>.
- [117] Q. Han, R. Setchi, S.L. Evans, Characterisation and milling time optimisation of nanocrystalline aluminium powder for selective laser melting, *Int. J. Adv. Manuf. Technol.* 88 (2017) 1429–1438, <https://doi.org/10.1007/s00170-016-8866-z>.
- [118] W. Xu, S. Xiao, X. Lu, G. Chen, C. Liu, X. Qu, Fabrication of commercial pure Ti by selective laser melting using hydride-dehydride titanium powders treated by ball milling, *J. Mater. Sci. Technol.* 35 (2019) 322–327, <https://doi.org/10.1016/j.jmst.2018.09.058>.
- [119] C. Suryanarayana, Mechanical alloying: a critical review, *Mater. Res. Lett.* 10 (2022) 619–647, <https://doi.org/10.1080/21663831.2022.2075243>.

- [120] J. Zhang, X. Zhang, M. Qian, Z. Jia, M. Imran, L. Geng, Recent progress in particulate reinforced aluminum composites fabricated via spark plasma sintering, *Crit. Rev. Solid State Mater. Sci.* (2023) 1–56, <https://doi.org/10.1080/10408436.2023.2223573>.
- [121] X. Yang, Z. Zhang, W. Gu, B. Wang, Y. Fan, Q. Miao, S. Zhao, B. Xie, Fabrication of ultra-low-cost pure Ti by selective laser melting using the mixed powders of hydride-dehydride titanium powders treated by ball milling and spherical powders, *Powder Metall.* 64 (2021) 35–42, <https://doi.org/10.1080/00325899.2020.1847848>.
- [122] J. Jin, S. Zhou, Y. Zhao, Q. Zhang, X. Wang, W. Li, D. Chen, L.-C. Zhang, Refined microstructure and enhanced wear resistance of titanium matrix composites produced by selective laser melting, *Opt. Laser Technol.* 134 (2021) 106644, <https://doi.org/10.1016/j.optlastec.2020.106644>.
- [123] H. Attar, K.G. Prashanth, L.-C. Zhang, M. Calin, I.V. Okulov, S. Scudino, C. Yang, J. Eckert, Effect of powder particle shape on the properties of in situ Ti–TiB composite materials produced by selective laser melting, *J. Mater. Sci. Technol.* 31 (2015) 1001–1005, <https://doi.org/10.1016/j.jmst.2015.08.007>.
- [124] X. Zhang, D. Li, Y. Zheng, P. Shojaei, M. Trabia, B. O'Toole, D. Lin, L. Mushongera, Y. Liao, In-situ synthesis of Ti₅Si₃-reinforced titanium matrix nanocomposite by selective laser melting: quasi-continuous reinforcement network and enhanced mechanical performance, *J. Mater. Process. Technol.* 309 (2022) 117752, <https://doi.org/10.1016/j.jmatprotec.2022.117752>.
- [125] C. Li, D. Gu, Y. Shen, G. Meng, Y. Li, In situ synthesis of Ti₅Si₃ matrix nanocomposites reinforced with nanoparticles by high-energy mechanical alloying, *Adv. Eng. Mater.* 13 (2011) 418–425, <https://doi.org/10.1002/adem.201000377>.
- [126] J. Zhuang, D. Gu, L. Xi, K. Lin, Y. Fang, R. Wang, Preparation method and underlying mechanism of MWCNTs/Ti6Al4V nanocomposite powder for selective laser melting additive manufacturing, *Powder Technol.* 368 (2020) 59–69, <https://doi.org/10.1016/j.powtec.2020.04.041>.
- [127] Q. Han, R. Setchi, S.L. Evans, Synthesis and characterisation of advanced ball-milled Al–Al₂O₃ nanocomposites for selective laser melting, *Powder Technol.* 297 (2016) 183–192, <https://doi.org/10.1016/j.powtec.2016.04.015>.
- [128] K. Shrivanioghaddam, S.U. Hamim, M. Karbalaie Akbari, S.M. Fakhroesini, H. Khayyam, A.H. Pakseresht, E. Ghasali, M. Zabet, K.S. Munir, S. Jia, J. P. Davim, M. Naebe, Carbon fiber reinforced metal matrix composites: fabrication processes and properties, *Compos. Part Appl. Sci. Manuf.* 92 (2017) 70–96, <https://doi.org/10.1016/j.compositesa.2016.10.032>.
- [129] S. Guo, Y. Li, J. Gu, J. Liu, Y. Peng, P. Wang, Q. Zhou, K. Wang, Microstructure and mechanical properties of Ti6Al4V/B₄C titanium matrix composite fabricated by selective laser melting (SLM), *J. Mater. Res. Technol.* 23 (2023) 1934–1946, <https://doi.org/10.1016/j.jmrt.2023.01.126>.
- [130] D. Gu, Y.-C. Hagedorn, W. Meiners, G. Meng, R.J.S. Batista, K. Wissenbach, R. Poprawe, Denatification behavior, microstructure evolution, and wear performance of selective laser melting processed commercially pure titanium, *Acta Mater.* 60 (2012) 3849–3860, <https://doi.org/10.1016/j.actamat.2012.04.006>.
- [131] D. Zhu, L. Zhang, W. Wu, L. Lu, J. Song, X. Ni, W. Zhu, J. Zhao, S. Gu, X. Shan, Investigation on microstructure and hardness of in-situ (TiB+TiC)/Ti composite prepared by selective laser melting, *J. Phys. Conf. Ser.* 1838 (2021) 012039, <https://doi.org/10.1088/1742-6596/1838/1/012039>.
- [132] D. Gu, Y. Shen, Z. Lu, Preparation of TiN–Ti₅Si₃ in-situ composites by selective laser melting, *Mater. Lett.* 63 (2009) 1577–1579, <https://doi.org/10.1016/j.matlet.2009.04.010>.
- [133] X. Yang, Z. Zhang, B. Wang, W. Ma, W. Wang, W. Chen, N. Kang, S. Liu, Microstructure, mechanical properties and corrosion performance of selective laser melting Ti/GNPs composite with a porous structure, *J. Cent. South Univ.* 28 (2021) 2257–2268, <https://doi.org/10.1007/s11771-021-4767-x>.
- [134] B. Zhou, J. Zhou, H. Li, F. Lin, A study of the microstructures and mechanical properties of Ti6Al4V fabricated by SLM under vacuum, *Mater. Sci. Eng. A* 724 (2018) 1–10, <https://doi.org/10.1016/j.msea.2018.03.021>.
- [135] Z. Zhou, Y. Liu, X. Liu, Q. Zhan, K. Wang, Microstructure evolution and mechanical properties of in-situ Ti6Al4V–TiB composites manufactured by selective laser melting, *Compos. Part B Eng.* 207 (2021) 108567, <https://doi.org/10.1016/j.compositesb.2020.108567>.
- [136] H. Wang, D. He, W. Huang, X. Chen, Y. Wang, L. Huang, Study on the fabricating process of LaB₆ reinforced Ti6Al4V by selective laser melting, *Mater. Today Commun.* 35 (2023) 106312, <https://doi.org/10.1016/j.mtcomm.2023.106312>.
- [137] G. Chen, Q. Zhai, Z. Ma, X. Yin, Q. Zhang, H. Zhou, L. Meng, K. Wang, S. Wang, L. Wang, Effect of Cr content on microstructure, mechanical properties and corrosion behavior of Ti6Al4V alloy produced by selective laser melting, *Mater. Technol.* 37 (2022) 1062–1074, <https://doi.org/10.1080/10667857.2021.1921098>.
- [138] Z. Zhao, S. Wang, W. Du, P. Bai, Z. Zhang, L. Wang, J. Wang, D. Tie, Interfacial structures and strengthening mechanisms of in situ synthesized TiC reinforced Ti6Al4V composites by selective laser melting, *Ceram. Int.* 47 (2021) 34127–34136, <https://doi.org/10.1016/j.ceramint.2021.08.323>.
- [139] Z. Zhou, Y. Liu, X. Liu, Q. Zhan, K. Wang, Microstructure evolution and mechanical properties of in-situ Ti6Al4V–TiB composites manufactured by selective laser melting, *Compos. Part B Eng.* 207 (2021) 108567, <https://doi.org/10.1016/j.compositesb.2020.108567>.
- [140] C. Yang, Z. Zhao, P. Bai, W. Du, S. Zhang, Nano-SiC whisker-reinforced Ti6Al4V matrix composites manufactured by selective laser melting: fine equiaxed grain formation mechanism and mechanical properties, *J. Mater. Process. Technol.* 317 (2023) 117981, <https://doi.org/10.1016/j.jmatprotec.2023.117981>.
- [141] O.A. Mohamed, S.H. Masood, W. Xu, Nickel-titanium shape memory alloys made by selective laser melting: a review on process optimisation, *Adv. Manuf.* 10 (2022) 24–58, <https://doi.org/10.1007/s40436-021-00376-9>.
- [142] M. Xia, A. Liu, H. Wang, Y. Lin, N. Li, M. Zhang, H. Ding, Microstructure evolution and its effect on mechanical response of the multi-phase reinforced Ti-based composites by laser powder-bed fusion, *J. Alloys Compd.* 782 (2019) 506–515, <https://doi.org/10.1016/j.jallcom.2018.12.182>.
- [143] Y.-H. Siao, C.-D. Wen, Examination of molten pool with Marangoni flow and evaporation effect by simulation and experiment in selective laser melting, *Int. Commun. Heat Mass Transf.* 125 (2021) 105325, <https://doi.org/10.1016/j.icheatmasstransfer.2021.105325>.
- [144] C. Poletti, M. Balog, T. Schubert, V. Liedtke, C. Edtmaier, Production of titanium matrix composites reinforced with SiC particles, *Compos. Sci. Technol.* 68 (2008) 2171–2177, <https://doi.org/10.1016/j.compscitech.2008.03.018>.
- [145] Y. Wen, T. Guo, Y. Zhou, H. Bai, Z. Wang, Nanoindentation characterization on microhardness of micron-level TiC and TiB reinforcements in in-situ synthesized (TiC+TiB)/Ti-6Al-4V composite, *Front. Mater.* 6 (2019) 205, <https://doi.org/10.3389/fmats.2019.0205>.
- [146] J. Chen, L. Zhou, J. Liang, B. Liu, J. Liu, R. Chen, X. Deng, S. Wu, M. Huang, Effect of initial WC particle size on grain growth behavior and gradient structure formation of bilayer functionally graded cemented carbides, *Mater. Chem. Phys.* 271 (2021) 124919, <https://doi.org/10.1016/j.matchemphys.2021.124919>.
- [147] W. Zhang, L. Wang, Z. Feng, Y. Chen, Research progress on selective laser melting (SLM) of magnesium alloys: a review, *Optik* 207 (2020) 163842, <https://doi.org/10.1016/j.ijleo.2019.163842>.
- [148] J.A. Otte, J. Zou, M.S. Dargusch, High strength and ductility of titanium matrix composites by nanoscale design in selective laser melting, *J. Mater. Sci. Technol.* 118 (2022) 114–127, <https://doi.org/10.1016/j.jmst.2021.12.020>.
- [149] Y. Su, S.-C. Luo, L. Meng, P. Gao, Z.-M. Wang, Selective laser melting of in situ TiB/Ti6Al4V composites: formability, microstructure evolution and mechanical performance, *Acta Metall. Sin. Engl. Lett.* 33 (2020) 774–788, <https://doi.org/10.1007/s40195-020-01021-3>.
- [150] G. Soundarapandiyar, C.L.A. Leung, C. Johnston, B. Chen, R.H.U. Khan, P. McNutt, A. Bhatt, R.C. Atwood, P.D. Lee, M.E. Fitzpatrick, In situ monitoring the effects of Ti6Al4V powder oxidation during laser powder bed fusion additive manufacturing, *Int. J. Mach. Tools Manuf.* 190 (2023) 104049, <https://doi.org/10.1016/j.ijmactools.2023.104049>.
- [151] C. Cai, C. Radoslaw, J. Zhang, Q. Yan, S. Wen, B. Song, Y. Shi, In-situ preparation and formation of TiB/Ti-6Al-4V nanocomposite via laser additive manufacturing: microstructure evolution and tribological behavior, *Powder Technol.* 342 (2019) 73–84, <https://doi.org/10.1016/j.powtec.2018.09.088>.
- [152] A. DeMartino, T.Y. Ansell, A. Nieto, Effects of laser energy density on carbon-nanotube-reinforced titanium composites printed via selective laser melting, *Adv. Eng. Mater.* 24 (2022) 2100737, <https://doi.org/10.1002/adem.202100737>.
- [153] I. Polozov, V. Sufiarov, A. Kanyukov, A. Popovich, Selective Laser Melting of Ti2AlNb-based intermetallic alloy using elemental powders: effect of process parameters and post-treatment on microstructure, composition, and properties, *Intermetallics* 112 (2019) 106554, <https://doi.org/10.1016/j.intermet.2019.106554>.
- [154] H. Attar, S. Ehtemam-Haghighi, D. Kent, X. Wu, M.S. Dargusch, Comparative study of commercially pure titanium produced by laser engineered net shaping, selective laser melting and casting processes, *Mater. Sci. Eng. A* 705 (2017) 385–393, <https://doi.org/10.1016/j.msea.2017.08.103>.
- [155] C. Qiu, C. Panwisawas, M. Ward, H.C. Basoalto, J.W. Brooks, M.M. Attallah, On the role of melt flow into the surface structure and porosity development during selective laser melting, *Acta Mater.* 96 (2015) 72–79, <https://doi.org/10.1016/j.actamat.2015.06.004>.

- [156] P. Akbari, F. Ogoke, N.-Y. Kao, K. Meidani, C.-Y. Yeh, W. Lee, A. Barati Farimani, MeltPoolNet: melt pool characteristic prediction in Metal Additive Manufacturing using machine learning, *Addit. Manuf.* 55 (2022) 102817, <https://doi.org/10.1016/j.addma.2022.102817>.
- [157] K.L. Raju, S. Thapliyal, S. Sigatapu, A.K. Shukla, G. Bajargan, B. Pant, Process parameter dependent machine learning model for densification prediction of selective laser melted Al-50Si alloy and its validation, *J. Mater. Eng. Perform.* 31 (2022) 8451–8458, <https://doi.org/10.1007/s11665-022-06831-3>.
- [158] E. Abele, M. Kniepkamp, Analysis and optimisation of vertical surface roughness in micro selective laser melting, *Surf. Topogr. Metrol. Prop.* 3 (2015) 034007, <https://doi.org/10.1088/2051-672X/3/3/034007>.
- [159] I. Yadroitsev, I. Smurov, Surface morphology in selective laser melting of metal powders, *Phys. Procedia* 12 (2011) 264–270, <https://doi.org/10.1016/j.phpro.2011.03.034>.
- [160] M. Xia, D. Gu, G. Yu, D. Dai, H. Chen, Q. Shi, Influence of hatch spacing on heat and mass transfer, thermodynamics and laser processability during additive manufacturing of Inconel 718 alloy, *Int. J. Mach. Tools Manuf.* 109 (2016) 147–157, <https://doi.org/10.1016/j.ijmactools.2016.07.010>.
- [161] Z. Li, R. Xu, Z. Zhang, I. Kucukkoc, The influence of scan length on fabricating thin-walled components in selective laser melting, *Int. J. Mach. Tools Manuf.* 126 (2018) 1–12, <https://doi.org/10.1016/j.ijmactools.2017.11.012>.
- [162] Y. Du, T. Mukherjee, T. DebRoy, Physics-informed machine learning and mechanistic modeling of additive manufacturing to reduce defects, *Appl. Mater. Today* 24 (2021) 101123, <https://doi.org/10.1016/j.apmt.2021.101123>.
- [163] H. Li, D. Jia, Z. Yang, X. Liao, H. Jin, D. Cai, Y. Zhou, Effect of heat treatment on microstructure evolution and mechanical properties of selective laser melted Ti-6Al-4V and TiB/Ti-6Al-4V composite: a comparative study, *Mater. Sci. Eng. A* 801 (2021) 140415, <https://doi.org/10.1016/j.msea.2020.140415>.
- [164] X.-Y. Zhang, G. Fang, S. Leeftang, A.J. Böttger, A.A. Zadpoor, J. Zhou, Effect of subtransus heat treatment on the microstructure and mechanical properties of additively manufactured Ti-6Al-4V alloy, *J. Alloys Compd.* 735 (2018) 1562–1575, <https://doi.org/10.1016/j.jallcom.2017.11.263>.
- [165] R.M. Baitimerov, P.A. Lykov, L.V. Radionova, Influence of heat treatment on microstructure and mechanical properties of selective laser melted Ti6Al4V alloy, *Solid State Phenom.* 284 (2018) 615–620, <https://doi.org/10.4028/www.scientific.net/SSP.284.615>.
- [166] C.V. Funch, A. Palmas, K. Somlo, E.H. Valente, X. Cheng, K. Poullos, M. Villa, M.A.J. Somers, T.L. Christiansen, Targeted heat treatment of additively manufactured Ti-6Al-4V for controlled formation of Bi-lamellar microstructures, *J. Mater. Sci. Technol.* 81 (2021) 67–76, <https://doi.org/10.1016/j.jmst.2021.01.004>.
- [167] E. Sallica-Leva, R. Caram, A.L. Jardini, J.B. Fogagnolo, Ductility improvement due to martensite α' decomposition in porous Ti-6Al-4V parts produced by selective laser melting for orthopedic implants, *J. Mech. Behav. Biomed. Mater.* 54 (2016) 149–158, <https://doi.org/10.1016/j.jmbbm.2015.09.020>.
- [168] Z. Zhou, Y. Liu, X. Liu, Constructing a bimodal microstructure via cyclic thermal treatment in selective laser melted Ti6Al4V-5vol%TiB composite, *Mater. Sci. Eng. A* 861 (2022) 144354, <https://doi.org/10.1016/j.msea.2022.144354>.
- [169] J. Zhang, B. Song, C. Cai, L. Zhang, Y. Shi, Tailorable microstructure and mechanical properties of selective laser melted TiB/Ti-6Al-4V composite by heat treatment, *Adv. Powder Mater.* 1 (2022) 100010, <https://doi.org/10.1016/j.apmate.2021.10.001>.
- [170] Z. Zhou, Y. Liu, X. Liu, Constructing targeted bi-lamellar microstructure via heat treatment for high compressive strength and plasticity in selective laser melted Ti6Al4V-5vol%TiB composite, *Mater. Sci. Eng. A* 844 (2022) 143173, <https://doi.org/10.1016/j.msea.2022.143173>.
- [171] H. Li, D. Jia, Z. Yang, Y. Zhou, Achieving near equiaxed α -Ti grains and significantly improved plasticity via heat treatment of TiB reinforced titanium matrix composite manufactured by selective laser melting, *J. Alloys Compd.* 836 (2020) 155344, <https://doi.org/10.1016/j.jallcom.2020.155344>.
- [172] Z. Zhao, C. Dong, D. Kong, L. Wang, X. Ni, L. Zhang, W. Wu, L. Zhu, X. Li, Influence of pore defects on the mechanical property and corrosion behavior of SLM 18Ni300 maraging steel, *Mater. Charact.* 182 (2021) 111514, <https://doi.org/10.1016/j.matchar.2021.111514>.
- [173] J. Lu, L. Zhuo, Additive manufacturing of titanium alloys via selective laser melting: fabrication, microstructure, post-processing, performance and prospect, *Int. J. Refract. Met. Hard Mater.* 111 (2023) 106110, <https://doi.org/10.1016/j.ijrmhm.2023.106110>.
- [174] X. Zhang, C.J. Yocom, B. Mao, Y. Liao, Microstructure Evolution during Selective Laser Melting of Metallic Materials: A Review, *Laser Appl.*, 2019.
- [175] S. Liu, H. Guo, *Balling Behavior of Selective Laser Melting (SLM) Magnesium Alloy*, 2020.
- [176] D. Gu, Y. Shen, Balling phenomena in direct laser sintering of stainless steel powder: metallurgical mechanisms and control methods, *Mater. Des.* 30 (2009) 2903–2910, <https://doi.org/10.1016/j.matdes.2009.01.013>.
- [177] X. Zhou, X. Liu, D. Zhang, Z. Shen, W. Liu, Balling phenomena in selective laser melted tungsten, *J. Mater. Process. Technol.* 222 (2015) 33–42, <https://doi.org/10.1016/j.jmatprotec.2015.02.032>.
- [178] R. Li, J. Liu, Y. Shi, L. Wang, W. Jiang, Balling behavior of stainless steel and nickel powder during selective laser melting process, *Int. J. Adv. Manuf. Technol.* 59 (2012) 1025–1035, <https://doi.org/10.1007/s00170-011-3566-1>.
- [179] K. Wei, M. Gao, Z. Wang, X. Zeng, Effect of energy input on formability, microstructure and mechanical properties of selective laser melted AZ91D magnesium alloy, *Mater. Sci. Eng. A* 611 (2014) 212–222, <https://doi.org/10.1016/j.msea.2014.05.092>.
- [180] C. Liu, M. Zhang, C. Chen, Effect of laser processing parameters on porosity, microstructure and mechanical properties of porous Mg-Ca alloys produced by laser additive manufacturing, *Mater. Sci. Eng. A* 703 (2017) 359–371, <https://doi.org/10.1016/j.msea.2017.07.031>.
- [181] M. Boutaous, X. Liu, D.A. Siginer, S. Xin, Balling phenomenon in metallic laser based 3D printing process, *Int. J. Therm. Sci.* 167 (2021) 107011, <https://doi.org/10.1016/j.ijthermalsci.2021.107011>.
- [182] D. Dai, D. Gu, Q. Ge, Y. Li, X. Shi, Y. Sun, S. Li, Mesoscopic study of thermal behavior, fluid dynamics and surface morphology during selective laser melting of Ti-based composites, *Comput. Mater. Sci.* 177 (2020) 109598, <https://doi.org/10.1016/j.commatsci.2020.109598>.
- [183] G. Chen, R.Z. Liu, Y.-D. Qiu, Y. Yang, J.M. Wu, S.F. Wen, J. Liu, Y.S. Shi, H.B. Tan, Effect of laser parameters on microstructure and phase evolution of Ti-Si-C composites prepared by selective laser melting, *Mater. Today Commun.* 24 (2020) 101114, <https://doi.org/10.1016/j.mtcomm.2020.101114>.
- [184] A. Reinhart, T. Ansell, W. Smith, A. Nieto, Oxide reinforced Ti64 composites processed by selective laser melting, *J. Mater. Eng. Perform.* 30 (2021) 6949–6960, <https://doi.org/10.1007/s11665-021-06077-5>.
- [185] P. Ansari, M.U. Salamci, On the selective laser melting based additive manufacturing of AlSi10Mg: the process parameter investigation through multiphysics simulation and experimental validation, *J. Alloys Compd.* 890 (2022) 161873, <https://doi.org/10.1016/j.jallcom.2021.161873>.
- [186] S.A. Khairallah, A.T. Anderson, A. Rubenchik, W.E. King, Laser powder-bed fusion additive manufacturing: physics of complex melt flow and formation mechanisms of pores, spatter, and denudation zones, *Acta Mater.* 108 (2016) 36–45, <https://doi.org/10.1016/j.actamat.2016.02.014>.
- [187] A.A. Martin, N.P. Calta, S.A. Khairallah, J. Wang, P.J. Depond, A.Y. Fong, V. Thampy, G.M. Guss, A.M. Kiss, K.H. Stone, C.J. Tassone, J. Nelson Weker, M. F. Toney, T. Van Buuren, M.J. Matthews, Dynamics of pore formation during laser powder bed fusion additive manufacturing, *Nat. Commun.* 10 (2019) 1987, <https://doi.org/10.1038/s41467-019-10009-2>.
- [188] K.D. Traxel, A. Bandyopadhyay, Selective laser melting of Ti6Al4V-B₂C-BN in situ reactive composites, *J. Mater. Res. Technol.* 18 (2022) 2654–2671, <https://doi.org/10.1016/j.jmrt.2022.03.092>.
- [189] Y. Zheng, K. Zhang, T.T. Liu, W.H. Liao, C.D. Zhang, H. Shao, Cracks of alumina ceramics by selective laser melting, *Ceram. Int.* 45 (2019) 175–184, <https://doi.org/10.1016/j.ceramint.2018.09.149>.
- [190] C. Rans, J. Michielssen, M. Walker, W. Wang, L.T. Hoen-Velterop, Beyond the orthogonal: on the influence of build orientation on fatigue crack growth in SLM Ti-6Al-4V, *Int. J. Fatigue* 116 (2018) 344–354, <https://doi.org/10.1016/j.ijfatigue.2018.06.038>.
- [191] N. Kalentics, N. Sohrabi, H.G. Tabasi, S. Griffiths, J. Jhabvala, C. Leinenbach, A. Burn, R.E. Logé, Healing cracks in selective laser melting by 3D laser shock peening, *Addit. Manuf.* 30 (2019) 100881, <https://doi.org/10.1016/j.addma.2019.100881>.
- [192] C. Han, Y. Li, Q. Wang, D. Cai, Q. Wei, L. Yang, S. Wen, J. Liu, Y. Shi, Titanium/hydroxyapatite (Ti/HA) gradient materials with quasi-continuous ratios fabricated by SLM: material interface and fracture toughness, *Mater. Des.* 141 (2018) 256–266, <https://doi.org/10.1016/j.matdes.2017.12.037>.

- [193] J.S. Moya, S. Lopez-Esteban, C. Pecharrómán, The challenge of ceramic/metal microcomposites and nanocomposites, *Prog. Mater. Sci.* 52 (2007) 1017–1090, <https://doi.org/10.1016/j.pmatsci.2006.09.003>.
- [194] J. Wang, L. Li, P. Lin, J. Wang, Effect of TiC particle size on the microstructure and tensile properties of TiC_p/Ti6Al4V composites fabricated by laser melting deposition, *Opt. Laser Technol.* 105 (2018) 195–206, <https://doi.org/10.1016/j.optlastec.2018.03.009>.
- [195] M. Ahmadi, S.A.A.B. Tabary, D. Rahmatbadi, M.S. Ebrahimi, K. Abrinia, R. Hashemi, Review of selective laser melting of magnesium alloys: advantages, microstructure and mechanical characterizations, defects, challenges, and applications, *J. Mater. Res. Technol.* 19 (2022) 1537–1562, <https://doi.org/10.1016/j.jmrt.2022.05.102>.
- [196] B. Guo, M. Song, J. Yi, S. Ni, T. Shen, Y. Du, Improving the mechanical properties of carbon nanotubes reinforced pure aluminum matrix composites by achieving non-equilibrium interface, *Mater. Des.* 120 (2017) 56–65, <https://doi.org/10.1016/j.matdes.2017.01.096>.
- [197] F. Ma, T. Wang, P. Liu, W. Li, X. Liu, X. Chen, D. Pan, W. Lu, Mechanical properties and strengthening effects of in situ (TiB+TiC)/Ti-1100 composite at elevated temperatures, *Mater. Sci. Eng. A* 654 (2016) 352–358, <https://doi.org/10.1016/j.msea.2015.12.071>.
- [198] M. Wang, Y. Zhao, L.-D. Wang, Y.-P. Zhu, X.-J. Wang, J. Sheng, Z.-Y. Yang, H.-L. Shi, Z.-D. Shi, W.-D. Fei, Achieving high strength and ductility in graphene/magnesium composite via an in-situ reaction wetting process, *Carbon* 139 (2018) 954–963, <https://doi.org/10.1016/j.carbon.2018.08.009>.
- [199] A. Zafari, E.W. Lui, K. Xia, Deformation-free geometric recrystallisation in a metastable β -Ti alloy produced by selective laser melting, *Mater. Res. Lett.* 8 (2020) 117–122, <https://doi.org/10.1080/21663831.2020.1713244>.
- [200] Q. Wang, K. Zhang, D. Qiu, W. Niu, Additive manufacturing of high-strength commercially pure titanium through lanthanum oxide addition, *Mater. Charact.* 176 (2021) 111074, <https://doi.org/10.1016/j.matchar.2021.111074>.
- [201] M. Alizadeh, H.A. Beni, Strength prediction of the ARBed Al/Al 2 O 3/B 4 C nano-composites using Orowan model, *Mater. Res. Bull.* 59 (2014) 290–294, <https://doi.org/10.1016/j.materresbull.2014.07.034>.
- [202] A. Sanaty-Zadeh, Comparison between current models for the strength of particulate-reinforced metal matrix nanocomposites with emphasis on consideration of Hall–Petch effect, *Mater. Sci. Eng. A* 531 (2012) 112–118, <https://doi.org/10.1016/j.msea.2011.10.043>.
- [203] A. Issariyapat, P. Visuttipitukul, J. Umeda, K. Kondoh, Refined grain formation behavior and strengthening mechanism of α -titanium with nitrogen fabricated by selective laser melting, *Addit. Manuf.* 36 (2020) 101537, <https://doi.org/10.1016/j.addma.2020.101537>.
- [204] L. Xinwei, S. Shi, H. Shuang, H. Xiaogang, Z. Qiang, L. Hongxing, L. Wenwu, S. Yusheng, D. Hui, Microstructure, solidification behavior and mechanical properties of Al-Si-Mg-Ti/TiC fabricated by selective laser melting, *Addit. Manuf.* 34 (2020) 101326, <https://doi.org/10.1016/j.addma.2020.101326>.
- [205] B. Ou, L. Lu, Q. Wang, Q. He, Y. Xie, J. Yan, Mechanical properties of TC11 titanium alloy and graphene nanoplatelets/TC11 composites prepared by selective laser melting, *Int. J. Mol. Sci.* 23 (2022) 6134, <https://doi.org/10.3390/ijms23116134>.
- [206] L. Huang, Q. An, L. Geng, S. Wang, S. Jiang, X. Cui, R. Zhang, F. Sun, Y. Jiao, X. Chen, C. Wang, Multiscale architecture and superior high-temperature performance of discontinuously reinforced titanium matrix composites, *Adv. Mater.* 33 (2021) 2000688, <https://doi.org/10.1002/adma.202000688>.
- [207] Y. Fang, M.-K. Kim, Y. Zhang, Z. Duan, Q. Yuan, J. Suhr, Particulate-reinforced iron-based metal matrix composites fabricated by selective laser melting: a systematic review, *J. Manuf. Process.* 74 (2022) 592–639, <https://doi.org/10.1016/j.jmapro.2021.12.018>.
- [208] M.E. Korkmaz, M.K. Gupta, G. Robak, K. Moj, G.M. Krolczyk, M. Kuntoğlu, Development of lattice structure with selective laser melting process: a state of the art on properties, future trends and challenges, *J. Manuf. Process.* 81 (2022) 1040–1063, <https://doi.org/10.1016/j.jmapro.2022.07.051>.
- [209] N. Kang, P. Coddet, Q. Liu, H. Liao, C. Coddet, In-situ TiB/near α Ti matrix composites manufactured by selective laser melting, *Addit. Manuf.* 11 (2016) 1–6, <https://doi.org/10.1016/j.addma.2016.04.001>.
- [210] M. Chlewicka, A. Dobkowska, R. Sitek, B. Adamczyk-Cieślak, J. Mizera, Microstructure and corrosion resistance characteristics of Ti–AlN composite produced by selective laser melting, *Mater. Corros.* 73 (2022) 451–459, <https://doi.org/10.1002/maco.202112703>.
- [211] Q. Yan, B. Chen, J.S. Li, Super-high-strength graphene/titanium composites fabricated by selective laser melting, *Carbon* 174 (2021) 451–462, <https://doi.org/10.1016/j.carbon.2020.12.047>.
- [212] W.M. Tucho, V.H. Lysne, H. Austbø, A. Sjolyst-Kverneland, V. Hansen, Investigation of effects of process parameters on microstructure and hardness of SLM manufactured SS316L, *J. Alloys Compd.* 740 (2018) 910–925, <https://doi.org/10.1016/j.jallcom.2018.01.098>.
- [213] H. Yang, X. Chen, G. Huang, J. Song, J. She, J. Tan, K. Zheng, Y. Jin, B. Jiang, F. Pan, Microstructures and mechanical properties of titanium-reinforced magnesium matrix composites: review and perspective, *J. Magnes. Alloys* 10 (2022) 2311–2333, <https://doi.org/10.1016/j.jma.2022.07.008>.
- [214] H. Tang, X. Xi, C. Gao, Z. Liu, J. Zhang, W. Zhang, Z. Xiao, J.H. Rao, Microstructure evolution and strengthening mechanisms of a high-performance TiN-reinforced Al–Mn–Mg–Sc–Zr alloy processed by laser powder bed fusion, *J. Mater. Sci. Technol.* 187 (2024) 86–100, <https://doi.org/10.1016/j.jmst.2023.11.033>.
- [215] M. Xia, A. Liu, Z. Hou, N. Li, Z. Chen, H. Ding, Microstructure growth behavior and its evolution mechanism during laser additive manufacture of in-situ reinforced (TiB+TiC)/Ti composite, *J. Alloys Compd.* 728 (2017) 436–444, <https://doi.org/10.1016/j.jallcom.2017.09.033>.
- [216] J. Han, J. Yang, H. Yu, J. Yin, M. Gao, Z. Wang, X. Zeng, Microstructure and mechanical property of selective laser melted Ti6Al4V dependence on laser energy density, *Rapid Prototyp. J.* 23 (2017) 217–226, <https://doi.org/10.1108/RPJ-12-2015-0193>.
- [217] Z. Zheng, X. Jin, Y. Bai, Y. Yang, C. Ni, W.F. Lu, H. Wang, Microstructure and anisotropic mechanical properties of selective laser melted Ti6Al4V alloy under different scanning strategies, *Mater. Sci. Eng. A* 831 (2022) 142236, <https://doi.org/10.1016/j.msea.2021.142236>.
- [218] X. Miao, X. Liu, P. Lu, J. Han, W. Duan, M. Wu, Influence of scanning strategy on the performances of GO-reinforced Ti6Al4V nanocomposites manufactured by SLM, *Metals* 10 (2020) 1379, <https://doi.org/10.3390/met10101379>.
- [219] J. Peterson, A. Issariyapat, J. Umeda, K. Kondoh, The effects of heat treatment and carbon content on the microstructure and mechanical properties of laser powder bed fusion Ti-6Al-4V with dissolved TiC particles, *J. Alloys Compd.* 920 (2022) 165930, <https://doi.org/10.1016/j.jallcom.2022.165930>.
- [220] A. Hattal, T. Chauveau, M. Djemai, J.J. Fouchet, B. Bacroix, G. Dirras, Effect of nano-yttria stabilized zirconia addition on the microstructure and mechanical properties of Ti6Al4V parts manufactured by selective laser melting, *Mater. Des.* 180 (2019) 107909, <https://doi.org/10.1016/j.matdes.2019.107909>.
- [221] D. Kong, L. Wang, G. Zhu, Y. Zhou, X. Ni, J. Song, L. Zhang, W. Wu, W. Wu, C. Man, D. Shu, B. Sun, C. Dong, Heat treatment effects on the metastable microstructure, mechanical property and corrosion behavior of Al-added CoCrFeMnNi alloys fabricated by laser powder bed fusion, *J. Mater. Sci. Technol.* 138 (2023) 171–182, <https://doi.org/10.1016/j.jmst.2022.08.018>.
- [222] Z. Zhou, Y. Liu, New insights into the evolution of TiB whisker and TiC particle during selective laser melting of titanium matrix composites, *Mater. Sci. Eng. A* 877 (2023) 145200, <https://doi.org/10.1016/j.msea.2023.145200>.
- [223] A. Khorasani, I. Gibson, U.S. Awan, A. Ghaderi, The effect of SLM process parameters on density, hardness, tensile strength and surface quality of Ti-6Al-4V, *Addit. Manuf.* 25 (2019) 176–186, <https://doi.org/10.1016/j.addma.2018.09.002>.
- [224] X. Wang, J. Yu, J. Liu, L. Chen, Q. Yang, H. Wei, J. Sun, Z. Wang, Z. Zhang, G. Zhao, J. Van Humbeeck, Effect of process parameters on the phase transformation behavior and tensile properties of NiTi shape memory alloys fabricated by selective laser melting, *Addit. Manuf.* 36 (2020) 101545, <https://doi.org/10.1016/j.addma.2020.101545>.
- [225] W.-C. Lin, Y.-J. Chang, T.-H. Hsu, S. Gorsse, F. Sun, T. Furuahara, A.-C. Yeh, Microstructure and tensile property of a precipitation strengthened high entropy alloy processed by selective laser melting and post heat treatment, *Addit. Manuf.* 36 (2020) 101601, <https://doi.org/10.1016/j.addma.2020.101601>.
- [226] A. Dareh Baghi, S. Nafisi, R. Hashemi, H. Ebendorff-Heidepriem, R. Ghomashchi, Effective post processing of SLM fabricated Ti-6Al-4V alloy: machining vs thermal treatment, *J. Manuf. Process.* 68 (2021) 1031–1046, <https://doi.org/10.1016/j.jmapro.2021.06.035>.
- [227] W.-S. Shin, B. Son, W. Song, H. Sohn, H. Jang, Y.-J. Kim, C. Park, Heat treatment effect on the microstructure, mechanical properties, and wear behaviors of stainless steel 316L prepared via selective laser melting, *Mater. Sci. Eng. A* 806 (2021) 140805, <https://doi.org/10.1016/j.msea.2021.140805>.

- [228] J.U. Lee, Y.K. Kim, S.M. Seo, K.A. Lee, Effects of hot isostatic pressing treatment on the microstructure and tensile properties of Ni-based superalloy CM247LC manufactured by selective laser melting, *Mater. Sci. Eng. A* 841 (2022) 143083, <https://doi.org/10.1016/j.msea.2022.143083>.
- [229] J. Liu, Q. Sun, C. Zhou, X. Wang, H. Li, K. Guo, J. Sun, Achieving Ti6Al4V alloys with both high strength and ductility via selective laser melting, *Mater. Sci. Eng. A* 766 (2019) 138319, <https://doi.org/10.1016/j.msea.2019.138319>.
- [230] Y. Lu, Y. Gan, J. Lin, S. Guo, S. Wu, J. Lin, Effect of laser speeds on the mechanical property and corrosion resistance of CoCrW alloy fabricated by SLM, *Rapid Prototyp. J.* 23 (2017) 28–33, <https://doi.org/10.1108/RPJ-07-2015-0085>.
- [231] Y. Zhu, J. Zou, H. Yang, Wear performance of metal parts fabricated by selective laser melting: a literature review, *J. Zhejiang Univ. - Sci.* 19 (2018) 95–110, <https://doi.org/10.1631/jzus.A1700328>.
- [232] Y. Yang, C. Ling, Y. Li, S. Peng, D. Xie, L. Shen, Z. Tian, C. Shuai, Microstructure development and biodegradation behavior of additively manufactured Mg-Zn-Gd alloy with LPSO structure, *J. Mater. Sci. Technol.* 144 (2023) 1–14, <https://doi.org/10.1016/j.jmst.2022.09.059>.
- [233] X. Yue, N. Qu, X. Ma, H. Li, Anodic electrochemical behaviors of in situ synthesized (TiB+TiC)/Ti6Al4V composites in NaNO₃ and NaCl electrolyte, *Corros. Sci.* 204 (2022) 110379, <https://doi.org/10.1016/j.corsci.2022.110379>.
- [234] S. Zhou, Y. Zhao, X. Wang, W. Li, D. Chen, T.B. Sercombe, Enhanced corrosion resistance of Ti-5 wt.% TiN composite compared to commercial pure Ti produced by selective laser melting in HCl solution, *J. Alloys Compd.* 820 (2020) 153422, <https://doi.org/10.1016/j.jallcom.2019.153422>.
- [235] J. Jin, S. Zhou, W. Zhang, K. Li, Y. Liu, D. Chen, L.-C. Zhang, Effect of ceramic types on the microstructure and corrosion behavior of titanium matrix composites produced by selective laser melting, *J. Alloys Compd.* 918 (2022) 165704, <https://doi.org/10.1016/j.jallcom.2022.165704>.
- [236] H. Wang, K. Su, L. Su, P. Liang, P. Ji, C. Wang, Comparison of 3D-printed porous tantalum and titanium scaffolds on osteointegration and osteogenesis, *Mater. Sci. Eng. C* 104 (2019) 109908, <https://doi.org/10.1016/j.msec.2019.109908>.
- [237] D. Zhao, C. Han, Y. Li, J. Li, K. Zhou, Q. Wei, J. Liu, Y. Shi, Improvement on mechanical properties and corrosion resistance of titanium-tantalum alloys in-situ fabricated via selective laser melting, *J. Alloys Compd.* 804 (2019) 288–298, <https://doi.org/10.1016/j.jallcom.2019.06.307>.
- [238] H. Attar, S. Ehtemam-Haghighi, D. Kent, I.V. Okulov, H. Wendrock, M. Bönisch, A.S. Volegov, M. Calin, J. Eckert, M.S. Dargusch, Nanoindentation and wear properties of Ti and Ti-TiB composite materials produced by selective laser melting, *Mater. Sci. Eng. A* 688 (2017) 20–26, <https://doi.org/10.1016/j.msea.2017.01.096>.
- [239] B. AlMangour, D. Grzesiak, J.-M. Yang, In situ formation of TiC-particle-reinforced stainless steel matrix nanocomposites during ball milling: feedstock powder preparation for selective laser melting at various energy densities, *Powder Technol.* 326 (2018) 467–478, <https://doi.org/10.1016/j.powtec.2017.11.064>.
- [240] D. Gu, G. Zhang, Selective laser melting of novel nanocomposites parts with enhanced tribological performance: nanocrystalline TiC/Ti nanocomposites parts were built via SLM technology and the densification, microstructures, microhardness and tribological Performance were investigated, *Virtual Phys. Prototyp.* 8 (2013) 11–18, <https://doi.org/10.1080/17452759.2013.772319>.
- [241] L. Xi, K. Ding, D. Gu, S. Guo, M. Cao, J. Zhuang, K. Lin, I. Okulov, B. Sarac, J. Eckert, K.G. Prashanth, Interfacial structure and wear properties of selective laser melted Ti/(TiC+TiN) composites with high content of reinforcements, *J. Alloys Compd.* 870 (2021) 159436, <https://doi.org/10.1016/j.jallcom.2021.159436>.
- [242] L. Wu, Z. Zhao, P. Bai, W. Zhao, Y. Li, M. Liang, H. Liao, P. Huo, J. Li, Wear resistance of graphene nano-platelets (GNPs) reinforced AlSi10Mg matrix composite prepared by SLM, *Appl. Surf. Sci.* 503 (2020) 144156, <https://doi.org/10.1016/j.apsusc.2019.144156>.
- [243] S. Zhang, Z. Chen, P. Wei, W. Liu, Y. Zou, Y. Lei, S. Yao, S. Zhang, B. Lu, L. Zhang, Wear properties of graphene/zirconia biphasic nano-reinforced aluminium matrix composites prepared by SLM, *Mater. Today Commun.* 30 (2022) 103009, <https://doi.org/10.1016/j.mtcomm.2021.103009>.
- [244] Y. Han, Y. Zhang, H. Jing, D. Lin, L. Zhao, L. Xu, P. Xin, Selective laser melting of low-content graphene nanoplatelets reinforced 316L austenitic stainless steel matrix: strength enhancement without affecting ductility, *Addit. Manuf.* 34 (2020) 101381, <https://doi.org/10.1016/j.addma.2020.101381>.
- [245] Y.K. Xiao, H. Chen, Z.Y. Bian, T.T. Sun, H. Ding, Q. Yang, Y. Wu, Q. Lian, Z. Chen, H.W. Wang, Enhancing strength and ductility of AlSi10Mg fabricated by selective laser melting by TiB₂ nanoparticles, *J. Mater. Sci. Technol.* 109 (2022) 254–266, <https://doi.org/10.1016/j.jmst.2021.08.030>.
- [246] D. Ivanov, A. Travyanov, P. Petrovskiy, V. Cheverikin, E. Alekseeva, A. Khvan, I. Logachev, Evolution of structure and properties of the nickel-based alloy EP718 after the SLM growth and after different types of heat and mechanical treatment, *Addit. Manuf.* 18 (2017) 269–275, <https://doi.org/10.1016/j.addma.2017.10.015>.